Università degli Studi di Padova

Dipartimento di Biologia

SCUOLA DI DOTTORATO DI RICERCA IN BIOSCIENZE E BIOTECNOLOGIE

INDIRIZZO BIOLOGIA CELLULARE

CICLO XXVIII

Identification and characterization of a novel MICU1 splice variant

Direttore della Scuola : Ch.mo Prof. Paolo Bernardi

Coordinatore d'indirizzo: Ch.mo Prof. Paolo Bernardi

Supervisore: Dott.ssa Cristina Mammucari

Co-Supervisore: Dott.ssa Anna Raffaello

Dottorando : Denis Vecellio Reane

Table of contents

Abstract

The ability of mitochondria to take up Ca^{2+} plays a fundamental role in the regulation of several biological processes [1]. In the last five years, the molecular and functional characterization of the MCU machinery pictures this Ca^{2+} channel as one of the most sophisticated ion channels described so far [2]. These groundbreaking discoveries have opened a new era for the study of mitochondrial Ca^{2+} in cell physiology and will allow to deepen the knowledge on the tissues-specific properties of MCU [3] that are still poorly understood.

In this regard, we identified an alternative splice isoform (hereafter named MICU1.1) of the positive MCU modulator MICU1, characterized by the addition of a micro-exon coding for 4 amino acids (EFWQ), conserved in vertebrates. Interestingly, while MICU1 is ubiquitously expressed, MICU1.1 shows a peculiar tissues distribution, being highly expressed in tissues that display the greatest level of mitochondrial Ca^{2+} uptake, skeletal muscle and lower levels are found in brain.

Immunoprecipitation experiments performed in HeLa cells assessed that MICU1.1 efficiently interacts with MCU and MICU2. Furthermore, MICU1.1 is able to form homo- and heterodimers with MICU2, as well as MICU1. Nonetheless, the overexpression of MICU1.1 in HeLa cells causes a major increase of mitochondrial Ca^{2+} uptake upon histamine stimulation compared to conventional MICU1, without affecting neither cytosolic Ca^{2+} values nor the mitochondrial membrane potential. Strikingly, MICU2 overexpression in cells expressing MICU1.1 is unable to block the increase of mitochondrial Ca^{2+} uptake induced by MICU1.1. On the contrary, the co-expression of MICU1.1 together with MICU2 further increases mitochondrial Ca^{2+} uptake speed compared to cells overexpressing MICU1.1 alone. On the other hand, MICU1.1, when bound to MICU2, is able to act as gatekeeper of the channel at resting Ca^{2+} levels as well as MICU1-MICU2 heterodimer. Importantly, we found that MICU1.1-MICU2 overexpression induces the shift of the threshold of MCU opening towards lower Ca^{2+} concentrations.

Consistently with previous results on MICU1, MICU1.1 function is dependent on its ability to bind Ca^{2+}. Indeed, a MICU1.1 mutant, insensitive to Ca^{2+}, displays a dominant-negative effect on mitochondrial Ca^{2+} uptake. On the

contrary, MICU1.1 is less affected by the dominant-negative effect of mutated MICU2, insensitive to Ca^{2+} binding.

We also analysed the contribution of the extra-exon to the particular behaviour of MICU1.1. We observed that single mutations or deletions of these residues do not influence the effect of MICU1.1 on mitochondrial Ca^{2+} uptake. On the contrary, the substitution of all the four amino acids of the extra-exon with four alanine residues is sufficient to recapitulate MICU1 behaviour.

In conclusion, we characterized a transcript variant of MICU1, which is specifically expressed in excitable tissues, prevalently in skeletal muscle, and that shows a higher ability to activate MCU compared to conventional MICU1. Interestingly, MICU1.1 exerts a peculiar function when bound to MICU2. Overall, our data demonstrate a skeletal muscle-specific mitochondrial Ca^{2+} uptake machinery with a presumably unique function. Thus, in this tissue, mitochondrial Ca^{2+} can exert new, unexplored roles. Future experiments have to be performed to clarify its physiological and pathological relevance.

Riassunto

La capacità dei mitocondri di accumulare Ca^{2+} riveste un ruolo cruciale nella regolazione di numerosi processi fisiologici [1]. Negli ultimi cinque anni, la caratterizzazione dell'identità molecolare e funzionale del complesso dell'uniporto mitocondriale per il calcio (MCU) ha delineato questo canale come uno dei canali più complessi finora descritti [2]. Questa scoperta rivoluzionaria ha inaugurato una nuova era per lo studio del ruolo del Ca^{2+} mitocondriale nella fisiologia cellulare e ha permesso di approfondire i meccanismi di regolazione tessuto-specifici di MCU [3], ad oggi ancora poco chiari.

A questo proposito, abbiamo identificato una variante di splicing del modulatore positivo di MCU, MICU1. Questa variante di splicing, che abbiamo chiamato MICU1.1, è il risultato di un evento di splicing alternativo che determina l'aggiunta di un micro-esone, conservato in tutti i vertebrati, codificante per quattro aminoacidi (EFWQ). Mentre MICU1 è espresso, seppur a diversi livelli, in tutti i tessuti, MICU1.1 presenta una distribuzione peculiare. Infatti, MICU1.1 è molto espresso nei tessuti che sono noti avere un elevato ingresso di Ca^{2+} nei mitocondri, ovvero il muscolo scheletrico e il tessuto nervoso, mentre è assente in tutti gli altri. Esperimenti di immunoprecipitazione effettuati in cellule HeLa hanno dimostrato che MICU1.1 interagisce con MCU e MICU2. Inoltre, MICU1.1 è in grado di formare omodimeri e eterodimeri con MICU2, come già osservato per MICU1. Nonostante ciò, la sovraespressione di MICU1.1 in cellule HeLa causa un aumento dell'entrata di Ca^{2+} mitocondriale maggiore rispetto a MICU1, senza influenzare né i valori di Ca^{2+} citosolici né il potenziale di membrana mitocondriale. Sorprendentemente, la co-espressione di MICU2 in cellule sovraesprimenti MICU1.1 non limita l'incremento di ingresso di Ca^{2+} nei mitocondri indotto dalla sovraespressione di MICU1.1. Al contrario, la co-espressione di MICU1.1 e MICU2 causa un aumento della velocità di entrata di Ca^{2+} nei mitocondri, che risulta essere maggiore rispetto a quella osservata in seguito alla sola sovraespressione di MICU1.1. Tuttavia, in condizioni basali, MICU1.1, quando forma eterodimeri con MICU2, causa la chiusura del canale allo stesso modo dell'eterodimero MICU1-MICU2. Ciononostante, abbiamo osservato che la

sovraespressione di MICU1.1 con MICU2 induce un abbassamento della soglia di attivazione di MCU verso concentrazioni di Ca^{2+} più basse.

Come già dimostrato in precedenti studi su MICU1, anche la funzione di MICU1.1 dipende dalla capacità di questa proteina di legare Ca^{2+}. Infatti, un mutante di MICU1.1 insensibile ai livelli di Ca^{2+}, agisce da dominante negativo sull'entrata di Ca^{2+} nel mitocondrio.

Abbiamo anche dimostrato che il comportamento peculiare di MICU1.1 dipende dai residui che compongono l'esone addizionale. I risultati ottenuti dimostrano che la singola mutazione di uno di questi residui (in particolare la sostituzione con alanina o la delezione) non influenza l'effetto di MICU1.1 sull'ingresso di Ca^{2+} nel mitocondrio. Tuttavia, la sostituzione di tutti e quattro gli aminoacidi con l'aminoacido alanina è sufficiente a ristabilire il comportamento di MICU1.

In conclusione, durante il mio periodo di dottorato ho caratterizzato una variante di splicing di MICU1, che è selettivamente espressa in tessuti eccitabili e che attiva MCU più efficientemente di MICU1. Sorprendentemente, ho osservato che MICU1.1 esercita una funzione peculiare quando legato a MICU2. Complessivamente, i nostri dati dimostrano che nei tessuti eccitabili esiste un complesso molecolare per l'ingresso di Ca^{2+} nei mitocondri con una funzione unica. Quindi, in questi tessuti, l'ingresso di Ca^{2+} nei mitocondri riveste funzioni nuove e ancora inesplorate. Ulteriori studi saranno necessari per chiarire il ruolo di MICU1.1 in diverse condizioni fisiologiche e patologiche.

Introduction

Ca^{2+} Signalling

Cell signalling is an intricate system of communication that directs basic cellular activities and coordinates cell functions. The ability of cells to sense and correctly respond to their microenvironment is the basis of development, tissue repair, and immunity, as well as normal tissue homeostasis. For this purpose, during evolution a plethora of mechanisms has evolved in order to fulfill the huge request of communication. Many of these mechanisms converge on a relative small number of messenger molecules, which are responsible to trigger an appropriate intracellular response. These molecules, called second messengers, share some particular properties: they are rapidly released in response to stimuli and they are also rapidly neutralized, allowing time and space limitation of the signal. Importantly, second messengers enable the amplification of the starting stimulus [4].

The divalent ion calcium (Ca^{2+}) is one of the most important second messengers, as once it enters the cytosol it exerts allosteric regulatory effects on many enzymes and proteins, impacting nearly every aspect of cellular life. This is corroborated by the amount of energy that cells invest to affect changes in Ca^{2+} concentration ($[Ca^{2+}]$). Indeed, while complex molecules can be chemically altered, the only mechanisms that exert control over Ca^{2+} are chelation, subcellular compartmentalization and cell extrusion. For this purpose, hundreds of cellular proteins have been adapted to bind Ca^{2+}, in some cases simply to buffer or lower Ca^{2+} levels, and in others to trigger cellular processes [5]. Hundreds of proteins chelator of Ca^{2+} share a common Ca^{2+}-binding motif, the EF-hand domain [6].

The consequence of this precise control of $[Ca^{2+}]$ is a very steep gradient of Ca^{2+} across the plasma membrane of cells: cytosolic Ca^{2+} ($[Ca^{2+}]_{cyt}$) is maintained at 10-100 nM, while the extracellular milieu generally presents a $[Ca^{2+}]$ of over 1 mM [7].

Ca^{2+}, which acts as second messenger in the cell, is retrieved from two main sources: the extracellular milieu and the internal stores. The most important Ca^{2+}

store in the cell is the endoplasmic reticulum (ER) [7], but some recent studies demonstrated that also other organelles, such as the Golgi apparatus, the endosomes and lysosomes are able to contribute to Ca^{2+} signalling [8–10].

One of the most common mechanism of intracellular Ca^{2+} release from ER is represented by inositol 1,4,5-trisphosphate (IP_3), a second messenger that is released as a consequence of a plethora of external stimuli [11]. IP_3 induces the release of Ca^{2+} from the ER, acting on its receptor, IP_3 Receptor (IP_3R). This IP_3/Ca^{2+} signalling system is a key regulator of many cellular control mechanisms[11]. Once Ca^{2+} has carried out its signalling functions, it is rapidly removed from the cytoplasm by extrusion or by compartmentalization thanks to various pumps and exchangers [7], allowing intracellular [Ca^{2+}] to return to its resting conditions. The rapid release and re-uptake of Ca^{2+} result in waves of Ca^{2+} that propagate within the cell, whose mechanisms and actions must be defined for each cell and tissue type.

Mitochondria

The general framework

Mitochondria represent unique organelles within the complex endomembrane systems that characterize any eukaryotic cell. Beyond the pivotal task of these organelles in regulating the production of ATP, a complex mitochondrial biology has emerged in the last decades. Indeed, mitochondria participate in many other aspects of cell homeostasis such as aminoacid synthesis, lipid metabolism, Ca^{2+} signalling, reactive oxygen species (ROS) production and cell death regulation [12,13]. Accordingly, it is now widely accepted that mitochondrial dysfunction is associated with several physiopathological conditions, including neurodegenerative diseases (Alzheimer's, Hungtinton's, Parkinson's diseases), motoneuron disorders (amyotrophic lateral sclerosis), ischemia-reperfusion injury, diabetes, ageing and cancer [13–17].

The understanding of the pivotal role of mitochondria as integration point of different cellular signals, and how mitochondria translate these stimuli in biological responses represent a new challenge in biomedical research.

Two structurally and functionally different membranes delimitate mitochondrial matrix: the outer membrane (OMM), permeable to ions and metabolites up to 5000 Daltons (Da), and the highly selective inner membrane (IMM), characterized by invaginations, called cristae, which enclose the mitochondria matrix. These two membranes delimitate the intermembrane space (IMS). The cristae define internal compartments formed by profound invaginations originating from narrow tubular structures, called cristae junctions [18] that limit the diffusion of molecules from the intra-cristae space towards the IMS. This space delimitates a micro-environment where the mitochondrial Electron Transport Chain (ETC) complexes are hosted and other proteins are protected from random diffusion [18].

The most important task of mitochondria is ATP production by oxidative phosphorylation. In 60s, Peter Mitchell shed light on the process by which electron transfer is coupled to ATP synthesis, proposing for the first time an indirect mechanism, the chemiosmotic theory [19,20]. Indeed, he suggested that the flow of electrons through the respiratory ETC complexes drives protons across the IMM of mitochondria, creating an electrochemical proton gradient across the membrane [21,22]. The synthesis of ATP is driven by a reverse flow of protons down the gradient through the F_1/F_o ATPase. This big protein complex uses the energy relieved by proton flow down the electrochemical gradient to carry out ATP production. This electrochemical gradient across the IMM is reflected in a huge membrane potential difference ($\Delta\Psi_m$) of -180 mV (negative inside) [21,22].

Mitochondrial Ca^{2+} signalling

An historical perspective

About sixty years ago, even before of chemiosmotic theory, pioneering studies demonstrated that energized mitochondria can rapidly and efficiently accumulate Ca^{2+} [23–25]. In the following years, the basic properties of the mitochondrial Ca^{2+} transport were clarified: the accumulation of Ca^{2+} into the mitochondrial matrix through the ion-impermeable IMM occurs via an electrogenic pathway that involves the mitochondrial Ca^{2+} uniporter (MCU). This channel

allows the rapid accumulation of Ca^{2+} in the matrix, thanks to the steep electrochemical gradient that acts as an enormous driving force attracting the divalent ion. Ca^{2+} accumulation by MCU does not proceed until electrochemical equilibrium due to the activity of two main efflux pathways, the Na^{+}/Ca^{2+} (mNCX) and H^{+}/Ca^{2+} (mHCX) exchangers [26].

In the 80s, the accurate $[Ca^{2+}]_{cyt}$ measurement obtained with fluorescent indicators demonstrated that the low affinity of MCU would not allow substantial Ca^{2+} uptake into the organelle with the $[Ca^{2+}]_{cyt}$ revealed by measurements in basal and stimulated conditions. Thus, the study of the role of mitochondria in Ca^{2+} homeostasis became marginal.

The situation completely reversed with the development of genetically encoded Ca^{2+} probe specifically targeted to mitochondria [27]. Indeed, these probes allowed to follow the mitochondrial Ca^{2+} concentration ($[Ca^{2+}]_{mt}$) changes during cell stimulation upon agonist-induced $[Ca^{2+}]_{cyt}$ increases. It was observed that the speed and the amplitude of Ca^{2+} accumulation into mitochondria greatly exceed the values that were previously predicted on the basis of MCU properties in isolated mitochondria. In addition, upon agonist stimulation, $[Ca^{2+}]_{mt}$ reaches much higher values than the levels in the cytosol [27].

The microdomain concept

The discrepancy between this prompt response and the low affinity of the Ca^{2+} transporter was reconciled by the discovery that mitochondria are strategically located in close proximity of Ca^{2+} channels responsible of cytosolic Ca^{2+} waves [28]. Therefore, mitochondria sense microdomains of high $[Ca^{2+}]_{cyt}$ that meet the low affinity of the MCU. In detail, it has been observed that mitochondria form quasi-synaptic junctions with ER membranes thus allowing the close proximity of ER-resident Ca^{2+} channels to mitochondria [28–32]. Thanks to a GFP-based Ca^{2+} probe localized on the cytosolic surface of the OMM, it was demonstrated that, upon Ca^{2+} mobilization, the $[Ca^{2+}]$ in small regions of the mitochondrial surface reaches levels 5- to 10-fold higher than in the bulk cytosol [33]. This high $[Ca^{2+}]_{cyt}$ microdomains are sufficient to ensure a rapid Ca^{2+} entry through MCU, but on the other hand, thanks to the rapid dissipation of the Ca^{2+} transient, it acts as a safety

lock that prevents mitochondrial Ca^{2+} overload and vicious cycling of Ca^{2+} through mitochondrial membranes [7].

This peculiar organization is possible thanks to an ultra-specialized structure that allows the just-apposition of mitochondria to the Ca^{2+} release sites in the ER [34]. This structure, called mitochondria associated membrane (MAM), has been observed for the first time in the 90s [35], and has been estimated as 5-20% of the total mitochondrial surface [36,30].

Pleiotropic roles of mitochondrial Ca^{2+}

Mitochondria as cytosolic Ca^{2+} buffers

Mitochondria are able to act as high capacity buffers and they can sequester large amounts of Ca^{2+} from subcellular domains. In contrast to Ca^{2+}-binding proteins, mitochondria act as fixed buffers of high capacity and sequester large amounts of Ca^{2+} from sub-cellular domains [7].

This process influences cellular Ca^{2+} signals and hence cell function [1]. Furthermore, mitochondria can regulate the activity of Ca^{2+} channels: mitochondria buffering of Ca^{2+} nearby the release sites is able to prevent the Ca^{2+}-mediated inhibition of the channels [37]; on the contrary, mitochondrial Ca^{2+} accumulation can prevent the further activation of Ca^{2+} channels, by suppressing Ca^{2+}-dependent positive feedback [38].

One of the most crucial processes, in which mitochondrial Ca^{2+} buffering is involved, is the control of Ca^{2+} gradients in defined cellular domains. This is possible thanks to a strategic cellular localization of mitochondria, as observed in the synaptic termini of neurons and in pancreatic acinar cells [39,40]. In both cases, mitochondrial Ca^{2+} buffering is sufficient to restrict Ca^{2+} waves towards the secretory pole of these cells.

Mitochondrial Ca^{2+} regulation of cell death

Cell death pathways are strongly affected by $[Ca^{2+}]_{mt}$ [12,41]. Indeed, it is well established that mitochondria undergo to Ca^{2+} overload during several

physiological stresses and pathological conditions [12,41]. This causes the rapid collapse of the membrane potential and swelling of mitochondrial membranes, with consequent loss of pyridine nucleotides and cytochrome c. This process is strictly correlated to the bioenergetics state of the cells. Indeed, conditions of mitochondrial Ca^{2+} overload, accompanied by a bioenergetics crisis and ATP depletion, are followed by cell death by necrosis [42].

Furthermore, mitochondrial Ca^{2+} overload is also an important trigger of apoptosis, as observed during ischemia-reperfusion in the heart and excitotoxicity in neurons [12]. Indeed, Ca^{2+} can directly and positively stimulate mitochondrial permeability transition pore (mPTP) opening [12]. mPTP opening plays a key role in the intrinsic pathway of apoptosis. Indeed, its opening induces cristae remodelling and subsequent release in the cytosol of mitochondrial-residing pro-apoptotic factors, such as cytochrome c [43]. These events are key steps for the induction of caspase-dependent or -independent apoptosis. Normally, physiological $[Ca^{2+}]_{mt}$ oscillations do not induce mPTP opening, but become effective if paralleled by pro-apoptotic challenges [44].

Mitochondrial Ca^{2+} regulation of cell metabolism

The ability of mitochondria to accumulate Ca^{2+} is fundamental for the regulation of several mitochondria tasks. Indeed, mitochondrial Ca^{2+} is able to modulate ATP production by oxidative phosphorylation. This regulation is possible thanks to the Ca^{2+}-dependent regulation of three key enzymes of tricarboxylic acid (TCA) cycle, pyruvate dehydrogenase, isocitrate dehydrogenase and α-ketoglutarate dehydrogenase. Indeed, it has been demonstrated that a Ca^{2+}-dependent phosphatase can directly modulate the pyruvate dehydrogenase activity, while the direct binding of Ca^{2+} to isocitrate dehydrogenase and α-ketoglutarate dehydrogenase plays an important regulatory role [45]. The reactions catalysed by these enzymes are rate limiting steps of TCA cycle. Therefore the positive modulation by Ca^{2+} of these enzymes can reflect in a substantial increase of TCA cycle activity, thus in an increased feeding of ETC by NADH and $FADH_2$.

Moreover, the regulation of the TCA dehydrogenases is not the only mechanism by which mitochondrial Ca^{2+} regulates metabolism. Indeed, in the IMM

are present two aspartate/glutamate exchangers (termed aralar1 and citrin) that are able to sense Ca^{2+} thanks to EF-hand Ca^{2+}-binding domains. As a result, mitochondrial Ca^{2+} promotes metabolite transport inside the mitochondrial matrix that, in turn, fuels the TCA cycle [46].

Altogether, mitochondrial Ca^{2+} entry ensures prompt induction of aerobic metabolism paralleled by cell stimulation and, thus, activation of ATP-consuming processes in the cytosol.

The Mitochondrial Ca^{2+} Uniporter: molecular identity and structural complexity

From the first evidence that mitochondria are able to uptake Ca^{2+} in the 60s, we had to wait 50 years before the discovery of the molecular identity of the mitochondrial Ca^{2+} uniporter [47,48]. This was made possible by a seminal proteomic study that allowed to compile an inventory of gene products with mitochondrial localization, as proven by mass spectrometry and imaging studies (MitoCarta) [49]. In order to find candidates that fulfill the requirements to be the mitochondrial calcium uniporter, the MitoCarta database was examined with unbiased search constraints, crossing several criteria: (i) ubiquitous expression in mammalian tissues; (ii) a sequence compatible with that of a channel (i.e. with at least 2 putative transmembrane regions); (iii) presence in those organisms in which mitochondrial Ca^{2+} transport with the properties of MCU was reported and iv) absence in *Saccaromices cerevisiae* that shows no ruthenium red-sensitive mitochondrial Ca^{2+} uptake. Through this bioinformatic analysis, in 2011 our and Mootha's laboratories identified a protein, encoded by the CCDC109A gene, which satisfies all the requirements to be the *bona fide* mitochondrial calcium uniporter [47,48].

The pore forming subunits

MCU: the mitochondrial Ca^{2+} channel

CCDC109A was demonstrated to be the long sought mitochondrial calcium uniporter (MCU). Indeed, its overexpression is sufficient to strongly induce mitochondrial Ca^{2+} uptake upon cell stimulation and coherently its knockdown drastically abolishes mitochondrial Ca^{2+} uptake [47,48]. In addition, some insight into channel function were obtained, as negatively charged residues of the amino acid sequence separating the two transmembrane domains of the MCU were shown to be required for channel activity [47] and, furthermore, ruthenium red-binding sites were mapped in the same region [48].

Importantly, De Stefani and colleagues demonstrated that CCDC109A is necessary and sufficient to mediate mitochondrial Ca^{2+} uptake. Indeed, purified CCDC190A formed a high selective Ca^{2+} channel in planar lipid bilayer experiments. Moreover, the electrophysiological properties of the newly identified protein, matched those previously described in isolated mitochondria, and the Ca^{2+} current could be inhibited by ruthenium red and gadolinium, two well-known inhibitors of the MCU [47]. All together, the genomic, physiological, biochemical and pharmacological data firmly established CCDC109A as the pore-forming subunit of the mitochondrial Ca^{2+} uniporter and, from that time on, the name of CCDC109A was changed in Mitochondrial Calcium Uniporter, MCU.

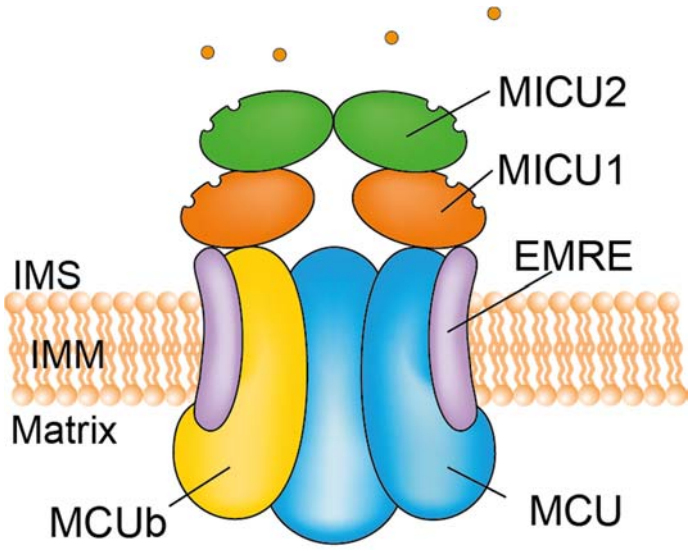

Figure 1 - Schematic representation of the mitochondrial calcium uniporter complex

In line with the pleiotropic roles of mitochondrial Ca^{2+} signalling, these works demonstrated that MCU exists in a large protein complex (~480 kD) [48], suggesting that many other proteins contribute to channel formation. Indeed, in the following years, several other components of MCU complex were identified (Figure 1).

MCUb: the dominant-negative regulator of MCU

Homology search with MCU protein sequence of the MitoCarta database identified a related gene (CCDC109B), named MCUb, located on *Mus musculus* chromosome 3 (chromosome 4 for the *Homo sapiens* orthologue) [50]. MCUb is present in vertebrates but absent in other organisms in which MCU is present (e.g., plants, kinetoplastids, Nematoda, and Arthropoda) and shares 50% of similarity with MCU. MCUb is characterized by two transmembrane domains similar in sequence to MCU, although some conserved differences in the primary sequence are present that prevent MCUb from forming a Ca^{2+}-permeable channel, thus acting as a dominant-negative subunit [50]. Thus, the incorporation of this protein in the MCU complex is sufficient to prevent mitochondrial Ca^{2+} uptake as shown in experiments in cell culture and in planar lipid bilayer. Interestingly, MCUb/MCU expression ratio varies greatly between tissues, suggesting that it might contribute to the spatiotemporal control of mitochondrial calcium uptake [50].

EMRE: the essential MCU regulator

The last player discovered as fundamental component of MCU complex is EMRE ("essential MCU regulator", previously known as C22orf32). It was identified through SILAC-based quantitative mass spectrometry of affinity-purified MCU complexes [51]. EMRE is a 10 kDa protein, present only in metazoan. It is composed of a single transmembrane domain that spans the IMM and possesses a highly conserved C-terminus rich in aspartate residues. Silencing of EMRE completely abrogates MCU activity in cells, even though MCU expression and oligomerization is preserved. This data is in contrast with experiments performed in our laboratory that show that MCU is sufficient to give rise to Ca^{2+} currents in planar lipid bilayer [47]. Interestingly, it was proposed that EMRE is required for

the interaction of MCU with MICU1 and MICU2, fundamental regulators of the channel (see below), since silencing of EMRE prevents MICU1 and MICU2 to coimmunoprecipitate with MCU [51]. However, this data is in contrast with bilayer experiments that showed that MICU1 is sufficient to induce MCU channel activity [52].

It is important to notice that MCU and MICU1 are conserved in plants, fungi and protozoa where EMRE is not present. Coherently, the same authors demonstrate that, when expressed in yeast, *Dictyostelium discoideum* MCU homologue conducts Ca^{2+} in the absence of an EMRE homologue while, in these systems, human MCU requires the presence of EMRE to act as a functional channel [53]. Interestingly, it has been recently shown, by patch-clamp experiments, that MCU responds to mitochondrial matrix [Ca^{2+}] through EMRE that thus acts as sensor of matrix [Ca^{2+}]. This function requires conserved acidic residues in the matrix-localized carboxyl tail of EMRE [54].

Given these contradictory data, further experiments are required to clarify the role of EMRE.

The regulatory subunits

One of the key features of mitochondrial Ca^{2+} uptake is the sigmoidal response to extra-mitochondrial [Ca^{2+}] (Figure 2). In resting conditions,

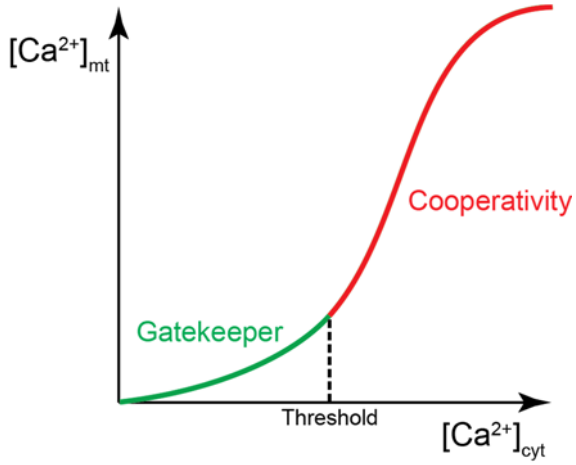

Figure 2 – Schematic diagram of cooperative activation of mitochondrial Ca^{2+} uptake

Mitochondrial Ca^{2+} concentration ($[Ca^{2+}]_{mt}$) dependence on cytosolic Ca^{2+} levels ($[Ca^{2+}]_{cyt}$). Ca^{2+} accumulates into mitochondria with a very low rate at low $[Ca^{2+}]_{cyt}$, thanks to the activity of the gatekeeper of the channel. When the $[Ca^{2+}]$ in the proximity of mitochondria reaches a threshold value (>10 mM), MCU activity undergoes cooperative activation that dramatically increases mitochondrial Ca^{2+} uptake. In green is represented the phase in which the gatekeeper is active, in red the cooperative activation of MCU.

mitochondrial Ca^{2+} uptake is inhibited despite the huge driving force for matrix cation accumulation. This mechanism prevents vicious cycling for Ca^{2+} accumulation, conspicuous energy drain, morphological alterations and release of apoptotic cofactors [1]. On the other hand, $[Ca^{2+}]_{mt}$ rapidly rises when the $[Ca^{2+}]_{cyt}$ in the proximity of mitochondria reaches a threshold value (>10 μM) [36,55,56]. Given the topology of the MCU, a small loop facing the intermembrane space and the N- and C-termini residing in the matrix [48,57], it seemed unlikely that MCU itself could be responsible for this fundamental property. Thus, the existence of a highly sophisticated gatekeeping mechanisms was predicted, including both negative modulators acting at low $[Ca^{2+}]$ and activators able to induce Ca^{2+} currents during cell stimulation (Figure 3).

MICU1: mitochondrial calcium uptake 1

Even before the molecular identification of MCU, Mootha's group discovered, through a bioinformatic search of the MitoCarta database followed by RNAi screening of the candidates, a mitochondrial protein whose expression clearly affects mitochondrial Ca^{2+} uptake. MICU1 (mitochondrial calcium uptake 1, formerly known as EFHA3) is evolutionarily conserved in vertebrates and in

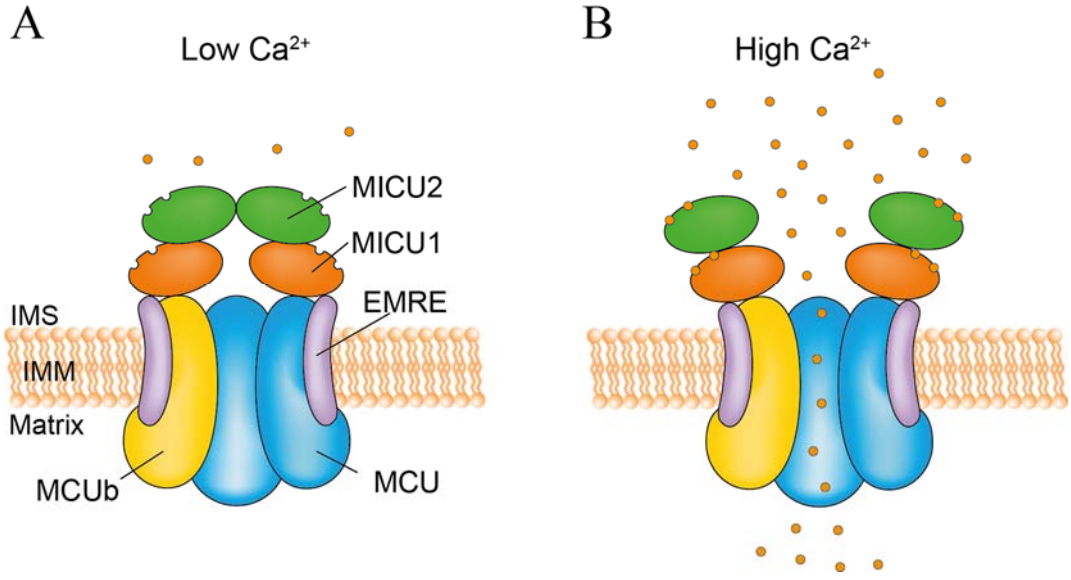

Figure 3 - Schematic representation of the mechanism controlling MCU activity by the MICU1-MICU2 heterodimer.

A) In resting conditions, MICU1-MICU2 heterodimer acts as gatekeeper of the MCU, thanks to the dominant inhibitory effect of MICU2;

B) Upon cell stimulation, increase in Ca^{2+} concentration triggers a conformational change that induces the loss of MICU2-dependent inhibition and activates MICU1-mediated cooperative activation of the MCU.

kinetoplastids but absent in yeast. Although some report are in contrast [58], it is widely accepted that MICU1 localizes in the IMS [59,60].

Importantly, MICU1 possesses two EF-hands domains and, accordingly, it was initially shown to be necessary for mitochondrial Ca^{2+} uptake since its silencing was shown to completely blunt mitochondrial Ca^{2+} uptake [61,62]. However, Madesh's group demonstrated that mitochondria lacking MICU1 are constitutively loaded with Ca^{2+} [63]. It was thus hypothesized that MICU1 is fundamental to prevent Ca^{2+} uptake at low $[Ca^{2+}]_{cyt}$. Complexity was added by the study performed by Hajnóczky's laboratory [59]. The gatekeeper role of MICU1 at low $[Ca^{2+}]_{cyt}$ was confirmed, but it was also shown that, in the absence of MICU1, the cooperativity of mitochondrial Ca^{2+} uptake is lost, suggesting that MICU1 plays a dual function depending on $[Ca^{2+}]_{cyt}$. Coherently, studies in human patients in which loss-of-function mutations in MICU1 gene cause a disease phenotype characterized by proximal myopathy, learning difficulties and a progressive extrapyramidal movement disorder, showed an increased mitochondrial Ca^{2+} load, both at basal $[Ca^{2+}]_{cyt}$ and after spontaneous, low-frequency, transient increases of cytoplasmic Ca^{2+} levels [64].

The genuine MCU gatekeeper: MICU2

All the studies discussed above preceded the identification of MICU1 paralogs [65], MICU2 (mitochondrial calcium uptake 2, formerly known as EFHA1) and MICU3 (mitochondrial calcium uptake 3, formerly known as EFHA2), also characterized by the presence of two highly conserved EF-hand domains. MICU2 shares a similar tissue distribution with MICU1 and the IMS localization [60] and, importantly, MICU2 forms an obligate heterodimer with MICU1 through a dysulfide bond [52] (Figure 1). MICU2 inhibits the channel activity of purified MCU in planar lipid bilayer and reduces channel opening at resting $[Ca^{2+}]_{cyt}$ in intact HeLa cells, thus ensuring minimal Ca^{2+} accumulation. Importantly, MICU2 protein stability depends on the presence of MICU1 [52,65,66], suggesting that the loss of the gatekeeping property of MCU in MICU1 silencing conditions [59,63] is due to the concomitant reduction of MICU2 expression. In addition, as $[Ca^{2+}]_{cyt}$ increases upon cell stimulation, Ca^{2+}-dependent

conformational changes of the MICU1-MICU2 dimer release MICU2-dependent inhibition (Figure 3A). At the same time, MICU1 stimulates MCU activity, acting as the cooperative activator of the channel (Figure 3B). Accordingly, a MICU2 mutant unable to bind Ca^{2+} acts as gatekeeper also in conditions of high $[Ca^{2+}]_{cyt}$, while, in the same conditions, the same MICU1 mutant loses the capability to cooperatively activate the channel [52,59].

Other regulators of MCU

MCU complex is emerging as one of the most sophisticated ion channel described so far. Indeed, beyond the subunits discussed above, some other proteins were indicated as MCU regulators, but they are not yet completely characterized and their roles are still controversial.

As for MICU3, its specific function is still unknown. Moreover, its restricted expression in the CNS and skeletal muscle [65] suggests a tissue-specific mitochondrial Ca^{2+} uptake modulation that needs to be thoroughly investigated in the near future.

Another protein whose role is not yet definitive is the Mitochondrial Ca^{2+} Uniporter Regulator 1 (MCUR1) (formerly known as coiled-coil domain-containing 90A or CCDC90A) [67]. Notably, MCUR1 has an orthologous in yeast which lacks uniporter activity, thus pointing to an indirect function of MCUR1 in regulating mitochondrial Ca^{2+} uptake. Indeed, in yeast and human cells, the silencing of MCUR1 produces a specific cytochrome c oxidase (COX) assembly defect, decreased mitochondrial membrane potential ($\Delta\Psi_m$) that causes reduced mitochondrial Ca^{2+} uptake [68], thus arguing for an indirect regulation of mitochondrial Ca^{2+} homeostasis. However, measurements of MCU-mediated Ca^{2+} currents by patch-clamp electrophysiology of mitoplasts showed that stable knockdown of MCUR1 diminishes MCU Ca^{2+} currents without affecting $\Delta\Psi_m$ [69]. Thus, further experiments are necessary to clarify the role of MCUR1.

Tissue-specific regulatory properties of MCU

For many decades, it was unclear whether MCU-dependent Ca^{2+} uptake was comparable among different tissues and whether $[Ca^{2+}]_{mt}$ could be modulated to respond to the different physiological needs of these tissues.

At the beginning of the 70s, the characterization of mitochondrial Ca^{2+} uptake in isolated mitochondria highlighted significant differences in the activity of MCU among different tissues [70]. In the following years, the complete definition of this phenomenon, through biochemical studies and the use of optical approach, did not allow the reliable control of the experimental conditions ($\Delta\Psi$, matrix pH and Ca^{2+} gradient across the IMM). As a consequence, substantial discrepancies in the measurements of mitochondrial Ca^{2+} uptake in the same tissue were reported [26,71].

These limitations were bypassed by the outstanding work of Clapham and colleagues: they, for the first time, were able to record by patch-clamp the MCU current (I_{MCU}) from IMM-derived mitoplasts, thus allowing the fine characterization of MCU electrophysiological properties [72]. In the following years, Kirichok and colleagues used the same approach to perform direct patch-clamp measurements of I_{MCU} in mitoplast derived from different tissues [3]. Their results led to the finding that I_{MCU} varies greatly among tissues. Strikingly, they showed that heart I_{MCU} is 30 times smaller than skeletal muscle I_{MCU} although in heart 37% of the volume is occupied by mitochondria, while in skeletal muscle only the 5% [3]. Nonetheless, skeletal muscle and heart mitochondrial Ca^{2+} currents share the same biophysical properties.

Despite the number of discoveries on the MCU complex components, the molecular basis of these differences are still poor understood. One of the most obvious explanation of the tissue-specificity of mitochondrial Ca^{2+} uptake is the differential expression of the MCU complex components. Indeed, several groups demonstrated that the expression of the members of the complex varies in different tissues and physiological conditions [47,48,50,61,65,66]. One of the most sticking example is MCUb. Indeed, MCUb/MCU ratio correlates with the Ca^{2+} measurement by patch-clamp [50]. Indeed, tissues characterized by low

mitochondrial Ca^{2+} transients, such as the heart, show a higher MCUb/MCU ratio, compared for example to skeletal muscle. Another MCU regulator that might contribute to these tissue-specific differences, that shows a peculiar tissue distribution is MICU3, whose expression is restricted to the central nervous system and, lower levels are found also in skeletal muscle [65].

It has been shown that one additional level of regulation of the rate of mitochondrial Ca^{2+} uptake in different tissues is represented by post-translational modifications of the components of the MCU complex. Indeed, Anderson and colleagues recently reported that MCU is phosphorylated and thus modulated by mitochondrial Ca^{2+}/calmodulin-dependent protein kinase II (CaMKII), and this regulation is a crucial mechanism that controls stress response in heart [73]. Indeed, CaMKII is activated during ischemia-reperfusion, myocardial infarction and neurohumoral injury, suggesting that phosphorylation of MCU, and thus the modulation of $[Ca^{2+}]_{mt}$, can couple disease stress to mitochondrial injury [73]. In support to this, the analysis of the crystal structure of the MCU N-terminal domain (NTD) suggests that the residue S92 is a CaMKII phosphorylation site [74]. Nonetheless, Kirichock's group claimed that the electrophysiological characterization of CaMKII modulation of MCU displayed properties that did not mimic those of the MCU [75]. Thus, further experiments are necessary to clarify the role of this regulatory mechanism on mitochondrial Ca^{2+} uptake.

Recent data showed that also post-transcriptional mechanisms control the activity of MCU in pathological conditions. Indeed, it has been shown that specific miRNAs control the expression of MCU. In detail, it has been demonstrated that miR-25 affects mitochondrial Ca^{2+} uptake acting on the translation of MCU mRNA [76]. Through this mechanism, miR-25 reduces mitochondrial Ca^{2+} uptake and confers resistance to Ca^{2+}-dependent apoptotic challenges. Interestingly, in human colon cancers and cancer-derived cells, miR-25 is overexpressed and MCU accordingly silenced. This result is strengthened by a recent study demonstrating that miR-25 can protect cardiomyocytes against oxidative stress through the modulation of MCU expression [77].

Overall, the study of the mechanisms that regulate mitochondrial Ca^{2+} uptake in different tissues and physiopathological conditions are just beginning to

emerge. Further efforts will be necessary to define the MCU complex components regulatory mechanisms.

The physiological role of mitochondrial Ca^{2+} uptake

In parallel with the elucidation of the molecular identity and function of the components of the MCU complex, a number of studies have been performed to better elucidate the function of Ca^{2+} transport in physiological and pathological conditions. In just five years we have assisted to an explosion of information regarding mitochondrial Ca^{2+} flux [2], and it shown no sign of slowing any time soon.

The most unexpected result was the characterization of the MCU full knockout mice ($MCU^{-/-}$), that was created thanks to the gene trap technique [78]. Surprisingly, the $MCU^{-/-}$ mice are viable and fertile although the mitochondria of these animals are not able to accumulate Ca^{2+}. Given the central role of mitochondrial Ca^{2+} in metabolic regulation, these mice were expected to die sometime during embryogenesis. Nonetheless, these mice are smaller than their wild type littermates and they only have modest defects in skeletal muscle strength. From a metabolic point of view, $MCU^{-/-}$ mice display reduced pyruvate dehydrogenase activity, without other major defects. Furthermore, the cells and tissues from these animals do not exhibit any marked protection from cell death, also followed by ischemia-reperfusion injury, although the mPTP opening is prevented [78]. These results opened a heated discussion among the scientists of the field, especially because the $MCU^{-/-}$ mice are viable only in a mixed genetic background, while the absence of mitochondrial Ca^{2+} uptake appears to be embryonically lethal in a pure background. Furthermore, compensatory mechanisms during embryonic development can not be excluded.

This latter mechanism is supported by the study of the role of mitochondrial Ca^{2+} uptake in skeletal muscle homeostasis performed in our laboratory [79]. Indeed, it has been demonstrated that overexpressing and silencing MCU specifically in skeletal muscle few days after birth and in adulthood using Adenoassociated viral vectors (AAVs) induces dramatic changes in muscle

trophism. In detail, MCU overexpression triggers skeletal muscle hypertrophy, while coherently MCU silencing causes muscle atrophy. Importantly, MCU overexpression protects muscles from the loss of muscle mass during denervation. As for the mechanism, known hypertrophy pathways, like IGF1-Akt/PKB and PGC-1α4, are responsible for the regulation of muscle size by MCU. In addition, RNA microarray analyses demonstrated that MCU modulation controls global gene expression, thus identifying a Ca^{2+}-dependent mitochondria-to-nucleus route that links mitochondrial function to the control of muscle mass [79,80].

Furthermore, the idea that in skeletal muscle mitochondrial Ca^{2+} uptake is fundamental for tissue homeostasis was strongly supported by the discovery of human patients with loss-of-function MICU1 mutations that trigger a neuronal and muscle pathological phenotype [64]. Altogether, these findings demonstrate that mitochondrial Ca^{2+} signalling in skeletal muscle plays an important role in muscle homeostasis.

Aim

Mitochondria are crucial players in cell physiology, since they are the integration centre of several processes, ranging from ATP production to regulation of cell death. In our laboratory, we are focused on the study of the role of mitochondrial Ca^{2+} in cell homeostasis.

The discovery of the mitochondrial Ca^{2+} uptake pore forming subunits and its regulatory subunits opened a new era for the study of the roles of mitochondrial Ca^{2+} in cell physiology but much is still controversial or unclear. One still unexplored paradigm of mitochondrial Ca^{2+} uptake is tissue-specificity. What is still obscure is whether variations of MCU activity are due to tissue-specific regulation of the MCU or to different tissue-specific expression of the MCU channel. Although several regulatory mechanisms emerged in the last years, many other efforts must be made to deepen the specific regulatory properties of MCU in the different tissues and physiopathological conditions.

The focus of my PhD research was to investigate new tissue-specific regulatory processes that modulate mitochondrial Ca^{2+} uptake. In this regard, we identified and characterized an alternative splice variant of MICU1, MICU1.1. I took advantage from the long-standing experience of our group in the analysis of cellular Ca^{2+} signals in order to investigate the regulation of mitochondrial Ca^{2+} homeostasis mediated by MICU1.1. My data demonstrate that alternative splicing mechanisms play a prominent role in regulating mitochondrial Ca^{2+} uptake in excitable tissues. Further studies are necessary in order to clarify the physiological and pathological relevance of this new regulatory process.

Results

Identification of an alternative splice variant of MICU1

We identified an alternative splice variant of MICU1, hereafter named MICU1.1, during a PCR experiment to clone the murine MICU1 from a skeletal

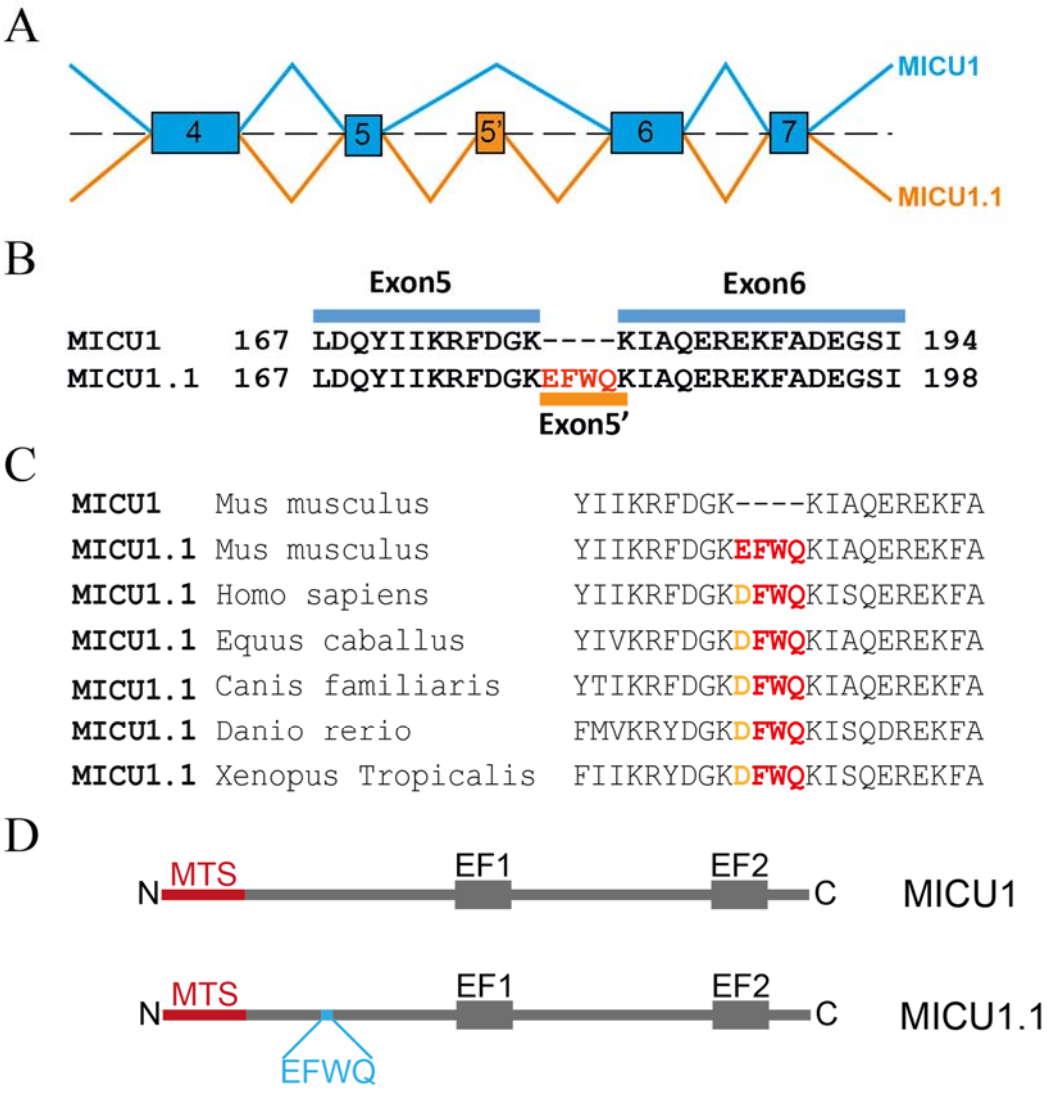

Figure 4– Identification of the alternative splice variant of MICU1, MICU1.1

A) Partial schematic of the MICU1 genomic locus. In-frame inclusion of exon 5' produces MICU1.1;

B) Exon 5' is a micro-exon that encodes for four amino acids;

C) Sequence alignment of conventional MICU1 and MICU1.1 of 7 different vertebrate species. Conservative differences are marked in orange, sequence identity is marked in red;

D) Domain structure of MICU1 and MICU1.1. N and C, N- and C-termini, respectively; MTS, mitochondrial targeting signal; EF1 and EF2, two EF-hand domains; EFWQ indicates the position of the extra-exon in MICU1.1 primary structure.

muscle cDNA library. MICU1.1 sequence is deposited in the NCBI database with accession number NM_001291443.

This alternative splice variant is created by the addition of an extra-exon (exon 5') between exon 5 and exon 6 (Figure 4A) that encodes for four amino acids (EFWQ) (Figure 4B). Intriguingly, MICU1.1 is present also in humans and is highly conserved in vertebrates (Figure 4C), suggesting that this alternative splicing event may serve a physiological function. Invertebrates do not seem to express this variant of MICU1, at least from a screening of the NCBI database. The extra-exon of MICU1.1 is located in a region with unknown function, far from the two EF-hand domains of MICU1 (Figure 4D). Interestingly, the extra-exon is localized in a domain which was not resolved in the crystal structure of MICU1 [81], suggesting that this region of the protein might be highly flexible and probably involved in protein-protein interactions.

MICU1.1 expression is restricted to brain and skeletal muscle

Since MICU1.1 is highly conserved in vertebrates, we investigated whether it might contribute to tissue-specific regulatory properties of the MCU complex. To address this question, we first measured MICU1.1 mRNA expression levels in different tissues by Real-Time PCR. The results obtained show that, unlike MICU1 that is ubiquitously expressed among tissues (Figure 5A and [47,65]), MICU1.1 presents a peculiar expression. Indeed, it is expressed specifically in skeletal muscle and, at lower levels, brain (Figure 5B). Intriguingly, in all the other tissues analysed its expression is undetectable (Figure 5B). It is interesting to notice that MICU1 and MICU1.1 are co-expressed in brain with a 1:1 MICU1/MICU1.1 ratio while, in skeletal muscle, MICU1.1 is the predominant form with a 1:8 MICU1/MICU1.1 ratio (Figure 5C), suggesting that a muscle-specific program controls mitochondrial Ca^{2+} uptake.

To further verify the tissue expression specificity of MICU1.1, we performed a conventional PCR using primers spanning exon 5' in order to discriminate the two isoforms by PCR products length. We thus separated the PCR

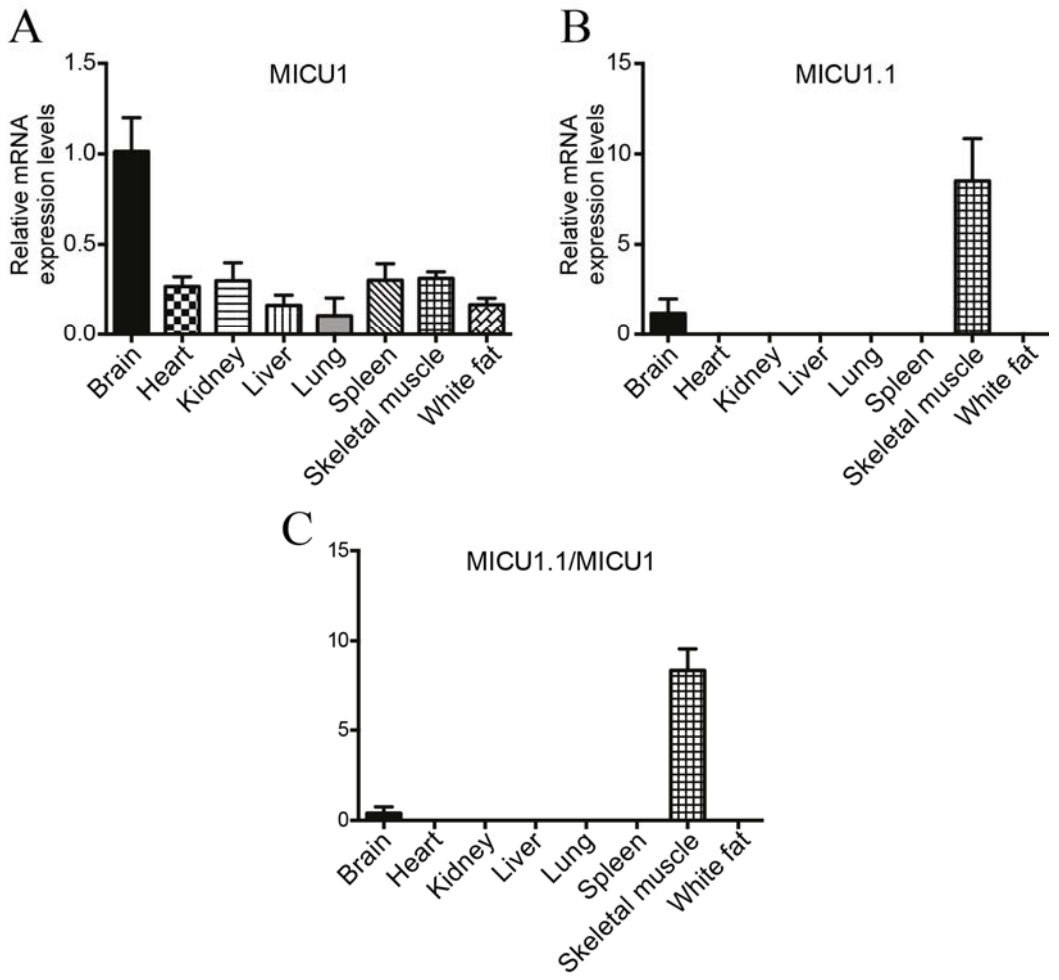

Figure 5 – MICU1.1 expression in mouse tissues

A) MICU1 relative expression levels in mouse tissues measured by Real-time PCR, normalized for Thioredoxin 1 (TNX1). Expression levels are normalized to brain, and presented as mean ± SD. n=4;

B) MICU1.1 relative expression levels in mouse tissues measured by Real-time PCR, normalized for Thioredoxin 1 (TNX1). Expression levels are normalized to brain, and presented as mean ± SD. n=4;

C) MICU1.1/MICU1 expression ratio among different mouse tissues (2^-ΔC_t MICU1.1/ 2^-ΔC_t MICU1 ratio).

products in an acrylamide gel that allows to discriminate nucleic acid fragments that differ only for few nucleotides (Figure 6A). This experiment confirms the results that we obtained by Real-Time PCR and highlights the abundance of MICU1.1 in skeletal muscle (Figure 6A).

With the same methodology, we also analysed the expression of MICU1.1 in C2C12 myoblasts and myotubes (Figure 6B). Interestingly, upon myotubes differentiation, MICU1.1 expression arises, suggesting that the control of MICU1.1 expression could be developmentally regulated (Figure 6B).

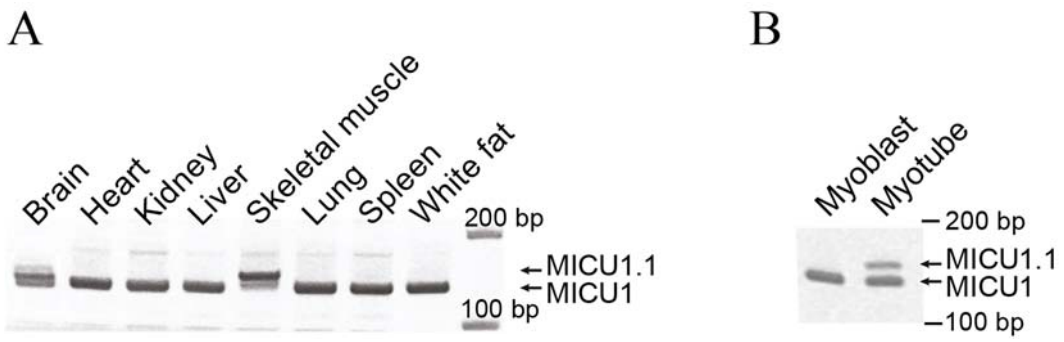

Figure 6 – MICU1.1 expression in different mouse tissues and C2C12 cells

A) Representative acrylamide gel of PCR products using primers spanning MICU1 extra-exon of cDNA of different mouse tissues. MICU1.1 produces a band of 152 bp; MICU1 of 140 bp;

B) Representative acrylamide gel of PCR products using primers spanning MICU1 extra-exon of cDNA derived by C2C12 myoblast cells and C2C12 myotubes 7 days after differentiation. MICU1.1 produces a band of 152 bp; MICU1 of 140 bp.

MICU1.1 subcellular localization and biochemical characterization

We then decided to evaluate whether MICU1.1 localizes to mitochondria as MICU1. In order to study this aspect, we performed an immunofluorescence experiment in HeLa cells transfected for 48 hours either with MICU1 or MICU1.1 tagged with a HA-tag (MICU1-HA and MICU1.1-HA, respectively). We detected the exogenous proteins thanks to the HA-tag and we used mitochondrially targeted red fluorescence protein (mtRFP) to identify mitochondria. We found that MICU1.1 specifically co-localizes with mtRFP, as well as MICU1 (Figure 7). This was an expected result since MICU1.1 mitochondrial targeting sequence is identical to that of MICU1 (Figure 7).

We then decided to characterize MICU1.1 from a biochemical point of view, to verify whether this splice variant is able to interact with the other MCU complex components as MICU1.

First, we evaluated the interaction of MICU1.1 with the pore forming subunit MCU (Figure 8A). In order to do this, we transfected HeLa cells with Flag-tagged MCU together with either HA-tagged MICU1 or HA-tagged MICU1.1. We immunoprecipitated MCU-Flag with α-Flag antibodies and we immuno-blotted using α-HA specific antibodies, in order to detect MICU1 and MICU1.1. The

results show that MICU1.1 is able to interact with MCU as well as MICU1 (Figure 8A), since the α-Flag antibody immunoprecipitated both MICU1 and MICU1.1.

We conducted a similar experiment to evaluate the ability of MICU1.1 to interact with MICU2 (Figure 8B). We first performed a co-immunoprecipitation experiment by overexpressing Flag-tagged MICU2 in HeLa cells together with HA-tagged MICU1 and MICU1.1. We immunoprecipitated MICU2-Flag with α-Flag antibodies and we analysed its interaction with MICU1 and MICU1.1 by immunoblotting with α-HA antibodies. We did not observe any difference between MICU1 and MICU1.1 in the capability to interact with MICU2 (Figure 8B).

It has been shown that MICU1 can form homo- and heterodimers with MICU2 through dysulfide bonds [52]. This occurs between the cysteine in position 465 of MICU1 and the cysteine 410 of MICU2, since mutation of these residues

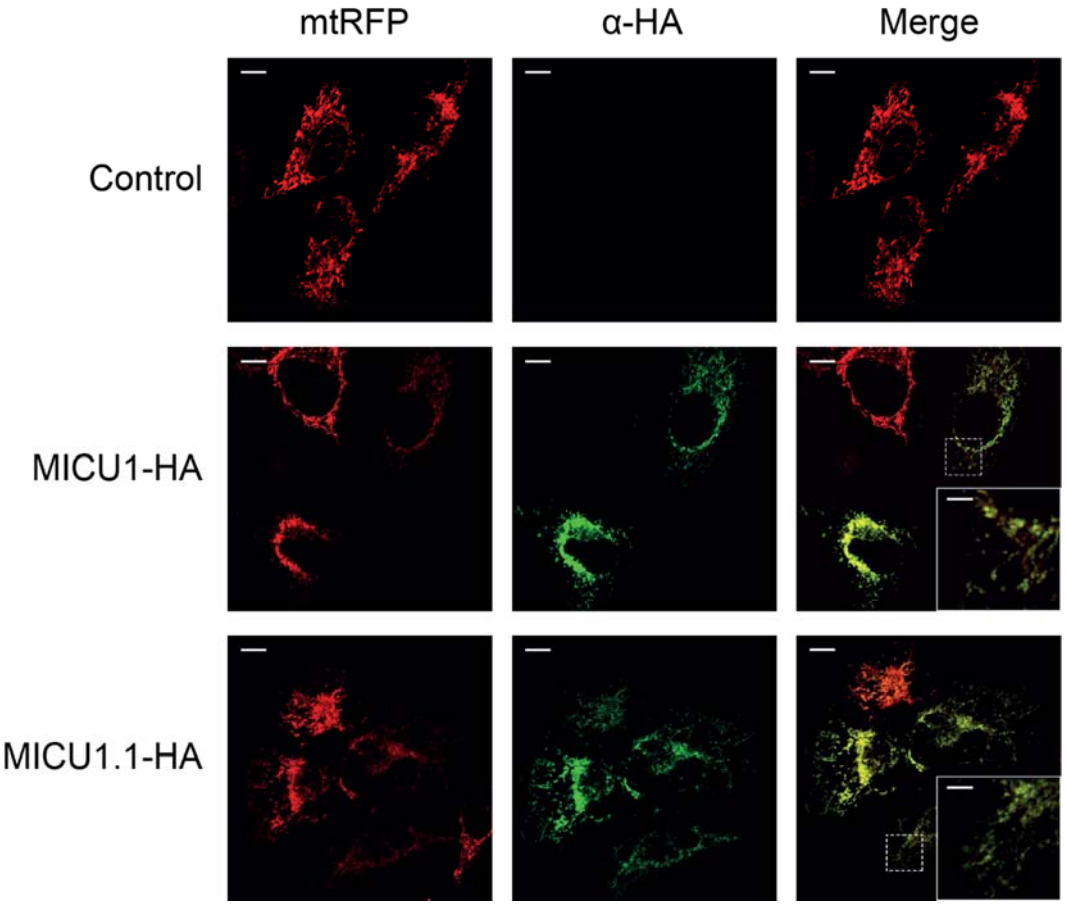

Figure 7- MICU1.1 localizes to mitochondria.

Immunolocalization of MICU1 and MICU1.1. HeLa cells were transfected with mtRFP together with either pcDNA3.1, MICU1-HA or MICU1.1-HA. After 48 h, cells were fixed and immunocytochemistry was performed with α-HA antibody followed by incubation with Alexa488-secondary antibodies as described in the Materials and methods section. Confocal images were taken (scale bar: 10 μm) and a region is expanded to appreciate the mitochondrial localization (scale bar: 3 μm).

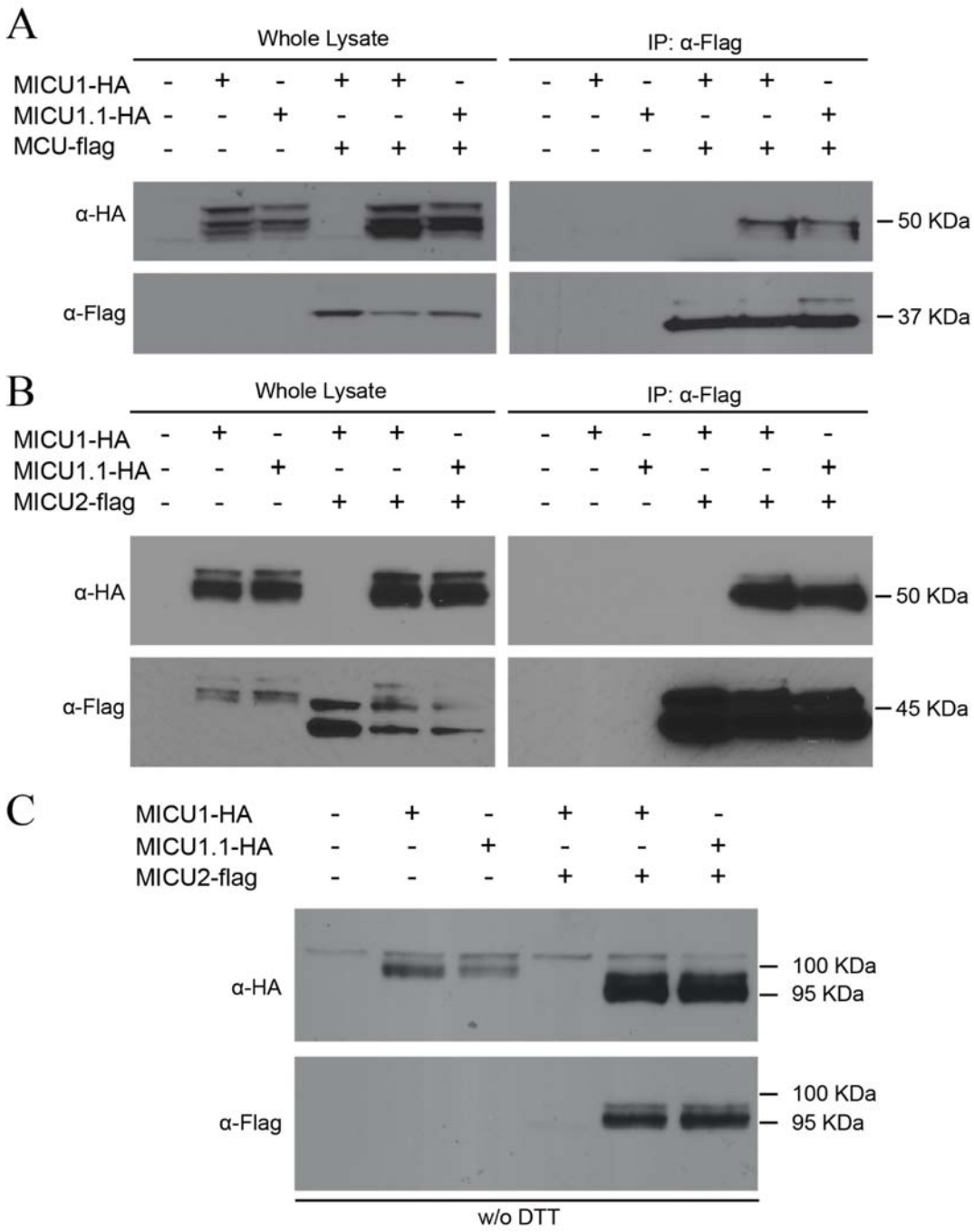

Figure 8 – Biochemical characterization of MICU1.1

A) Co-immunoprecipitation experiments. HeLa cells were transfected with the indicated constructs. Flag-tagged MCU was immunoprecipitated from whole-cell lysate with a specific α-Flag agarose-conjugated antibody. The precipitated proteins were immunoblotted with α-Flag and α-HA antibodies;

B) Co-immunoprecipitation experiments. HeLa cells were transfected with the indicated constructs. Flag-tagged MICU2 was immunoprecipitated from whole-cell lysate with a specific α-Flag agarose-conjugated antibody. The precipitated proteins were immunoblotted with α-Flag and α-HA antibodies;

C) Homo- or heterodimer formation. HeLa cells were harvested after 48 hours of transfection with the indicated constructs and total proteins were extracted and subjected to western blotting analysis with α-Flag and α-HA antibodies. SDS-PAGE was performed in the absence of DTT.

prevents the formation of the disulphide bond [52]. We thus tested the ability of MICU1.1 to homo- and heterodimerize with MICU2 by performing a SDS-PAGE in non-reducing conditions. The expected molecular weight of the homodimer is 100 kDa, being MICU1 a 50 kDa protein, while a 95 kDa band is expected for the heterodimeric form, being MICU2 a 45 kDa protein. Figure 8C shows that when MICU1.1 is overexpressed alone is able to homodimerize and, when co-expressed with MICU2, the prevalent form is the heterodimer, as observed also for MICU1[52].

In previous studies, it was demonstrated that MCU is present in high molecular weight complexes using blue native polyacrylamide gel electrophoresis (BN-PAGE) and western blot (WB) analysis [48,65]. To verify that MICU1.1 does not alter the composition and the stoichiometry of the MCU complex, we performed a similar experiment to assess the molecular weight of the MCU complex containing MICU1 and MICU1.1. For this purpose, we purified mitochondria from mouse skeletal muscle, where MICU1.1 is the prevalent form, and from mouse liver, where MICU1 is the only isoform expressed. Samples were prepared through tissue homogenization and subsequent differential centrifugations to isolate the tissue fraction enriched of mitochondria. The mitochondria fractions were then treated with a non-ionic surfactant (n-Dodecyl β-D-maltoside, DDM) to extract the mitochondrial proteins and preserving their macro-molecular complexes. The samples were then loaded in a BN-PAGE and protein complexes were separated by electrophoresis. The gel was blotted on a PVDF membrane and incubated with an α-MICU1 specific antibody, that can recognize both MICU1 and MICU1.1. Figure 9A shows that the MCU complex present in skeletal muscle mitochondria, containing prevalently MICU1.1, does not differ from the liver complex, containing MICU1. To further confirm that MICU1.1 forms the same super-complexes as MICU1, we performed BN-PAGE of affinity-purified recombinant MICU1.1-MICU2 heterodimers. Since MICU1-MICU2 heterodimer formation relays on a disulphide bond, we could not produce functional heterodimers in *Escherichia coli*, since this system can not ensure the eukaryotic post-translational modifications. Thus, we decided to express MICU1 together with MICU2 in eukaryotic cells. For this reason, we used the baculovirus/insect cells system that allows to efficiently

produce recombinant proteins with the appropriated post-translational modifications of eukaryotic cells. Thus, MICU1-MICU2 and MICU1.1-MICU2 heterodimers were expressed in insect cells and the heterodimers were affinity-purified thanks to a 6xHis tag fused to the recombinant proteins. After affinity-purification, these proteins were loaded in a BN-PAGE, separated according to the molecular weights and immunoblotted using an α-MICU2 specific antibody. We observed three different protein complexes that are compatible with the dimeric, tetrameric and hexameric forms of MICU1-MICU2 complex (Figure 9B), on the basis of the predicted molecular weight of MICU1-MICU2 heterodimer (95 kDa).

Together, these results clearly show that MICU1.1 is indistinguishable from MICU1 in the capability to interact with the other components of the MCU complex and to form high molecular weight complexes.

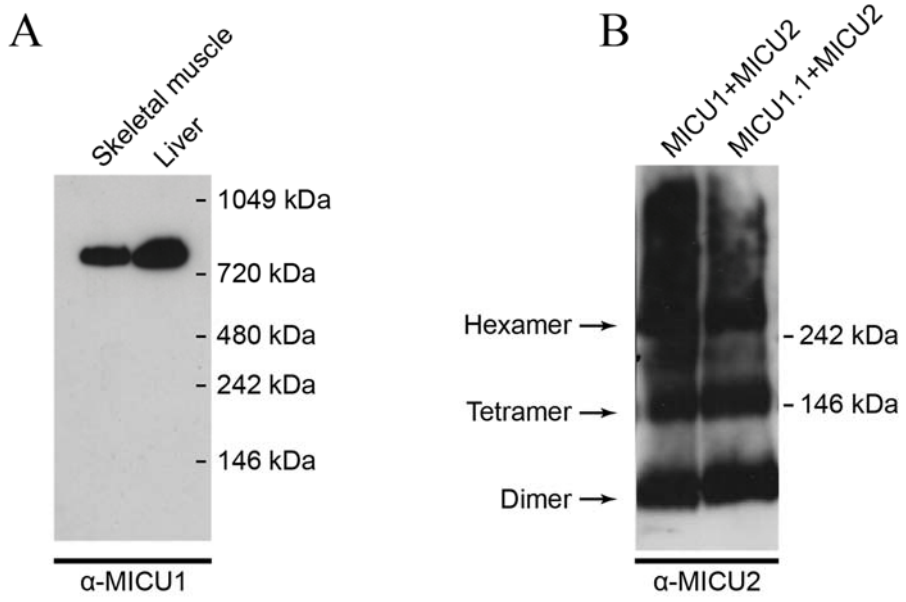

Figure 9 – MICU1 and MICU1.1 supercomplexes characterization

A) BN-PAGE of mitochondrial enriched fraction derived from mouse skeletal muscle and liver. The gel were immunoblotted with α-MICU1 antibody to assess the molecular weight of the MCU complex containing MICU1 and MICU1.1. Skeletal muscle prevalently expresses MICU1.1, while liver only expresses MICU1;

B) BN-PAGE of MICU1-MICU2 and MICU1.1-MICU2 heterodimers purified through affinity-chromatography from insect cell line upon baculovirus infection. The separated protein complexes were immunoblotted with α-MICU2 antibody. Based on predicted molecular weights, the possibly supercomplex of dimers are indicated on the left.

MICU1.1 acts as a strong MCU activator at high $[Ca^{2+}]_{cyt}$

Since MICU1.1 shows a peculiar tissue distribution and is highly conserved among vertebrates, we asked whether it displays a specific role in regulating mitochondrial Ca^{2+} uptake. To answer to this question, we decided to first asses the effect of MICU1.1 overexpression on mitochondrial Ca^{2+} uptake in intact HeLa cells. We evaluated mitochondrial Ca^{2+} uptake thanks to mitochondrially targeted aequorin upon maximal histamine stimulation (100 µM), as already performed [47,50,52]. It has been shown that MICU1 overexpression stimulates mitochondrial Ca^{2+} uptake when overexpressed in HeLa cells [52]. Strikingly, the overexpression

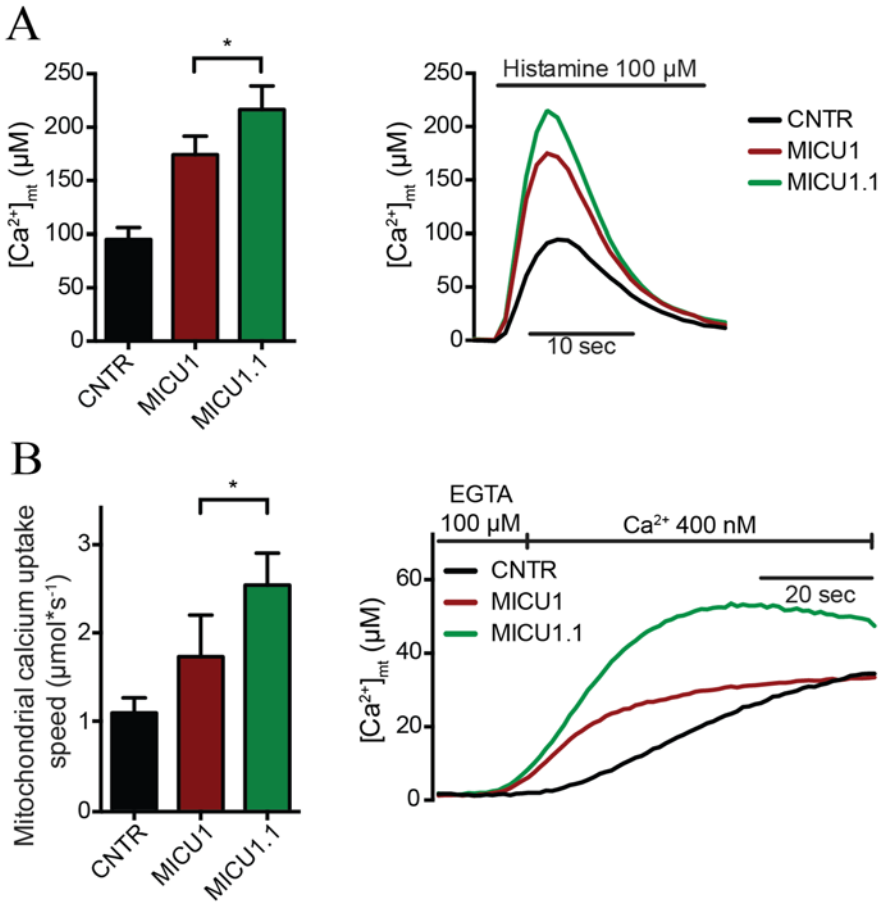

Figure 10 - MICU1.1 acts as a strong MCU activator in stimulated intact cells

*A) $[Ca^{2+}]_{mt}$ measurements in intact HeLa cells overexpressing for 24 hours the indicated constructs together with mitochondrially targeted aequorin. Cells were challenged with maximal histamine stimulation (100 µM). The bar diagram (left panel) represents the mean peak ± SD. n=10. The panel on the right shows representative traces of the experiment. *p<0.05;*

*B) $[Ca^{2+}]_{mt}$ measurements in permeabilized HeLa cells overexpressing for 24 hours indicated constructs together with mitochondrially targeted aequorin upon exposure to 400 nM $[Ca^{2+}]$. On the left, bar diagram representing the mean $[Ca^{2+}]_{mt}$ speed ± SD. The panel on the right shows representative traces of the experiment. Where indicated the perfusion medium was switched from IB/EGTA (Ca^{2+}-free) to IB/Ca^{2+} (400 nM Ca^{2+}). n=4, *p<0.05.*

of MICU1.1 causes a major increase of mitochondrial Ca^{2+} uptake that significantly exceeds the one induced by the overexpression of MICU1 (Figure 10A). In order to selectively investigate the specific contribution of the mitochondrial Ca^{2+} uptake machinery, we decided to measure mitochondrial Ca^{2+} uptake speed in digitonin-permeabilized HeLa cells. This experiment allows the evaluation of the properties of the mitochondrial Ca^{2+} uptake independently of the ER Ca^{2+} release and the formations of microdomains of high $[Ca^{2+}]$ in close proximity to mitochondrial Ca^{2+} channels. These experiments are performed initially by perfusing cells for 60

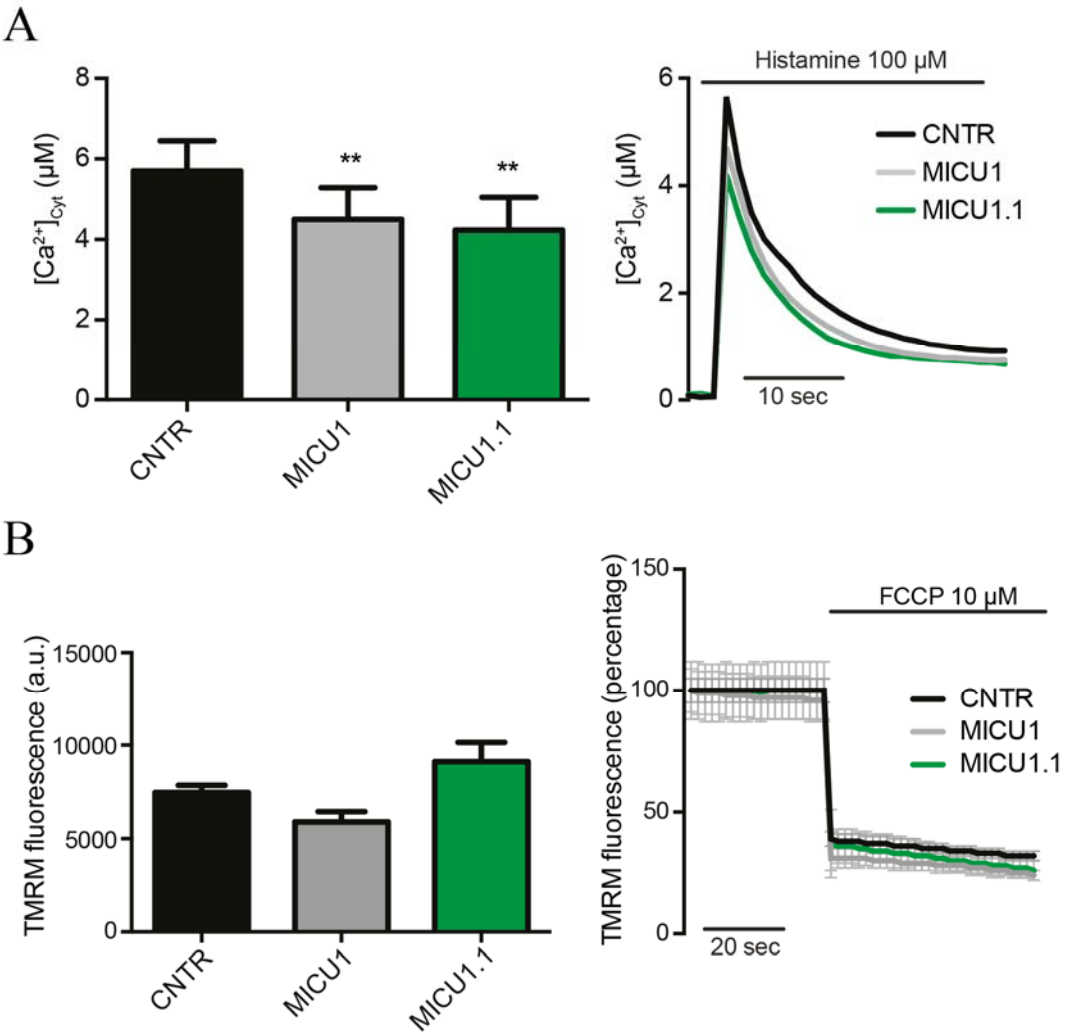

Figure 11 – $[Ca^{2+}]_{cyt}$ transients and membrane potential ($\Delta\Psi$) in MICU1 and MICU1.1 overexpressing cells

*A. $[Ca^{2+}]_{cyt}$ measurements in intact HeLa cells overexpressing for 24 hours the indicated constructs together with cytosolic aequorin. Cells were challenged with maximal histamine stimulation (100 μM). The bar diagram (left panel) represents the mean peak ± SD n=9. The panel on the right shows representative traces of the experiment. ** $p<0.01$;*

B. Hela cells, overexpressing for 24 hours the indicated constructs, were loaded with TMRM and TMRM fluorescence measurements were performed. Where indicated 10 μM FCCP were added. a.u., arbitrary units. On the right, representative traces of the experiment. The bar diagram (left panel) represents the mean ± SD, n=20.

seconds with EGTA-containing Ca^{2+}-free intracellular buffer (IB/EGTA). Cells are then perfused with the same buffer with 50 μM digitonin for 60 seconds and washed with IB/EGTA buffer for other 60 seconds. Ca^{2+} accumulation is initiated by switching the perfusion buffer to IB containing an EGTA-buffered [Ca^{2+}] of 400 nM. In line with the experiment in intact cells, MICU1.1 increases mitochondrial Ca^{2+} uptake rate by almost 50% (Figure 10B).

We then asked whether the effect of MICU1.1 on mitochondrial Ca^{2+} uptake was secondary to changes in $[Ca^{2+}]_{cyt}$ or in the driving force for Ca^{2+} accumulation (i.e. a collapse of mitochondrial membrane potential, ΔΨ). We thus measured cytosolic Ca^{2+} transients by overexpressing in HeLa cells cytosolic aequorin together with MICU1 or MICU1.1 for 24 hours and we stimulated cells with histamine (100 μM). The greater mitochondrial response of MICU1 and MICU1.1 overexpression is not secondary to alterations of the cytosolic response. Rather, a significant reduction in the cytosolic Ca^{2+} transient is observed both in cells overexpressing MICU1 and MICU1.1, most likely due to increased Ca^{2+} clearance by mitochondria (Figure 11A).

As to the driving force for Ca^{2+} uptake, we measured mitochondrial membrane potential (ΔΨ) using the fluorescence probe tetramethylrhodamine methyl ester (TMRM). The overexpression of both MICU1 and MICU1.1 does not alter the mitochondrial membrane potential (Figure 11B), indicating that the increase of mitochondrial Ca^{2+} uptake observed is specifically due to MICU1.1-mediated activation of MCU.

Electrophysiological characterization of MICU1.1

In order to study the regulatory properties of MICU1 and MICU1.1 on MCU channel activity, we performed a series of electrophysiological experiments taking advantage from a well-establish technique of planar lipid bilayer, as previously reported [47,50,52].

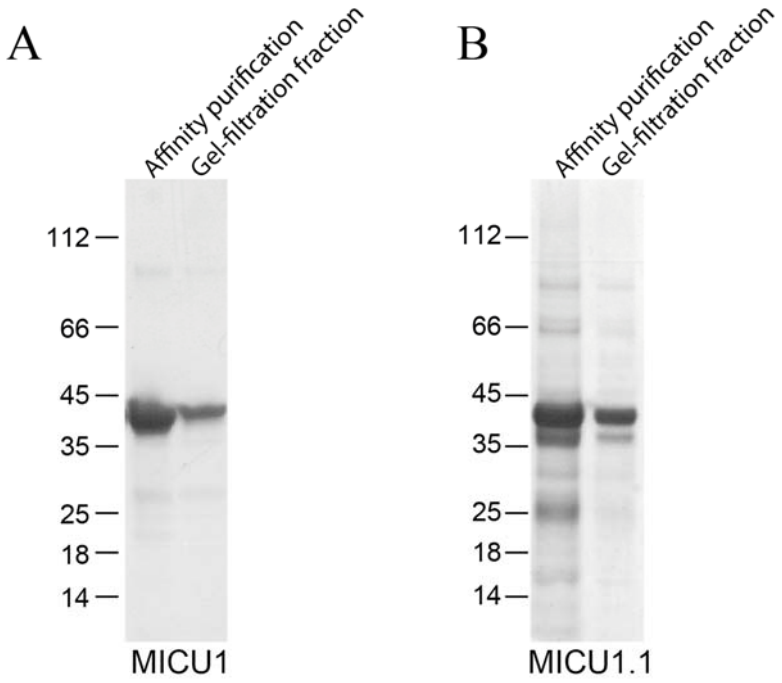

Figure 12 – Expression and purification of recombinant MICU1 and MICU1.1

A) SDS-PAGE stained with G250 colloidal Coomassie of MICU1. Lane 1: protein sample obtained after the affinity-purification. Lane 2: protein sample after gel-filtration chromatography;

B) SDS-PAGE stained with G250 colloidal Coomassie of MICU1.1. Lane 1: protein sample obtained after the affinity-purification. Lane 2: protein sample after gel-filtration chromatography.

Recombinant MCU was prepared by *in vitro* expression using an eukaryotic cell-free translation system, in order to obtain a pure MCU preparation without contamination of bacterial proteins. On the contrary, recombinant MICU1 and MICU1.1 were expressed in *Escherichia coli*. We removed the mitochondrial targeting sequence of both MICU1 and MICU1.1 (1-53) and to avoid protein aggregation and the first 43 amino acids after the predicted cleavage site of the MTS (MICU1$^{\Delta 1\text{-}96}$ and MICU1.1$^{\Delta 1\text{-}96}$), as previously performed for the crystallization of MICU1 [82]. Bacteria were lysed by French press to avoid the use of detergents and the proteins of interest were purified by affinity chromatography tandem to size-exclusion chromatography, to increase the purity of recombinant MICU1 and MICU1.1. The protein samples obtained by the affinity chromatography and the fractions obtain by gel filtration chromatography, containing the proteins of interest, were separated by SDS-PAGE and stained with G-250 colloidal Coomassie to assess the presence of contaminant proteins. Figure 12 shows that the gel

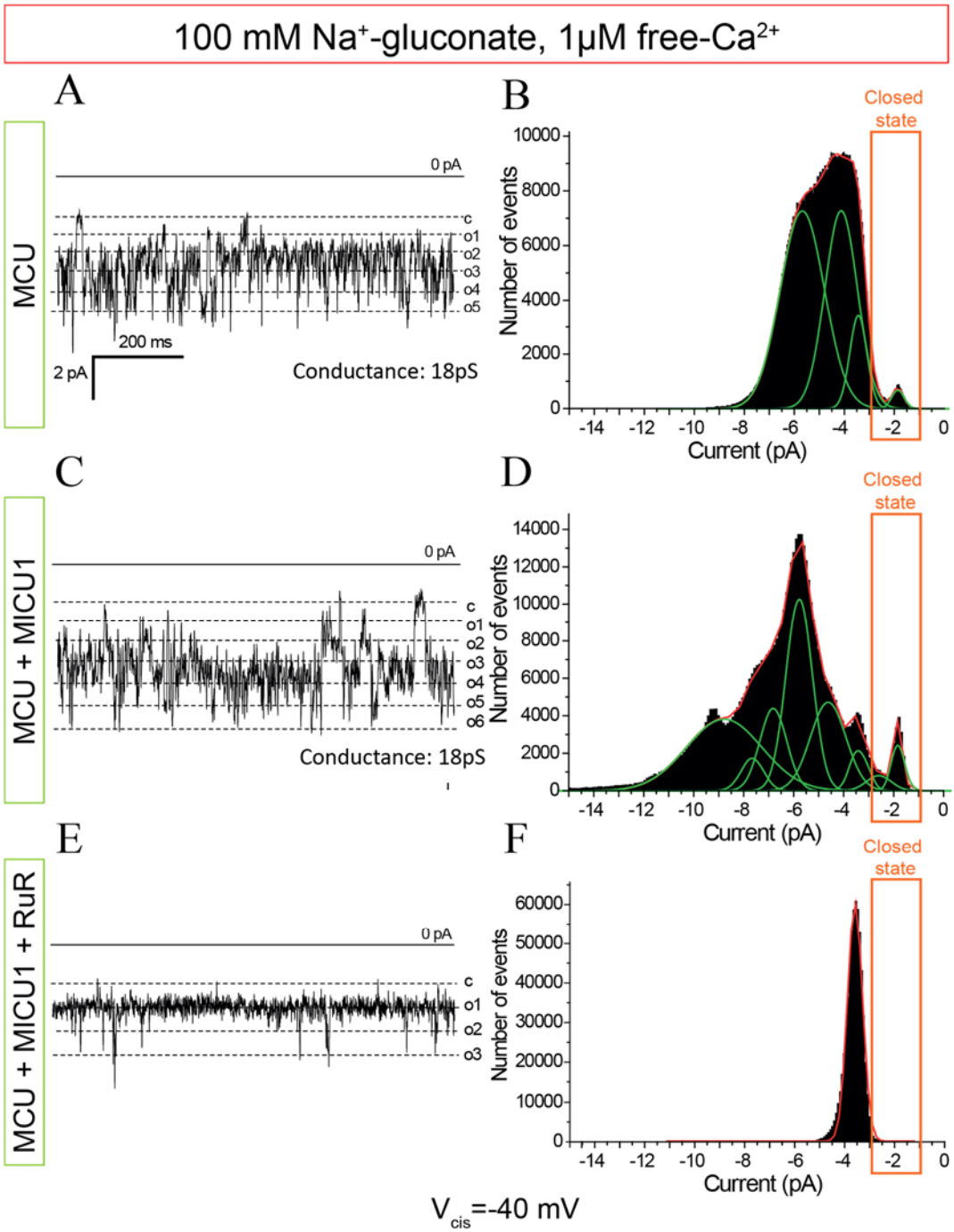

Figure 13 – MICU1 modulation of MCU activity recorded in planar lipid bilayer experiments

A) Representative trace of in vitro expressed MCU activity recorded in 1 µM EGTA-buffered free-[Ca^{2+}] solution during the application of -40 mV in the cis compartment. Dashed lines indicate the different opening states. c: closed state; while "o" indicates different state in which the channels are opened;

B) Amplitude histograms were obtained by analysing 60 seconds long traces. Gaussian fits of the multipeak histgram (red) and MCU current (green) were obtained using the Origin 7.5 software. The closed state is indicated in the figure;

C) Representative trace of MCU activity after the addition of purified recombinant MICU1.1, performed as in A;

D) Amplitude histograms after the addition of MICU1 performed as in B.uthenium red (RuR), performed as in A;

E) Representative trace of MCU activity after the addition of purified recombinant MICU1 and ruthenium red (RuR), performed as in A;

F) Amplitude histograms after the addition of MICU1 and RuR performed as in B.

filtration chromatography fraction, that was chosen for the planar lipid bilayer experiments, contains only the band of predicted molecular weight of MICU1 and MICU1.1.

Since we demonstrated that MICU1.1 strongly activates MCU at high [Ca^{2+}], we decided to perform the planar lipid bilayer experiments in EGTA-buffered solution containing 1 μM free-[Ca^{2+}]. All the experiments were begun with the recording of MCU activity during the application of the voltage of -40 mV to assess the incorporation of MCU into the planar lipid bilayer. Subsequently, MICU1 or MICU1.1 were added in the *cis* and *trans* compartments and changes in MCU activity were recorded. The experiments were concluded with the addition of the specific MCU inhibitor, ruthenium red (RuR) [83], that allows to identify the basal state with zero open channels. As already observed, MCU activity in a Ca^{2+} containing solution (1 μM) displayed a conductance of 18 pS, in accordance with our previous data [52]. In these conditions, in the example reported shown in Figure 13A, 5 distinct current levels were detectable, that correspond to 5 different opened channels at the same time, but most of the time the measured current level corresponded to 2-3 opened channel levels (Figure 13A). Upon addition of the MICU1 to the same membrane during the same experiment, further activation of MCU was achieved, as possible to observe on the representative current traces: after addition of MICU1 the main current level corresponded to the continuous activity of 4 channels (Figure 13C). Finally, addition of ruthenium red to both sides drastically reduced channel activity (Figure 13E). In order to better evaluate the effect of MICU1 on MCU activity, amplitude histograms were obtained from the current traces before and after the addition of MICU1. These histograms show the number of events at a certain current value in a 60 second-long current trace (Figure 13B, D, F). Thus, the height and the position of the peaks on the histograms give an indirect information about the time the channel spends in the open state with respect to the closed state. In these conditions, it is appreciable that MICU1 powerfully activates MCU, since the number of open channels drastically increase (Figure 13D). Similar results were obtained in other 3 experiments, while in further 2 cases addition of MICU1 to MCU in Ca^{2+}-containing medium did not result in an increase of channel activity, for unknown reasons.

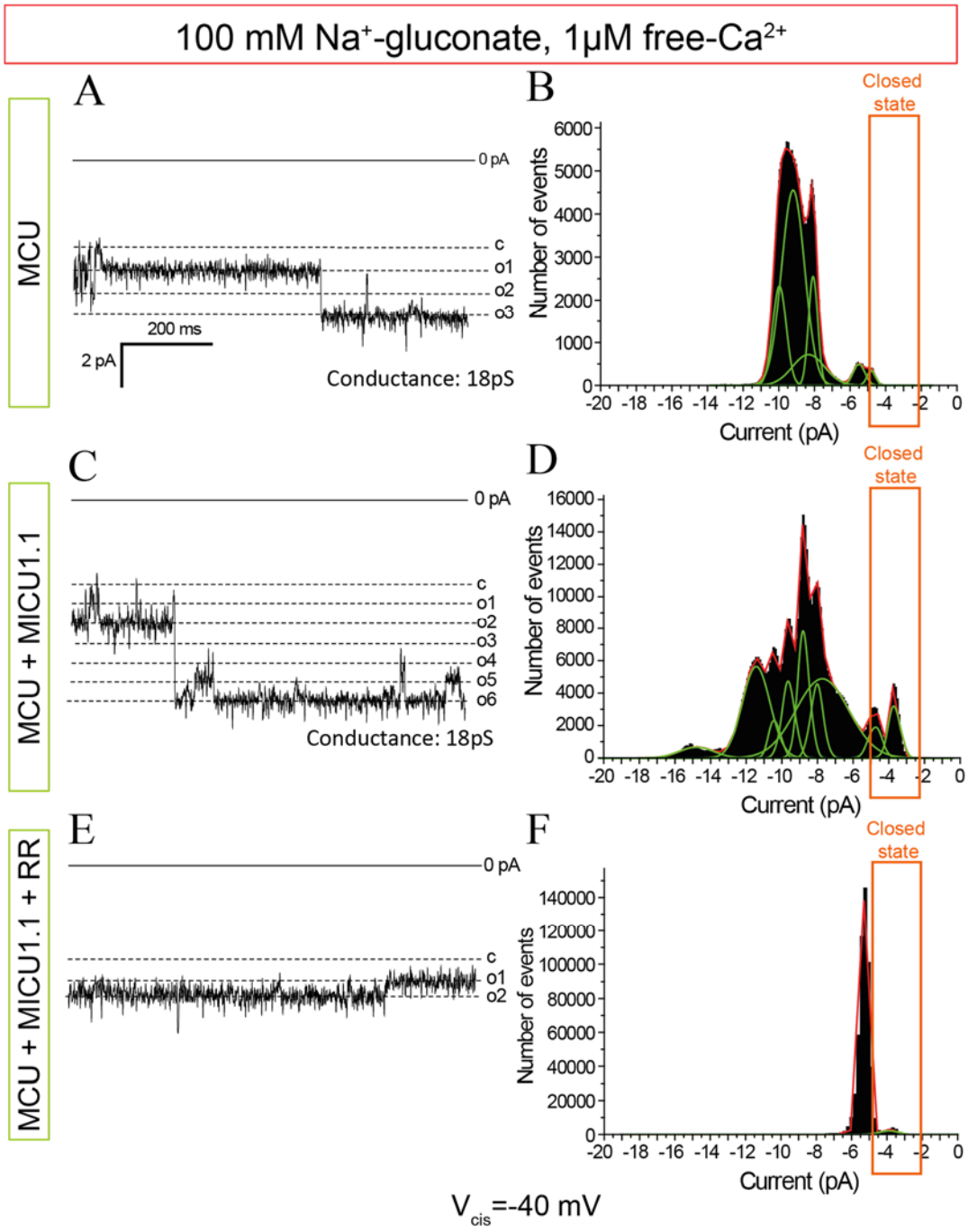

Figure 14 – MICU1.1 modulation of MCU activity recorded in planar lipid bilayer experiments

A) Representative trace of in vitro expressed MCU activity recorded in 1 µM EGTA-buffered free-[Ca^{2+}] solution during the application of -40 mV in the cis compartment. Dashed lines indicate the different opening states. c: closed state; while "o" indicates different state in which the channels are opened;

B) Amplitude histograms were obtained by analysing 60 seconds long traces. Gaussian fits of the multipeak histgram (red) and MCU current (green) were obtained using the Origin 7.5 software. The closed state is indicated in the figure;

C) Representative trace of MCU activity after the addition of purified recombinant MICU1.1, performed as in A;

D) Amplitude histograms after the addition of MICU1.1 performed as in B;

E) Representative trace of MCU activity after the addition of purified recombinant MICU1.1 and ruthenium red (RuR), performed as in A;

F) Amplitude histograms after the addition of MICU1.1 and RuR performed as in B.

In the same experimental conditions, we evaluated the ability of MICU1.1 to modulate the MCU activity. As before, MCU conductance in Ca^{2+} containing solution is of 18 pS. In the example shown in Figure 14A, in these conditions, 3 distinct current levels were detectable and the average number of open channels is 2 (Figure 14A). Upon addition of MICU1.1, we achieved a very strong activation of MCU with 5-6 open channel levels for most of the time (Figure 14C). From the respective amplitude histograms, we observed that MICU1.1 strongly activates MCU, increasing the number of events at high open state compared with the trace recorded with MCU alone (Figure 14D). In the amplitude histograms not all separate current levels raising form the opening of 1 to 6 channels could be resolved because of the flickering behavior and because of the relatively low probability of finding all six channels open. From these histograms, it can not be fully appreciated whether or not MICU1.1 activates MCU in a more efficient manner compared with MICU1, but qualitatively (on the basis of amplitude histograms and current traces), this strong activatory effect was recorded in other 7 experiments.

MICU1.1-induced mitochondrial Ca^{2+} uptake is not inhibited by the gatekeeper MICU2

As already shown, MICU2 overexpression in HeLa cells is sufficient to reduce $[Ca^{2+}]_{mt}$ uptake of about 20% in stimulated cells compared with control cells [52]. These data, indicating an inverse correlation between MICU2 levels and MCU activity, confirm the role of MICU2 as the authentic MCU gatekeeper (Figure 3). In line with the gatekeeper function of MICU2, it has been demonstrated that when MICU1 and MICU2 are both overexpressed, thus leading to an increase of the heterodimer only, the MICU1-dependent potentiation of mitochondrial Ca^{2+} responses is almost abolished [52]. We asked whether MICU2 overexpression leads to the same effect on MICU1.1. We thus overexpressed in HeLa cells mitochondrially targeted aequorin together with MICU1.1 and MICU2, thus leading to an increase of the heterodimer only. Strikingly, MICU2 overexpression fails to inhibit the increase of mitochondrial Ca^{2+} uptake due to the overexpression of MICU1.1 (Figure 15A).

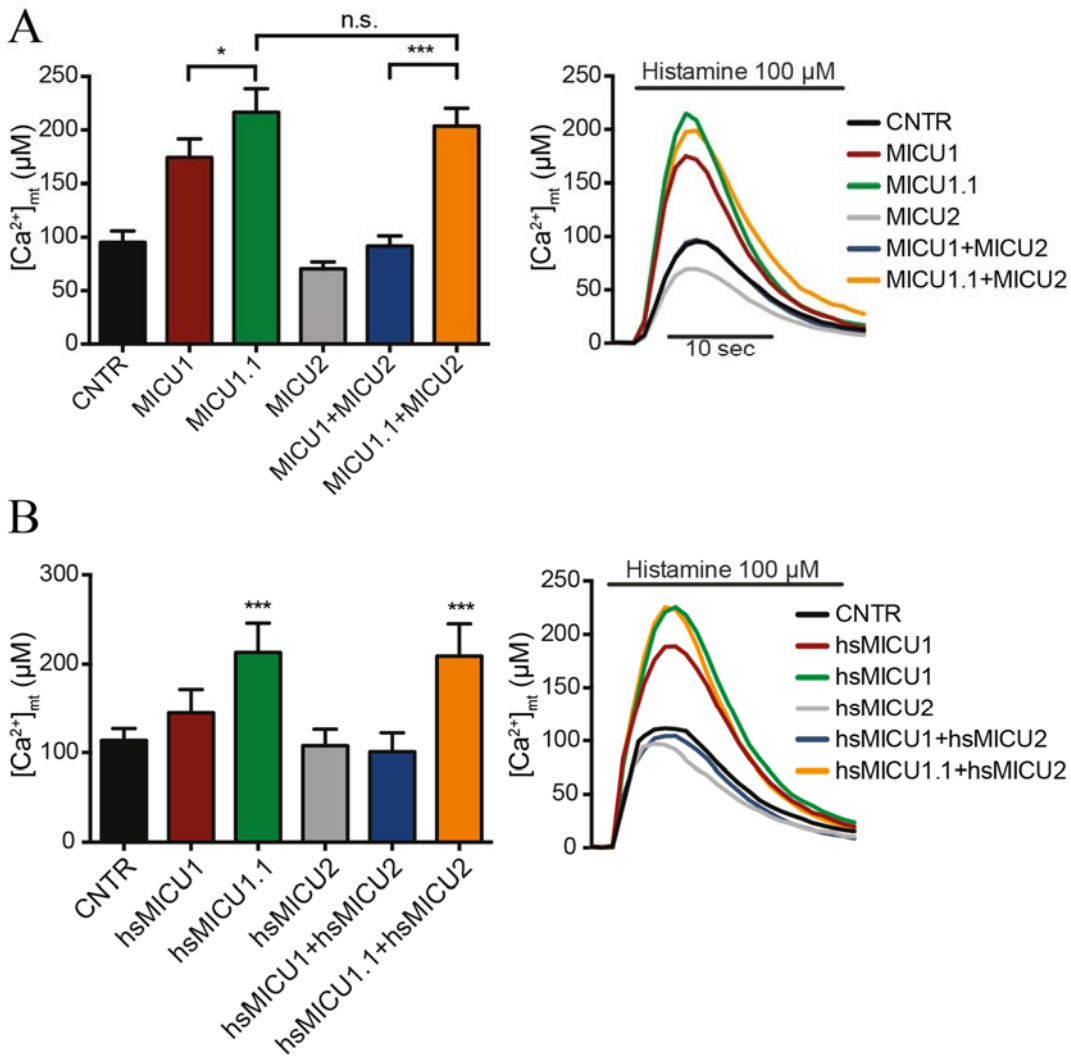

Figure 15 – Murine and human MICU1.1-induced mitochondrial Ca^{2+} uptake is not inhibited by the gatekeeper MICU2.

*A) $[Ca^{2+}]_{mt}$ measurements in intact HeLa cells overexpressing for 24 hours the indicated constructs together with mitochondrially targeted aequorin. Cells were challenged with maximal histamine stimulation (100 μM). The bar diagram (left panel) represents the mean peak ± SD. n=10. On the right, representative traces of the experiment. *p<0.05, ***p<0.005, n.s. non-significant;*

*B) $[Ca^{2+}]_{mt}$ measurements in intact HeLa cells overexpressing for 24 hours human isoforms (hs) of MICU1, MICU1.1 and MICU2 together with mitochondrially targeted aequorin. Cells were challenged with maximal histamine stimulation (100 μM). The bar diagram (left panel) represents the mean peak ± SD. n=10. The panel on the right shows representative traces of the experiment. *p<0.05, ***p<0.005, n.s. non-significant.*

We also wondered whether human MICU1.1 exerts the same effect on $[Ca^{2+}]_{mt}$. For this purpose, we cloned human MICU1 (hsMICU1), human MICU1.1 (hsMICU1.1) and human MICU2 (hsMICU2) from a *Homo sapiens* skeletal muscle cDNA library and we measured mitochondrial Ca^{2+} uptake in the same conditions as in Figure 15A. This experiment clearly shows that also human MICU1.1 is a potent activator of mitochondrial Ca^{2+} uptake and that MICU2 is not able to inhibit its function (Figure 15B).

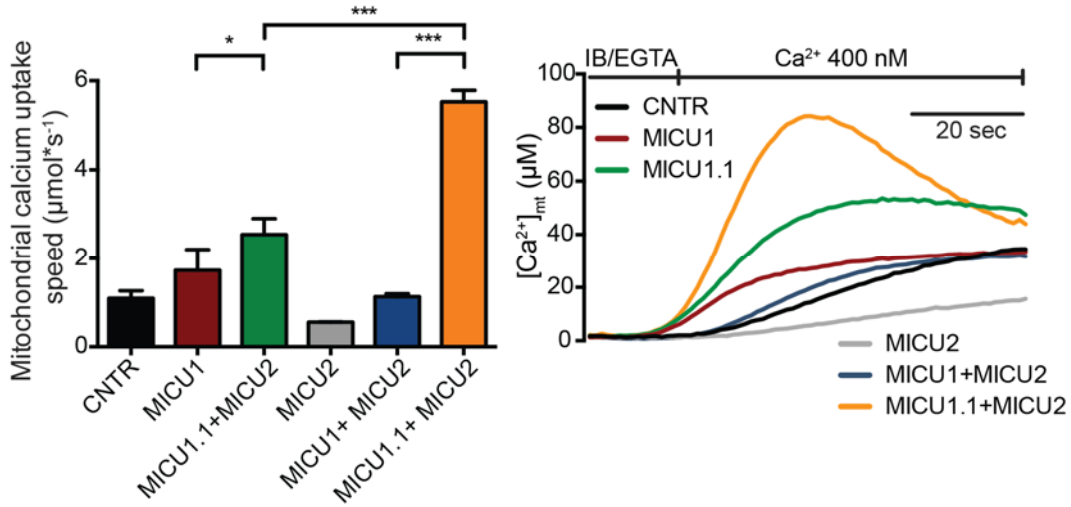

Figure 16 – Cells overexpressing MICU1.1 together with MICU2 display a synergistic induction of mitochondrial Ca^{2+} uptake speed

*$[Ca^{2+}]_{mt}$ measurements in permeabilized HeLa cells overexpressing for 24 hours the indicated constructs together with mitochondrially targeted aequorin upon exposure to 400 nM $[Ca^{2+}]$. The panel on the right shows representative traces of the experiment. Where indicated the perfusion medium was switched from IB/EGTA (Ca^{2+}-free) to IB/Ca^{2+} (400 nM Ca^{2+}). On the left, bar diagram representing the mean $[Ca^{2+}]_{mt}$ speed ± SD n=4. *p<0.05, ***p<0.005.*

To further characterize this peculiar behaviour of MICU1.1, we decided to measure mitochondrial Ca^{2+} uptake speed in permeabilized HeLa cells. We thus performed a similar experiment of that shown in Figure 10B. The overexpression of MICU2 alone is sufficient to reduce the speed of mitochondrial Ca^{2+} uptake compared to control cells. The gatekeeper effect of MICU2 is particularly evident when MICU2 is co-expressed with MICU1. Indeed, in this condition, we observed that mitochondrial Ca^{2+} uptake speed increase due to MICU1 overexpression is blocked. Strikingly, when we measured mitochondrial Ca^{2+} uptake speed in cells overexpressing MICU1.1 together with MICU2, we found that mitochondrial Ca^{2+} uptake speed is further increased, far more than in cells overexpressing MICU1.1 alone (Figure 16).

Finally, we tested whether endogenous MICU1, together with overexpressed MICU1.1, is partially responsible of the observed effect. To verify this, we silenced endogenous human MICU1 and we rescued the knockdown by overexpressing either mouse MICU1 or mouse MICU1.1. The effect of MICU1 knockdown is efficiently rescued by MICU1 transfection in HeLa cells, since in this condition the $[Ca^{2+}]_{mt}$ peak is undistinguishable from control cells (Figure 17). On the other hand, MICU1 knockdown rescued by MICU1.1 transfection displays a $[Ca^{2+}]_{mt}$ peak significantly higher compared to control cells (Figure 17), indicating

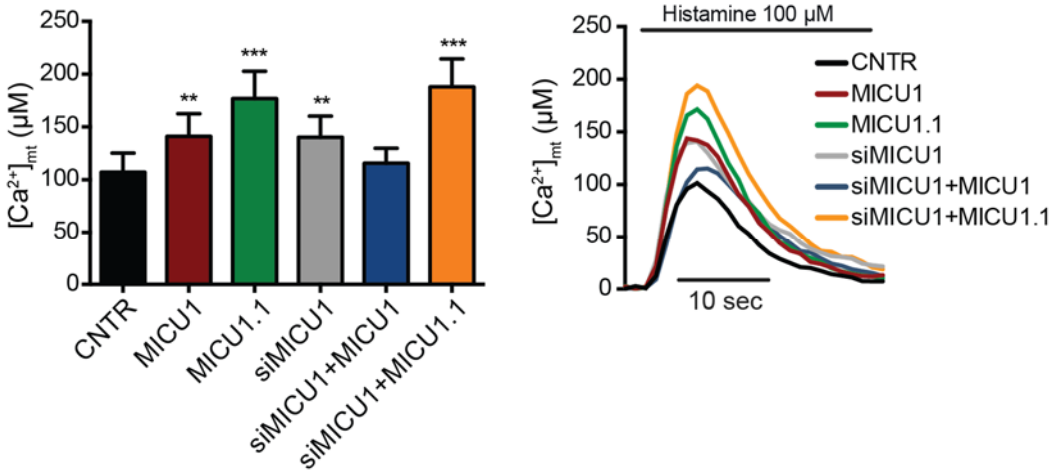

Figure 17 – Effect of MICU1.1 on mitochondrial Ca^{2+} uptake in HeLa cells silenced for endogenous MICU1.

*$[Ca^{2+}]_{mt}$ measurements in intact HeLa cells transfected for 24 hours with the indicated constructs and siRNA together with mitochondrially targeted aequorin. Cells were challenged with maximal histamine stimulation (100 μM). On the left, bar diagram representing the mean peak ± SD. n=9. On the right, representative traces of the experiment. **p<0.01, **p<0.01, ***p<0.005, n.s. non-significant.*

that the effect of MICU1.1 on mitochondrial Ca^{2+} uptake is independent from endogenous MICU1.

We concluded that, when mitochondria sense high Ca^{2+} levels, MICU1.1 is able to act as a strong MCU activator. Surprisingly, the heterodimerization with MICU2 not only fails to inhibit MICU1.1, but synergistically increases mitochondrial Ca^{2+} uptake speed.

MICU1.1 acts as gatekeeper of the MCU channel at resting $[Ca^{2+}]_{cyt}$

It has been demonstrated that while at high $[Ca^{2+}]_{cyt}$ the stimulatory effect of MICU1 allows the prompt response of mitochondria to Ca^{2+} signals generated in the cytoplasm, at low $[Ca^{2+}]_{cyt}$, the dominant effect of MICU2 largely shuts down MCU activity (Figure 3 and [52]). We thus asked whether also MICU1.1 is able to act as gatekeeper together with MICU2 in basal conditions as MICU1. To address this point, we performed an assay of gatekeeper reconstitution upon MCU overexpression in HeLa cells. To measure mitochondrial Ca^{2+} levels at resting conditions, we transfected a GFP-based Ca^{2+} probe targeted to mitochondria, 4mtGCaMP6f, as already performed [52]. The GCaMP6 family is a group of ultrasensitive, green fluorescent indicator proteins that enable reliable detection of

fast Ca^{2+} transients (excitation at 474 nm) [84]. GFP is circularly permutated in which the amino and carboxyl portions had been interchanged and reconnected by calmodulin (CaM) and the M13 domain of the myosin light chain kinase. This allows that, at low [Ca^{2+}], the circularly permutated GFP exists in a poorly fluorescent state, that increases after CaM Ca^{2+} binding and subsequent protein structural shift. This fluorescence protein presents an isosbestic point (410 nm) in the excitation spectrum in which fluorescence emission is not Ca^{2+}-dependent [84]. We exploited this property to normalize the traces for the probe expression: in this way, the ratio between 474 and 410 nm excitation wavelengths is proportional to [Ca^{2+}] but independent of probe expression. Thanks to this probe, we observed that, when we overexpressed MCU for 24 hours, we obtained a 3 times increase of mitochondrial Ca^{2+} levels in resting conditions. This is due to the presence of a large number of channels without their regulators. In this condition, we tried to reconstitute the regulated channel by overexpressing the components of the gatekeeper heterodimer MICU1-MICU2. In this configuration, co-expression of MCU together with MICU1 failed to recover normal resting $[Ca^{2+}]_{mt}$, showing just

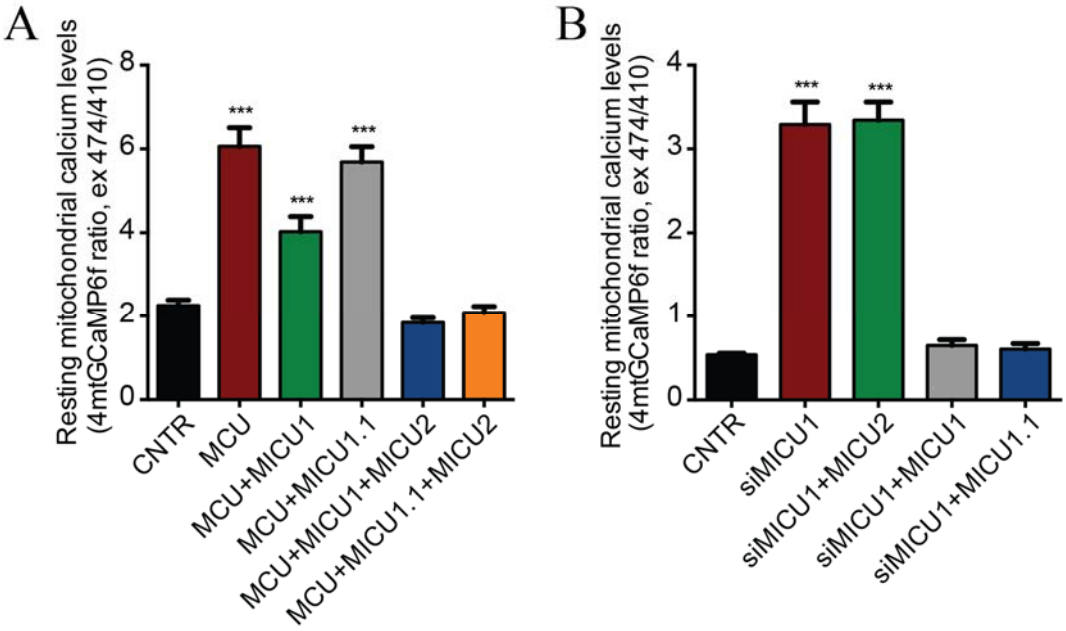

Figure 18 – The dimer MICU1.1-MICU2 acts as gatekeeper of MCU in resting conditions

*A) Resting mitochondrial Ca^{2+} levels in HeLa cells overexpressing the indicated constructs, evaluated through ratiometric imaging (Ex 474/410) of the mitochondrial targeted GCaMP6f. Data are presented as mean ± SE, ***p<0.005, n=15;*

*B) Resting mitochondrial Ca^{2+} levels in HeLa cells silenced for endogenous MICU1 and overexpressing MICU2, MICU1 or MICU1.1, evaluated through ratiometric imaging (Ex 474/410) of the mitochondrial targeted GCaMP6f. Data are presented as mean ± SE, ***p<0.005, n=15.*

a modest reduction, probably due to partial MICU2 stabilization [65]. On the contrary, the concomitant expression of MCU, MICU1 and MICU2, which substantially increases MICU1-MICU2 heterodimer formation, efficiently rescues normal values of basal $[Ca^{2+}]_{mt}$, as already shown [52]. On the other hand, in HeLa cells, transfected with MCU together with MICU1.1, we did not observe any difference in $[Ca^{2+}]_{mt}$ compared with cells overexpressing only MCU, suggesting that the homodimer MICU1.1, as MICU1, is not able to act as gatekeeper of MCU channel. When we overexpressed MCU, together with MICU1.1 and MICU2, we observed that mitochondrial Ca^{2+} levels in resting conditions return to the Ca^{2+} levels of control cells. This suggests that the heterodimer MICU1.1-MICU2 acts as a gatekeeper as MICU1-MICU2 at low $[Ca^{2+}]_{cyt}$ (Figure 18A).

To further verify these results, we decided to knockdown endogenous MICU1 using a specific siRNA in HeLa cells for 24 hours. The loss of MICU1 is sufficient to destabilize MICU2 proteins and thus leads MICU2 protein degradation [52,65]. Consequently, in this condition, we obtained the loss of the channel gatekeeper and, accordingly, a 6-times increase of basal mitochondrial Ca^{2+} levels. Thus, we tried to rescue the $[Ca^{2+}]_{mt}$ by co-expressing MICU2, MICU1 or MICU1.1. MICU2, when overexpressed alone, is not able to rescue the mitochondrial Ca^{2+} levels increase of basal mitochondrial $[Ca^{2+}]$. This is not an unexpected result since it has been shown that MICU2 can not act on MCU without the endogenous MICU1 [65,66]. On the contrary, we observed that the increase of mitochondrial basal Ca^{2+} levels is rescued by the overexpression of both MICU1 and MICU1.1 (Figure 18B).

Role of MICU1.1 in setting the threshold of mitochondrial Ca^{2+} uptake

Overall, we demonstrated that MICU1.1 is a strong activator of MCU at high $[Ca^{2+}]_{cyt}$, while in resting conditions it is able to act as gatekeeper together with MICU2. It has been demonstrated that MICU1 controls both $[Ca^{2+}]_{cyt}$ threshold and cooperativity of the MCU, with the latter being dependent on Ca^{2+} binding to the EF-hands domains of MICU1 [59]. Since the huge activation of MCU Ca^{2+} current

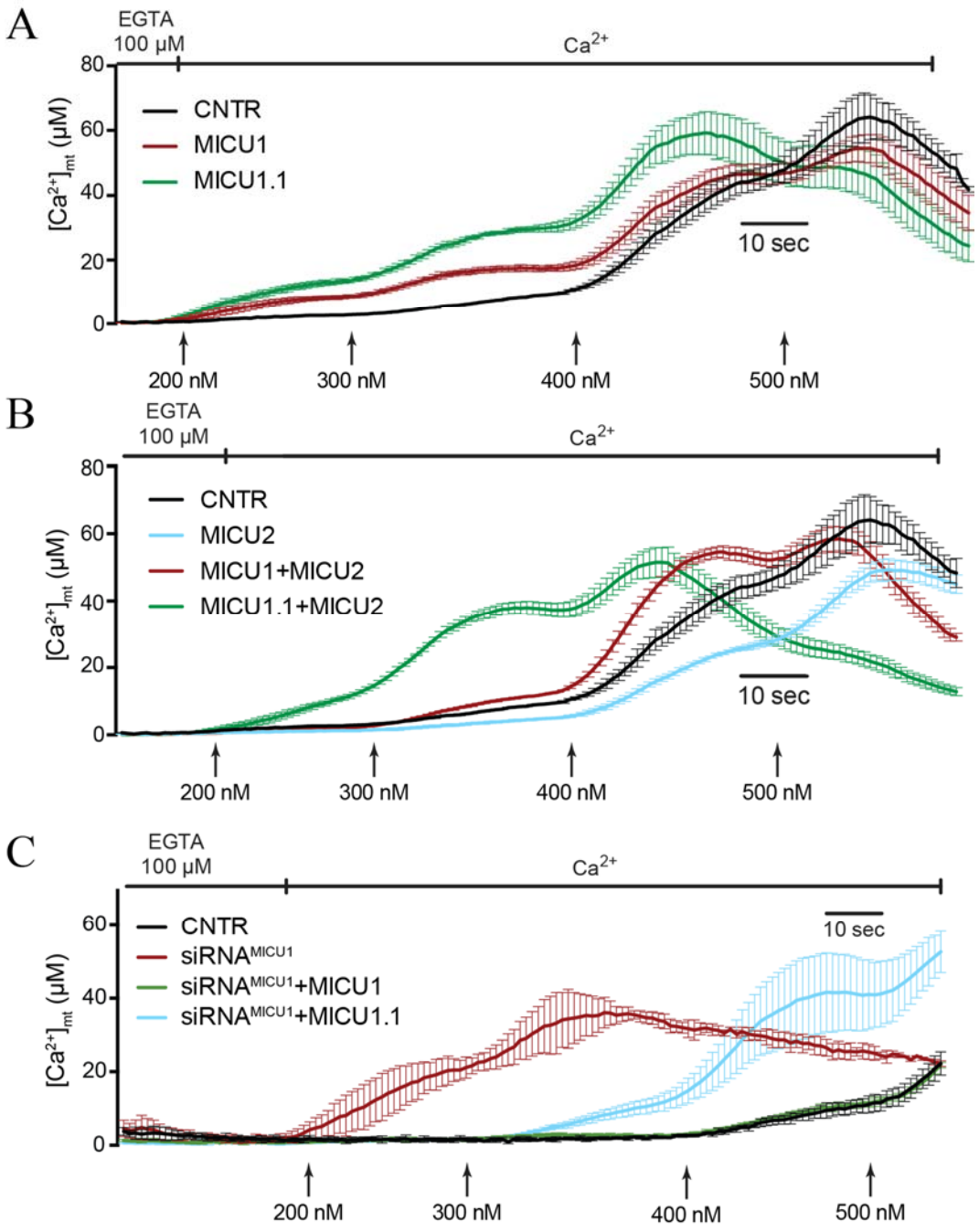

Figure 19 – Mitochondrial Ca^{2+} uptake kinetic at different Ca^{2+} concentration in MICU1.1 overexpressing cells

A) *$[Ca^{2+}]_{mt}$ measurements in permeabilized HeLa cells overexpressing either MICU1 or MICU1.1 together with mitochondrially targeted aequorin upon sequential exposure to crescent $[Ca^{2+}]$, as indicated in the graph. Data are presented as mean ± SD. n=4;*

B) *$[Ca^{2+}]_{mt}$ measurements in permeabilized HeLa cells overexpressing MICU1 and MICU1.1 together with MICU2. Mitochondrial Ca^{2+} uptake is monitored thanks to mitochondrially targeted aequorin light emission. Cells were perfused sequentially with solutions at crescent $[Ca^{2+}]$, as indicated in the graph. Data are presented as mean ± SD. n=4;*

C) *$[Ca^{2+}]_{mt}$ measurements in permeabilized HeLa cells overexpressing MICU1 and MICU1.1 upon silencing of endogenous MICU1. Mitochondrial Ca^{2+} uptake is monitored thanks to mitochondrially targeted aequorin light emission. Cells were perfused sequentially with solutions at crescent $[Ca^{2+}]$, as indicated in the graph. Data are presented as mean ± SD. n=4.*

upon overexpression of MICU1.1, we wondered whether this effect was mediated by changes in the threshold of initiation of mitochondrial Ca^{2+} uptake. To assess this, we measured mitochondrial Ca^{2+} uptake thanks to aequorin light emission in permeabilized HeLa cells. Thus, we perfused permeabilized cells sequentially with solutions containing increasing free-Ca^{2+} concentrations (from 200 nM to 600 nM), perfusing cells with each solution for the same period of time (30 seconds). First, we analyzed the effect of MICU1 and MICU1.1 overexpression in HeLa cells for 24 hours. As observed in the previous experiment (Figure 10B), the overexpression of MICU1.1 induces a prompter response at each [Ca^{2+}] compared to control cells and MICU1 overexpressing cells (Figure 19A).

On the contrary, as expected, MICU2 overexpression shows a negative modulation on mitochondrial Ca^{2+} uptake speed response. This is also observed when we co-expressed MICU1 together with MICU2. Indeed, the reconstitution of the MICU1-MICU2 heterodimer abrogates the faster and higher response caused by the overexpression of MICU1 upon perfusion of 300 nM free-[Ca^{2+}] solution. On the contrary, cells overexpressing the heterodimer MICU1.1-MICU2 present a sustained mitochondrial Ca^{2+} uptake at lower free [Ca^{2+}] (at 200 nM free-[Ca^{2+}] solution), at which control cells and cells overexpressing MICU1 together MICU2 do not initiate mitochondrial Ca^{2+} uptake (Figure 19B).

It has been recently published that mitochondrial Ca^{2+} uptake is regulated by a Ca^{2+}-dependent remodelling of the uniporter complex [85]. In this model, the dimer MICU1-MICU2 associates with MCU in a Ca^{2+}-dependent manner. Indeed, at low $[Ca^{2+}]_{cyt}$ levels, the dimer associates with MCU, while it dissociates upon increases of $[Ca^{2+}]_{cyt}$ [85]. We thus asked whether the huge increase of $[Ca^{2+}]_{mt}$ caused by the overexpression of MICU1.1 together with MICU2 was due to the dissociation of MICU1.1-MICU2 heterodimer from MCU. If this is the case, the overexpression of MICU1.1 should mimic the loss of the gatekeeper. To address this question, we measured mitochondrial uniporter threshold in permeabilized cells in which endogenous MICU1 was silenced by a specific siRNA (Figure 19C). To perform this experiment, as in Figure 19B, we measured $[Ca^{2+}]_{mt}$ in permeabilized HeLa cells by perfusing them sequentially with increasing free Ca^{2+} concentrations. We compared mitochondrial Ca^{2+} uptake of cells in silenced for endogenous

MICU1 for 24 hours, compared with cells in which this MICU1 knockdown was rescued by the overexpression of either MICU1 or MICU1.1. The results show that the silencing of MICU1 causes the complete loss of gatekeeper, since these cells display a $[Ca^{2+}]_{mt}$ uptake even at very low free-$[Ca^{2+}]$ concentrations (200 nM) (Figure 19C). In line with previous results, MICU1.1 rescue affects the threshold of activation of MCU, shifting the threshold towards lower free-$[Ca^{2+}]$ (from 400 nM to 300 nM) compared with control cells (Figure 19C). Nevertheless, the response starts at higher $[Ca^{2+}]$ than in condition of total loss of the dimer MICU1-MICU2, suggesting that MICU1.1 does not induce the dissociation of the dimer.

Ca^{2+}-dependent functional regulation of the MICU complex

It has been shown that MICU1 and MICU2 are able to sense Ca^{2+} levels thanks to the two EF-hand domains present in their amino acid sequence. This is demonstrated by the functional behaviour displayed by MICU1 and MICU2 mutants ($MICU1^{EFmut}$ and $MICU2^{EFmut}$, respectively) in which the EF-hand domains lose the capability to bind Ca^{2+} [52,59,66]. Since MICU1 is activated upon Ca^{2+} binding, $MICU1^{EFmut}$ is locked in the 'inactive state'. As a consequence, its function is not affected in basal conditions when it is normally inactive while in conditions of high $[Ca^{2+}]_{cyt}$, $MICU1^{EFmut}$ loses the ability to operate as cooperative activator of MCU [59]. Since this Ca^{2+}-dependent activity of MICU1, we decided to evaluate the effects of EF-hand domains mutations on MICU1.1 activity. We thus created $MICU1.1^{EFmut}$-HA by mutating key residues of the two EF-hand domains (D237A, E248K, D427A, E438K) and we tested its effect on mitochondrial Ca^{2+} uptake in HeLa cells after 24 hours of transfection. We observed that $MICU1.1^{EFmut}$ reduces mitochondrial Ca^{2+} uptake of 40%, significantly less compared to $MICU1^{EFmut}$ effect (Figure 20A). However, the reduction is still significant if compared to control cells. On the other hand, the heterodimer $MICU1.1^{EFmut}$-MICU2 dramatically abrogates mitochondrial Ca^{2+} uptake as $MICU1^{EFmut}$-MICU2 dimer (Figure 20A).

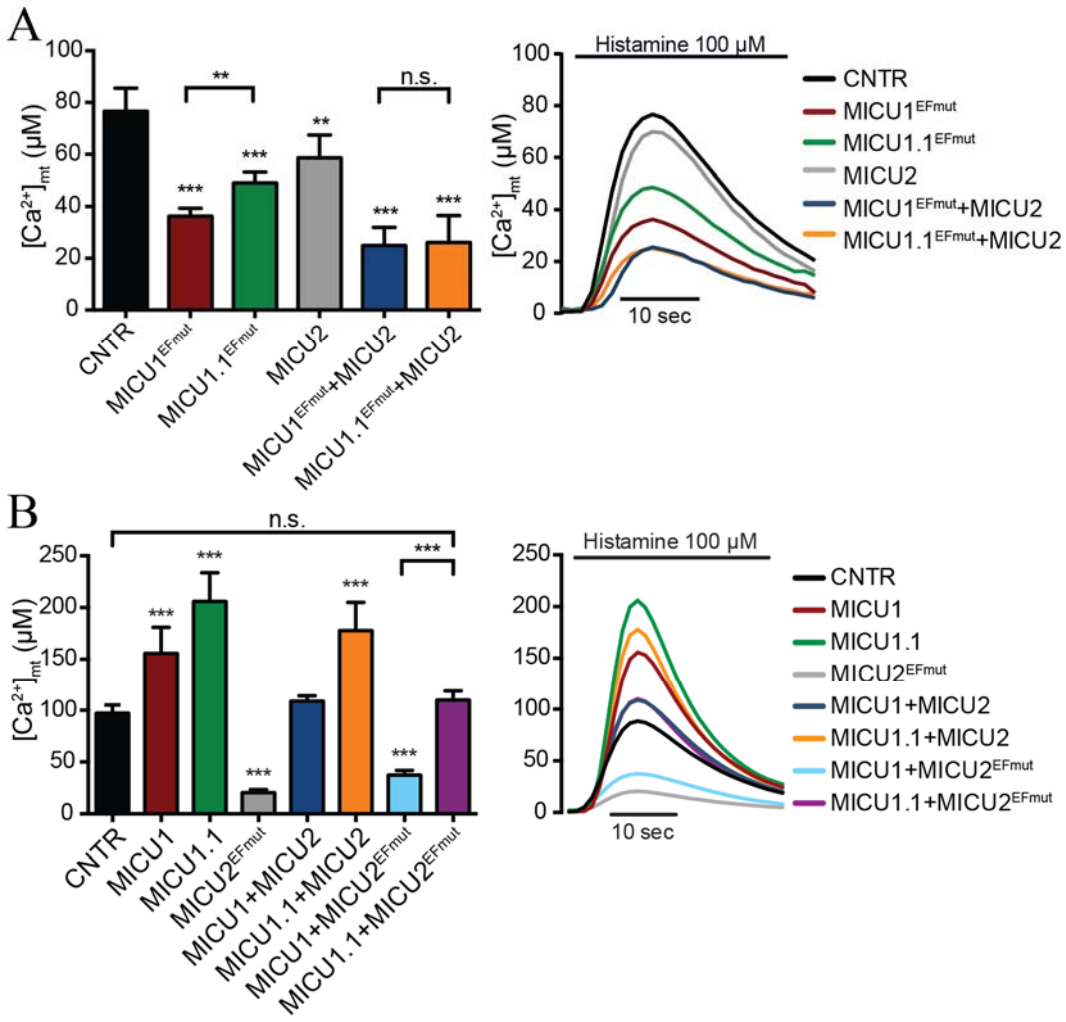

Figure 20 – Ca^{2+}-dependent functional effects of MICU1 and MICU2

*A) $[Ca^{2+}]_{mt}$ measurements in intact HeLa cells overexpressing for 24 hours the indicated constructs together with mitochondrially targeted aequorin. Cells were challenged with maximal histamine stimulation (100 μM). On the left, bar diagram representing the mean peak ± SD. n=5. The panel on the right shows representative traces of the experiment. **p<0.01, ***p<0.005, n.s. non-significant;.*

*B) $[Ca^{2+}]_{mt}$ measurements in intact HeLa cells overexpressing for 24 hours the indicated constructs together with mitochondrially targeted aequorin. Cells were challenged with maximal histamine stimulation (100 μM). On the left, bar diagram representing the mean peak ± SD. n=5. The panel on the right shows representative traces of the experiment. ***p<0.005, n.s. non-significant.*

We also assessed the effect of $MICU2^{EFmut}$ (D372A) on MICU1.1 activity. As already shown, this mutant is able to almost completely blunt mitochondrial Ca^{2+} uptake upon cell stimulation, since Ca^{2+} is unable to relieve MICU2 inhibition of the uniporter, regardless of Ca^{2+} concentration (Figure 20B and [52,66]). Co-expression of $MICU2^{EFmut}$ together with MICU1 is not able to re-establish normal $[Ca^{2+}]_{mt}$ uptake, highlighting the inhibitory role of apo-MICU2 on MCU activity (Figure 20B). Surprisingly, cells co-transfected with $MICU2^{EFmut}$ together with MICU1.1 display a $[Ca^{2+}]_{mt}$ peak comparable with the one in control cells (Figure

20B), suggesting that MICU1.1 activatory effect is less affected by MICU2 inhibition than conventional MICU1.

MICU1.1 behaviour depends on the residues that compose the extra-exon

We next wondered whether the amino acids that compose the extra-exon are responsible for MICU1.1 peculiar behaviour. To address this issue, we decided to create some MICU1.1 mutants of the extra-exon residues. First, we substituted each residue with alanine (MICU1.1^{E182A}, MICU1.1^{F183A}, MICU1.1^{W184A}, and MICU1.1^{Q185A}) in order to verify which of the four amino acids defines the strong activatory function of MICU1.1. We thus tested the effect of these mutants on HeLa cells mitochondrial Ca^{2+} uptake when co-expressed with MICU2 for 24 hours since in this condition we observed the most dramatic effect of MICU1.1. This allows us to detect more efficiently any effect of these mutants. Figure 21A clearly shows that all these mutants, when overexpressed together with MICU2, behave indistinguishably from MICU1.1 wild-type.

We then decided to evaluate the effects of MICU1.1 mutants in which we deleted one by one each of the residues of the extra-exon (MICU1$^{\Delta E182}$, MICU1$^{\Delta F183}$, MICU1$^{\Delta W184}$ and MICU1$^{\Delta Q185}$). We verified their ability to modulate $[Ca^{2+}]_{mt}$ uptake when co-expressed together with MICU2 in HeLa cells. Only the deletion of tryptophan causes a statistically significant difference in mitochondrial Ca^{2+} uptake compared to MICU1.1. However, this mutant increases dramatically mitochondrial Ca^{2+} uptake compared to MICU1 (Figure 21B). Overall, these data suggest that no residues of extra-exon are indispensable for the peculiar behaviour of MICU1.1.

To further verify the causative role of the extra-exon in defining the activatory properties of MICU1.1, we created another mutant in which we substituted all four residues in alanine (MICU1.1$^{E182A,\ F183A,\ W184A,\ Q185A}$, hereafter indicated as MICU1.1^{AAAA}). We expected that if this extra-exon has a role in defining the peculiar activatory property of MICU1.1, this mutation will completely abrogate the differences between MICU1.1 and MICU1. Thus, we evaluated the

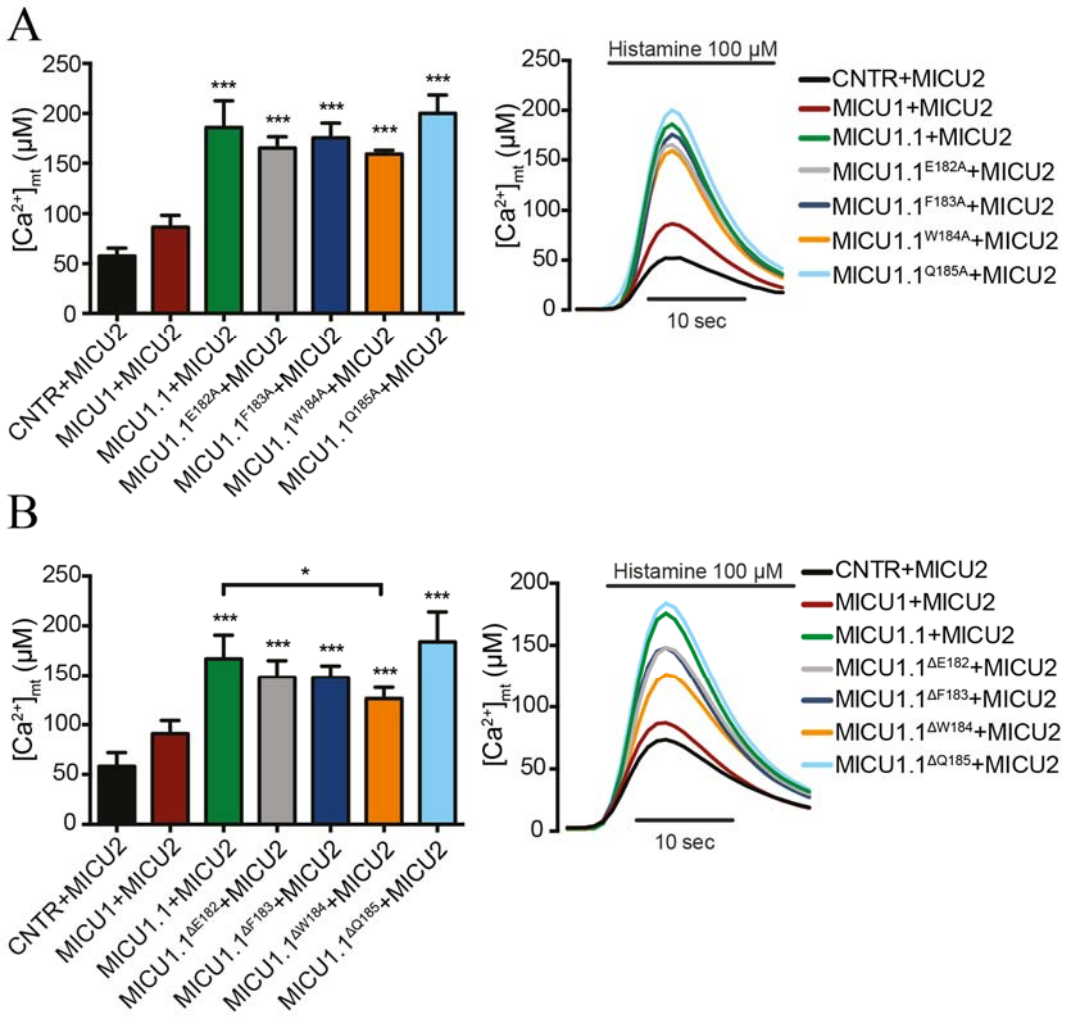

Figure 21 – Single mutations and deletions of the extra-exon amino acids do not alter MICU1.1 functional properties

A) *$[Ca^{2+}]_{mt}$ measurements in intact HeLa cells overexpressing for 24 hours the indicated constructs together with mitochondrially targeted aequorin. Cells were challenged with maximal histamine stimulation (100 μM). On the left, bar diagram representing the mean peak ± SD. n=4. On the right, representative traces of the experiment. ***p<0.005;*

B) *$[Ca^{2+}]_{mt}$ measurements in intact HeLa cells overexpressing for 24 hours the indicated constructs together with mitochondrially targeted aequorin. Cells were challenged with maximal histamine stimulation (100 μM). On the left, bar diagram representing the mean peak ± SD. n=5. *p<0.05. The panel on the right shows representative traces of the experiment. ***p<0.005.*

capability of MICU1.1^{AAAA} together with MICU2 to modulate mitochondrial Ca^{2+} uptake in HeLa cells after 24 hours of transfection (Figure 22A). As expected, this mutant evokes a mitochondrial Ca^{2+} uptake comparable with that observed in cells transfected with MICU1 together with MICU2 (Figure 22A).

We characterized also the MICU1.1^{AAAA} mutant in terms of mitochondrial Ca^{2+} uptake kinetic in permeabilized HeLa cells by perfusing them sequentially with different solutions at increasing free-$[Ca^{2+}]$, as performed above (Figure 19). First, we overexpressed MICU1.1^{AAAA} alone to assess the effect of MICU1.1^{AAAA}

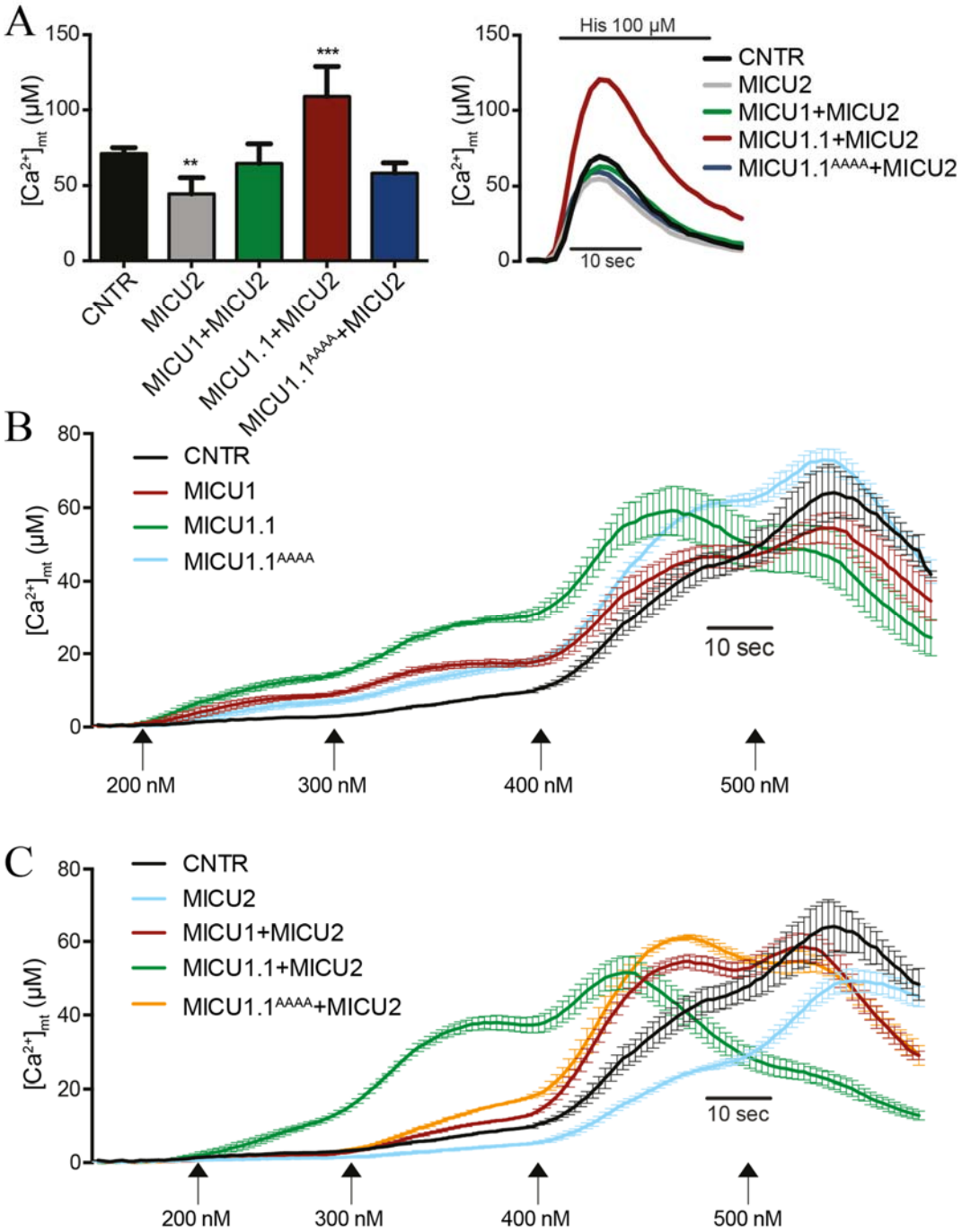

Figure 22 – The substitution mutant MICU1.1^{AAAA} alters MICU1.1 functional properties in intact and permeabilized cells

*A) $[Ca^{2+}]_{mt}$ measurements in intact HeLa cells overexpressing MICU1.1^{AAAA} together with MICU2 and with mitochondrially targeted aequorin. Cells were challenged with maximal histamine stimulation (100 μM). On the left, bar diagram representing the mean peak ± SD. n=6. On the right, representative traces of the experiment. **p<0.01, ***p<0.005;*

B) $[Ca^{2+}]_{mt}$ measurements in permeabilized HeLa cells overexpressing either MICU1.1^{AAAA}, MICU1.1 or MICU1 with mitochondrially targeted aequorin upon sequential exposure to crescent $[Ca^{2+}]$, as indicated in the graph. Data are presented as mean ± SD. n=4;

C) $[Ca^{2+}]_{mt}$ measurements in permeabilized HeLa cells overexpressing MICU1.1^{AAAA} together with MICU2 and mitochondrially targeted aequorin. Cells were perfused sequentially with solutions at crescent $[Ca^{2+}]$, as indicated in the graph. Data are presented as mean ± SD. n=4.

homodimer in modulating mitochondrial Ca^{2+} uptake (Figure 22B). In this condition, the kinetic profile of $MICU1^{AAAA}$ is indistinguishable from MICU1 (Figure 22B). We then verified the effect of this mutant when overexpressed together with MICU2 in HeLa cells. Also in this condition, we did not observe any difference with cells overexpressing MICU1-MICU2 (Figure 22C).

In conclusion, although single mutations of the extra-exon did not show a significant difference in MICU1.1 activity, the substitution of all four residues confirms that this domanin is responsible of the activatory function of MICU1.1

MICU1.1 expression levels during the progression of denervation atrophy

In order to establish whether the expression levels of MICU1.1 is affected in physiopathological conditions and since MICU1.1 is expressed prevalently in skeletal muscle, we focused our attention on skeletal muscle denervation atrophy.

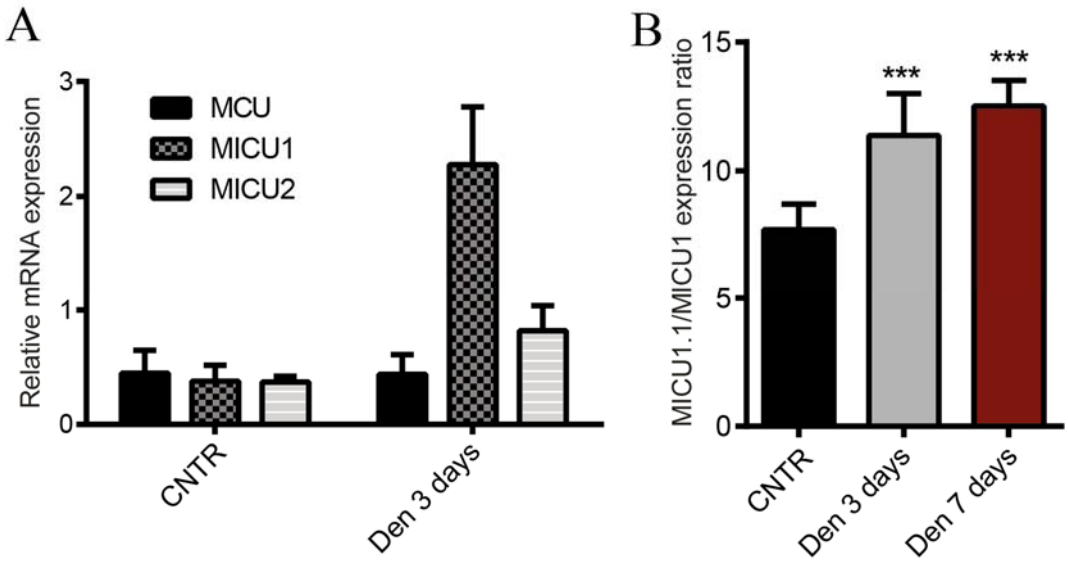

Figure 23 – MCU complex component expression levels during the progression of denervation atrophy.

*A) MCU, MICU1 and MICU2 relative mRNA expression levels in control mouse tibialis anterior (TA) muscles TA muscles denervated for 3 days measured by Real-time PCR, normalized for GAPDH. Expression levels are normalized for GAPDH and quantification data are expressed with ΔCt methods. Data are presented as mean ± SD. n=4 ***p<0.005;*

*B) MICU1.1/MICU1 expression ratio of control TA muscles and TA muscles after 3 and 7 days after denervation (2^ΔCt MICU1.1/ 2^ΔCt MICU1 ratio). Expression levels are normalized for GAPDH. Data are presented as mean ± SD. n=4 ***p<0.005.*

We analysed the expression of the uniporter complex components during the progression of denervation of tibialis anterior (TA) mouse muscles. For this purpose, we unilaterally cut the sciatic nerve of 4 mice for each condition to induce atrophy of the hindlimb and we collected TA muscles 3 and 7 days after denervation. It is well established that cutting the sciatic nerve produces significant atrophy of TA muscles in mouse models [86,87], and this catabolic state involves a precise transcriptional program [88–90]. In line with this, we found that the components of MCU are differentially regulated during denervation atrophy. Indeed, while the expression of pore-forming subunit MCU is not perturbed, MICU1, which comprises both MICU1 and MICU1.1, is strongly induced and, at lower extent, also MICU2 expression increases (Figure 23A). Noteworthy, in this condition, the ratio between MICU1.1 and MICU1 increases dramatically during the progression of atrophy, starting from a ratio of 8:1 in control muscles to a ratio of 14:1 at 7 days after the cut of the sciatic nerve (Figure 23B).

Discussion

The ability of mitochondria to accumulate Ca^{2+} is fundamental for the regulation of several biological processes. Importantly, mitochondrial Ca^{2+} uptake enables these organelles to shape cytosolic Ca^{2+} transients, resulting in mitochondrial control over intracellular Ca^{2+} signalling. Moreover, mitochondrial Ca^{2+} has a pivotal role in cell survival, since it has already been demonstrated that mitochondrial Ca^{2+} overload is an important trigger of apoptosis [1].

Another crucial function of mitochondrial Ca^{2+} is the modulation of ATP production by oxidative phosphorylation. Indeed, it has been demonstrated that Ca^{2+} can modulate mitochondrial metabolism [45]. This concept was strengthened by the evidence that mitochondrial Ca^{2+} controls the rate of autophagy, since it has been shown that decreased mitochondrial Ca^{2+} uptake results activation of AMPK, which activates pro-survival macroautophagy [91]. Altogether, these results strongly support the role of mitochondrial Ca^{2+} uptake in regulating essential cellular processes such as mitochondrial respiration and maintenance of normal cell bioenergetics.

Furthermore, it is known for many decades that the MCU complex exhibits tissue-specific properties. This concept was made stronger by experiments of direct patch-clamp recordings of the Ca^{2+} current through MCU (I_{MCU}) in mitoplasts derived from mitochondria of different tissues [3]. The molecular basis of these differences are still poorly understood and how this complex machinery is modulated in different tissues and physiopathological conditions is still an open question. One sticking and still mysterious example of this regulation is that MCU current (I_{MCU}) in mouse heart is extremely lower than in other mouse tissues [3]. In particular, in heart, I_{MCU} is 30 times smaller than in skeletal muscle although in heart mitochondria occupy the 37% of the volume, while in skeletal muscle only the 5%.

Tissue-specific differential expression of the components of the MCU complex as well as post-translational and post-transcriptional modifications could explain the different Ca^{2+} accumulation in different tissues. Indeed, it has been shown that all these mechanisms act on the regulation of MCU activity in different tissues in physiological and pathological conditions [50,76,77,92].

Here we found an additional new regulatory mechanism modulating mitochondrial Ca^{2+} uptake: alternative splicing. Indeed, during PCR experiments to clone murine MICU1 from a skeletal muscle cDNA library, we discovered an alternative splice isoform of MICU1 that we named MICU1.1. This variant is characterized by the addition of a micro-exon coding for 4 amino acids (EFWQ) located in the intron between exon 5 and exon 6.

We decided to study in detail this splice variant first because we found that MICU1.1 is present in humans and conserved in all vertebrates and second because other crucial modulators of Ca^{2+} homeostasis are subjected to alternative splicing events. Indeed, it has been recently discovered an alternative splice variant of STIM2, a pivotal player in the Store-Operated Ca^{2+} Entry (SOCE), in which a micro-exon insertion in STIM2 mRNA disables this variant from activating Orai1 [93,94].

Interestingly, MICU1.1 shows a peculiar tissue expression. Indeed, while MICU1 is ubiquitously expressed, MICU1.1 expression is restricted to tissues with the greatest levels of mitochondrial Ca^{2+} uptake, skeletal muscle and, at lower levels, brain. Strikingly, in skeletal muscle, MICU1.1 is the predominant isoform, suggesting that in this tissue it might play a peculiar function in regulating mitochondrial Ca^{2+} uptake.

We decided to characterize this splice variant first by evaluating its ability to interact with the other pore complex components. We observed no differences in the ability of MICU1.1 to interact with MCU and with MICU2. Furthermore, MICU1.1 can heterodimerize with MICU2 as well as MICU1 and it can also give rise to high molecular weight complexes of the same molecular weights as MICU1. Thus, MICU1.1 seems indistinguishable form MICU1 from the biochemical point of view (Figure 1). Noteworthy, the region in which the extra exon is inserted has not been resolved in the crystal structure of MICU1 [95], suggesting that is a flexible region possibly involved in interaction with known or unknown MCU complex components.

We then asked what was the effect of MICU1.1 on mitochondrial Ca^{2+} uptake. It has recently been demonstrated that MICU1 is the MCU activator at high $[Ca^{2+}]_{cyt}$ and for the prompt response of mitochondria to $[Ca^{2+}]_{cyt}$ increases (Figure

3B). On the other hand, MICU2 is MCU genuine gatekeeper that inhibits MCU activity at low $[Ca^{2+}]_{cyt}$ [52], ensuring minimal Ca^{2+} accumulation in the presence of a huge driving force for cation accumulation, thus preventing the deleterious effects of Ca^{2+} cycling and matrix overload (Figure 3A).

Surprisingly, MICU1.1, when overexpressed in HeLa cells, causes a major increase of mitochondrial Ca^{2+} uptake upon histamine stimulation that exceeds the one induced by the overexpression of MICU1. This effect is specific, as membrane potential is not perturbed by the overexpression of MICU1.1 and cytosolic Ca^{2+} is rather reduced, most likely due to increased Ca^{2+} clearance by mitochondria, as already observed for the overexpression of MCU [47]. We also confirmed that human MICU1.1 exerts the same activatory role on mitochondrial Ca^{2+} uptake.

We also checked whether endogenous MICU1 interferes with MICU1.1 effect, being the two variants able to form dimers. In MICU1 silenced HeLa cells, MICU1.1 overexpression exerts the same activatory effect on MCU.

Enhanced mitochondrial Ca^{2+} uptake mediated by MICU1.1 was confirmed also in permeabilized cells. This experiment allows the evaluation of mitochondrial Ca^{2+} uptake independently from Ca^{2+} released from the endoplasmic reticulum and the formation of microdomains of high $[Ca^{2+}]$ in close proximity to mitochondrial Ca^{2+} channels. Strikingly, MICU1.1 overexpression is accompanied by an increase of about the 50% of mitochondrial Ca^{2+} uptake speed compared to cells overexpressing MICU1.

Since this strong activatory effect of MICU1.1, we decided to better characterize the ability of MICU1.1 to modulate MCU activity trying to recapitulate the MCU machinery *in vitro* in planar lipid bilayer. These experiments demonstrate that MICU1.1 acts as a strong MCU activator in these conditions. Surprisingly, we did not observe major differences between MICU1 and MICU1.1. This could suggest that MICU1.1 is important in the threshold definition of MCU, reason why we did not detect a significant difference. Other experiments have to be performed to fully characterized MICU1.1, analyzing the behavior of MICU1.1 when heterodimerized with MICU2, a condition in which, differently from MICU1, we observed a cooperative activation of the MCU activity.

It is known that in physiological conditions the heterodimer MICU1-MICU2 is the prevalent form [52]. We thus studied the effect of this new splice variant in a more physiological condition. We thus overexpressed MICU1 and MICU1.1 together with MICU2 in HeLa cells in order to shift the balance towards the MICU1-MICU2 and MICU1.1-MICU2 heterodimers. It has been demonstrated that MICU2 prevents the mitochondrial Ca^{2+} uptake increase due to MICU1 [52] but, strikingly, MICU2, when overexpressed with MICU1.1, is unable to inhibit the induction of mitochondrial Ca^{2+} uptake caused by MICU1.1 overexpression. Moreover, in permeabilized cells mitochondrial Ca^{2+} uptake speed is not decreased, as observed overexpressing MICU1-MICU2 heterodimers but, unexpectedly, it increases far more than in cells transfected only with MICU1.1, suggesting that MICU2 synergistically activates mitochondrial Ca^{2+} uptake when bound to MICU1.1. Overall, we can conclude that MICU1.1-MICU2 heterodimer acts as a strong activator of the MCU complex in conditions of high $[Ca^{2+}]$.

Since it was shown that MICU2 acts as the gatekeeper of the channel at low $[Ca^{2+}]_{cyt}$ (Figure 3A) and our data demonstrate that the MICU1.1-MICU2 dimer acts as a strong activator of the channel at high $[Ca^{2+}]_{cyt}$, we decided to assess whether the MICU1.1-MICU2 heterodimer is able to act as gatekeeper of the channel in resting conditions. Surprisingly, the heterodimer MICU1.1-MICU2 is able to act as gatekeeper of the channel as well as MICU1-MICU2 heterodimer. We demonstrated this property by two gatekeeper reconstitution assays in which we analysed the effect of the different modulators in regulating the activity of free MCU oligomers, not bound to both MICU1 and MICU2. We obtained this by either overexpressing MCU, which favours the condition in which the channel is present in the mitochondrial membrane without its gatekeeper and by silencing MICU1, condition that destabilizes also MICU2 protein. Both this approaches clearly showed that also the MICU1.1-MICU2 dimer causes minimal Ca^{2+} uptake at low $[Ca^{2+}]_{cyt}$.

We then tried to deepen our knowledge of the mechanism by which the MICU1.1-MICU2 dimer strongly activates MCU at high $[Ca^{2+}]_{cyt}$. One possible mechanism is that the MICU1.1-MICU2 dimer cooperatively activates mitochondrial Ca^{2+} uptake at lower $[Ca^{2+}]_{cyt}$. We thus hypothesized that the

MICU1.1-MICU2 dimer can shift to the left the $[Ca^{2+}]_{cyt}$ mitochondrial Ca^{2+} uptake curve (Figure 2). To analyse this aspect, we performed an experiment in permeabilized conditions in which, after digitonin treatment, mitochondria were subjected to crescent $[Ca^{2+}]$. In these conditions, as hypothesized, mitochondria overexpressing MICU1.1 and MICU2 take up Ca^{2+} at $[Ca^{2+}]$ at which mitochondria transfected with the MICU1-MICU2 heterodimer show only a mild uptake.

These results highlight the possible role of the prevalent expression of MICU1.1 in excitable tissues where Ca^{2+} plays a pivotal functional role. We demonstrated that, at resting conditions, this splice isoform does not induce Ca^{2+} entry inside mitochondria, thus ensuring protection from Ca^{2+} overload and cell death but, upon cell stimulation, it ensures a fast and high Ca^{2+} entry in mitochondria even at low $[Ca^{2+}]_{cyt}$. Intriguing, this can be an important mechanism in excitable tissues where fast Ca^{2+} transients occur [96–98]. Indeed, we can speculate that in skeletal muscle the prevalent expression of MICU1.1 allows a prompt response of mitochondria metabolism, ensuring a sustained ATP production during resistance and strenuous exercise.

We also analysed the Ca^{2+}-dependent regulation of the MICU1.1-MICU2 heterodimer. For this purpose, we mutated the EF-hand motives of MICU1.1 ($MICU1.1^{EFmut}$) in order to prevent Ca^{2+} binding to this protein. As shown also for MICU1 [52,59,66], these domains are fundamental for MICU1.1 activity in stimulated cells, since their mutation completely abrogates MICU1.1 activity. We also overexpressed MICU1.1 with a MICU2 mutant whose EF-hands are unable to bind Ca^{2+} ($MICU2^{EFmut}$). It has been shown that this mutant is capable of inhibiting Ca^{2+} uptake also in conditions of high $[Ca^{2+}]_{cyt}$ and to prevent MICU1-dependent activation of MCU in stimulated cells. Interestingly, MICU1.1 is less affected by the dominant-negative effect of $MICU2^{EFmut}$, compared to MICU1. This result suggests that MICU1.1 regulation of MCU activity is partially independent from MICU2. Indeed, while MICU1 is subjected to a tight regulation by MICU2 at high $[Ca^{2+}]$, MICU1.1 seems to act, at least in part, independently from the gatekeeper function of MICU2.

We also asked whether one of the four additional residues was required for MICU1.1 activity. Our data demonstrate that neither the single substitution with

alanine nor the deletion of single amino acids influence significantly the activity of MICU1.1. Only the substitution of all the four amino acids of the extra-exon with alanine is able to blunt MICU1.1 activity, recapitulating MICU1 function. Further studies are necessary in order to understand whether double or triple mutations of the amino acids composing the extra exon can affect the peculiar behaviour of MICU1.1 and possibly, since MICU1 crystal structure is available [82], using bioinformatics analysis, we might predict the three-dimensional structure of this domain.

Overall, the newly identified alternative splice variant of MICU1 represents a novel mechanism of regulation of mitochondrial Ca^{2+} uptake in excitable tissues that contributes to explain the tissue-specific regulatory properties of MCU. Indeed, the peculiar expression profile of this splice variant correlates with the highest mitochondrial Ca^{2+} uptake currents [3].

Our hypothesis is that, in skeletal muscle, mitochondrial Ca^{2+} uptake is more efficient in order to sustain the huge ATP consumption needed for contraction. In the future, we will characterize the functional properties of this new isoform in regulating mitochondrial Ca^{2+} uptake in physiological contests. Indeed, we found that C2C12 mouse muscle cell line expresses this splice variant only upon myotube differentiation. We will take advantage from this system to understand the physiological role of this alternative splice variant in the skeletal muscle homeostasis *in vitro*. Specifically, we will modulate the expression of this variant and measure ATP production and oxygen consumption rate.

We will also analyse mitochondrial Ca^{2+} dynamics in skeletal muscle *in vivo*. First, we will evaluate the effects of an acute silencing of MICU1.1 and MICU2 through specific shRNA delivered by adeno-associated viruses (AAVs). Simultaneously, we will carry out experiments in which we will assess the effects of overexpressing MICU1.1 together with MICU2 by AAVs infection. We will evaluate the effects of these treatments on muscle trophism and on known signalling pathways involved in atrophy and hypertrophy.

Furthermore, we will specifically substitute the expression of MICU1.1 with MICU1 in skeletal muscle. To do this, we plan to remove MICU1.1 extra-exon by CRISPR/Cas9-mediated non homologous end joining (NHEJ) in postnatal muscle

tissues, following delivery of gene editing components using AAVs, as already performed [99]. In detail, we will produce AAV viral particles expressing Cas9 that we will inject in tibialis anterior mouse muscles together with an AAV expressing the guide RNA and GFP in order to visualize the infected fibers. CRISPR/Cas9-mediated NHEJ will thus create an internal genomic deletion to bypass the transcription of the MICU1.1 extra-exon. In this way, only MICU1 will be expressed and thus we will study the specific role of MICU1.1 in skeletal muscle. This approach has been recently used with success to correct the DMD mutations in postnatal muscle tissues in mdx mouse model [99].

Strong preliminary data support the hypothesis that MICU1.1 modulation of $[Ca^{2+}]_{mt}$ can be a major determinant of skeletal muscle homeostasis. First, it has been recently shown that the lack of MICU1, due to loss-of-function mutations preventing its expression, leads to mitochondrial Ca^{2+} overload under basal conditions, and this results in an autosomal recessive human disease with muscle phenotype characterized of proximal muscle weakness and learning difficulties [64]. Importantly, muscle weakness is accompanied by moderately to grossly elevated serum creatine kinase levels. In line with the symptoms, muscle biopsies showed myopathic features, with diffuse variation in fiber size, increased frequency of internal and central nuclei, and clusters of regenerating fibers. Second, it was recently demonstrated that mitochondrial Ca^{2+} has a dramatic trophic effect that impinges on two major hypertrophic pathways of skeletal muscle, PGC-1α4 and IGF1-Akt/PKB [79]. Microarray analyses demonstrated that MCU modulation controls global gene expression, thus identifying a Ca^{2+}-dependent mitochondria-to-nucleus route that links mitochondrial function to the control of muscle mass. Third, MCU knockout mice show clear metabolic and functional alterations of skeletal muscle [78].

Further evidence in support of the central role of mitochondrial Ca^{2+} in muscle homeostasis is provided by the observation that the components of the mitochondrial Ca^{2+} uniporter are differentially regulated during the catabolic state induced in TA mouse muscles by sciatic nerve dissection. Strikingly, the expression of the pore-forming subunit MCU is not perturbed, while the expression of the regulatory subunits MICU1 (which comprises both MICU1 and MICU1.1) and

MICU2 are significantly induced during the progression of atrophy. This result strongly suggests that mitochondrial Ca^{2+} modulation plays an important role in skeletal muscle fibers adaptation to physiological and pathological stresses. Noteworthy, in this condition the ratio between MICU1.1 and MICU1 increases dramatically, starting from a ratio of 8:1 to a ratio of 14:1 at 7 days after the cut of the sciatic nerve, suggesting a precise control of splicing events in pathological conditions of skeletal muscle.

Overall, these data demonstrate a muscle-specific mitochondrial Ca^{2+} uptake machinery with a presumably unique function and further experiments have to be performed to clarify its physiological and pathological relevance.

Materials and methods

Legend of abbreviation

bp = base pair;
cDNA = DNA complementary to RNA;
DDM = n-dodecyl-β-D-maltoside;
DMEM = Dulbecco's modified Eagle's medium;
FBS = fetal bovine serum;
g = gravity;
g = grams;
HCl = hydrochloric acid;
KCl = potassium chloride;
HS = horse serum;
Hz = Hertz
KH_2PO_4 = potassium phosphate;
M = molar;
min = minutes;
mL = milliliters;
ms = milli seconds;
NaCl= sodium chloride;
NaOH = sodium hydroxide;
Na_2HPO_4 = sodium hydrogen phosphate;
nm = nanometers;
$NaHCO_3$ = sodium bicarbonate;
PBS = Phosphate-buffered saline;
PCR = polymerase chain reaction;
rpm = revolutions per minute;
RT = room temperature;
SDS = sodium dodecyl sulfate;
s = seconds;
TA = tibialis anterior;
PFA = paraformaldehyde;
μL = microliters;

RNA extraction, reverse transcription, and quantitative Real-Time PCR

For the expression analysis of MICU1 and MICU1.1 in mouse tissues, adult male CD1 mice (28-30 g) were used. Skeletal muscle (tibialis anterior (TA)), heart, brain, spleen, lung, liver, kidney and visceral fat were excised from three age-matched animals. Total RNA was extracted through mechanical tissue homogenization in TRIZOL reagent (Thermo Fisher Scientific) following manufacturer instructions. The RNA was quantified with Nanodrop (Thermo Fisher Scientific) and 1 µg of total RNA of each samples was retro-transcribed with the cDNA synthesis kit SuperScript II (Thermo Fisher Scientific). Oligo(dT)$_{12-18}$ primer (Thermo Fisher Scientific) were used as a primer for first stand cDNA synthesis with reverse transcriptase. The obtained cDNA was analyzed by Real-Time PCR using the IQ5 thermocycler and the SYBR green chemistry (Bio-Rad). The primers were designed and analyzed with Primer3 [100]. Primers efficiency was tested by performing standard curves and the efficiency of all primers was between 90% and 110%. The housekeeping gene *TXN1* was used as an internal control for cDNA normalization. For quantification, expression levels were calculated by using the $2^{-\Delta\Delta Ct}$ method. Real-Time PCR primer sequences were as follows:

GAPDH:
Fw 5'-CACCATCTTCCAGGAGCGAG-3'
Rv 5'-CCTTCTCCATGGTGGTGAAGAC-3'

TXN1:
Fw 5'-GGCTTCAAGCTTTTCCTTGTT-3'
Rv 5'-TCCAATGTGGTGTTCCTTGA-3'

MICU1 all isoforms:
Fw 5'-AAGGCAGCATCTTCTACAGCC-3'
Rv 5'-CCTGCTCAAACTCCTCCATGT-3'

MICU1 splice variant specific (NM_144822.3):

Fw 5'-GCGCTTTGATGGAAAGAAAATTGC-3'
Rv 5'-TGTCTACCTCTCCGTCTCCA-3'

MICU1.1 splice variant specific (NM_001291443.1):
Fw 5'-CTTTGATGGAAAGGAGTTCTGGC-3'
Rv 5'-CCTCCATGTCTACCTCTCCGT-3'

MCU:
Fw 5'-AAAGGAGCCAAAAAGTCACG-3'
Rv 5'-AACGGCGTGAGTTACAAACA-3'

MICU2:
Fw 5'-TGGAGCACGACGGAGAGTAT-3'
Rv 5'-GCCAGCTTCTTGACCAGTGT-3'

The same samples of cDNA were used for standard PCR. Primers that span the extra-exon were designed with Primer3 and the PCR reaction was performed with 2x PCR master mix (Thermo Fisher Scientific). Electrophoresis separation of the PCR products was performed using acrylamide precast gels 20% in TBE buffer (Thermo Fisher Scientific) and DNA bands were detected thanks to GelRed nucleic acid gel stain (Biotium) after UV exposure. PCR primer sequences were as follows:

Fw: 5'-GAACACTTGGGCCTGGATCA-3'
Rv: 5'-GAAGGAGATGAGCCCACACT-3'

Product size 152 bp for MICU1.1 and 140 bp for MICU1.

Cell culture and transfection

HeLa cells and C2C12 cells (ATCC) were cultured in DMEM (Thermo Fisher Scientific), supplemented with 10% FBS (Thermo Fisher Scientific), containing penicillin (100 U/ml) and streptomycin (100 μg/ml). Fully confluent C2C12 cells were differentiated in myotubes for 7 days using DMEM supplemented with 2% HS (Life Technologies)

Cells were transfected with a standard Ca^{2+}-phosphate procedure. Briefly, the solution containing the desired amount of DNA and 250 mM $CaCl_2$ was added quickly to an equal volume of HEPES Buffered Solution (HBS, 280 mM NaCl, 50 mM Hepes, 1.5 mM Na_2HPO_4, pH 7.12). The solution was then added directly to the cell monolayer. 8-16 hours after addition of the transfection mix, cells were washed with PBS until the excess of precipitate is completely removed. Experiments were carried out 24-36 hours after transfection. Mock vectors (i.e., pcDNA3.1 or pEGFP-N1) were used as controls in all overexpression experiments. In parallel, a non-targeting siRNA (i.e., siRNA-scrambled) was used as a control in all silencing experiments.

siRNA and constructs

Mouse MICU1.1 was amplified from mouse skeletal muscle cDNA by For the cloning of MICU1.1-HA in pcDNA3.1:

fw: 5'-CGGATCCGCCACCATGTTTCGTCTTAACACCCT-3'
rv: 5'-GCTCGAGTCACAGGGAAGCGTAGTCAGGCACATCGTAGGGGTATTTGG GCAGAGCAAAGTCCC-3'

The PCR fragment was cloned into BamHI and XhoI sites in pcDNA3.1 (Thermo Fisher Scientific).

To silence MICU1 specific leading siRNA sequences were designed:

siRNA-MICU1#1: 5'-UCUGAAGGGAAAGCUGACAAU-3'

All the siRNAs and the non-targeting siRNA (siRNA-scrambled, MISSION siRNA Universal Negative Control #1, cat no. SIC001) were purchased from Sigma-Aldrich. pcDNA3.1-MCU-Flag, pcDNA3.1-MICU1-HA, pcDNA3.1-MICU2-Flag, pcDNA3.1-MICU1^{EFmut}-HA, pcDNA3.1-MICU2^{EFmut}-Flag, pcDNA3.1-4mtGCaMP6f were previously described [47,52].

Mutagenesis

To create the mutant MICU1.1^{D233A,E244K,D423A,E434K}, pcDNA3.1-MICU1.1-HA was mutagenized using the following primers:

5'-
TGAAATTGCTTTCAAGATGTTT**GCC**TTGAATGGAGACGGAGAGGTAGACATGGAG**AA**
GTTTGAGCAGGTTCAGAGC-3'
5'-
GTGGTGTTCGCGCTCTTT**GCC**TGTGATGGCAATGGGGAGCTGAGCAACAAG**AAG**TTC
GTTTCCATCATGAAGC-3'

To create the mutant MICU1.1^{E182A}, pcDNA3.1-MICU1.1-HA was mutagenized using the following primers:

5'-TAAAGCGCTTTGATGGAAAG**GCT**TTCTGGCAGAAAATTGCCCAG-3'

To create the mutant MICU1.1^{F183A}, pcDNA3.1-MICU1.1-HA was mutagenized using the following primers:

5'-AGCGCTTTGATGGAAAGGAG**GCT**TGGCAGAAAATTGCCCAGGA-3'

To create the mutant MICU1.1^{W184A}, pcDNA3.1-MICU1.1-HA was mutagenized using the following primers:

5'-CGCTTTGATGGAAAGGAGTTC**GCG**CAGAAAATTGCCCAGGAAC-3'

To create the mutant MICU1.1^{Q185A}, pcDNA3.1-MICU1.1-HA was mutagenized using the following primers:

5' TTTGATGGAAAGGAGTTCTGG**GCG**AAAATTGCCCAGGAACGAG 3'

To create the mutant MICU1.1$^{\Delta E182}$, pcDNA3.1-MICU1.1-HA was mutagenized using the following primers:

5'-AATAAAGCGCTTTGATGGAAAGTTCTGGCAGAAAATTGCCCAG-3'

To create the mutant MICU1.1$^{\Delta F183}$, pcDNA3.1-MICU1.1-HA was mutagenized using the following primers:

5'-AGCGCTTTGATGGAAAGGAGTGGCAGAAAATTGCCCAGGA-3'

To create the mutant MICU1.1$^{\Delta W184}$, pcDNA3.1-MICU1.1-HA was mutagenized using the following primers:

5'-CGCTTTGATGGAAAGGAGTTCCAGAAAATTGCCCAGGAACG-3'

To create the mutant MICU1.1$^{\Delta Q184}$, pcDNA3.1-MICU1.1-HA was mutagenized using the following primers:

5'-TTTGATGGAAAGGAGTTCTGGAAAATTGCCCAGGAACGAGAA-3'

To create the mutant MICU1.1^{E182A,F183A,W184A,Q185A}, pcDNA3.1-MICU1.1-HA was mutagenized using the following primers:

5'-TAAAGCGCTTTGATGGAAAG**GCCGCCGCCGCC**AAAATTGCCCAGGAACGAGAA-3ì

Mutagenesis was performed as previously described [101,102].

Western blotting and Antibodies

To monitor endogenous and overexpressed proteins, cells were lysated in RIPA-buffer (150 mM NaCl, 50 mM Tris, 1 mM EGTA, 1% Triton X-100, 0.1% SDS) and after 30' of incubation on ice, 40 μg of total proteins were loaded, according to BCA quantification (Thermo Fisher Scientific). Proteins were separated by SDS-PAGE electrophoresis, in commercial 4-12% acrylamide gels (Thermo Fisher Scientific) and transferred on nitrocellulose membranes (Thermo Fisher Scientific) by wet electrophoretic transfer. Blots were blocked 1 hour at RT

with 5% non-fat dry milk (BioRad) in TBS-tween (0.5M Tris, 1.5M NaCl, 0.01% Tween) solution and incubated at 4°C with primary antibodies. Secondary antibodies were incubated 1 hour at RT. Washes after antibody incubations were done on an orbital shaker, three times for 10 minutes each, with TBS-tween. We used the following antibodies: α-Flag and α-HA (1:1000, Cell Signaling Technologies), α-MICU1 (1:1000, Sigma-Aldrich), α-MICU2 (1:1000, Abcam). Secondary, isotype-specific HRP-conjugated antibodies (1:5000) were purchased from BioRad.

Co-immunoprecipitation

For co-immunoprecipitation experiments, HeLa cells were transfected with a calcium-phosphate procedure. After 48 hours of expression cells were lysate in an appropriate volume of lysis buffer (150 mM NaCl, 0.5% DDM, 50 mM Tris-HCl pH 7.4, 1 mM EGTA-Tris pH 7.4 and Complete EDTA-free protease inhibitor mixture (Roche Applied Science)). 1 mg of proteins from the different conditions was incubated with 20 µL of monoclonal α-Flag-Agarose antibody (Sigma-Aldrich) overnight in rotation. The day after, agarose beads were washed 3 times with lysis buffer and the immune-complexes were broken by heating at 95°C for 5 minutes in SDS-sample buffer (Thermo Fischer Scientific). The co-immunoprecipitated proteins were separated by SDS-PAGE gel electrophoresis, transferred to nitrocellulose membrane (Thermo Fisher Scientific) and stained with Ponceau S solution.

Mitochondrial purification from mouse tissues

Purification of mitochondria was performed from mice skeletal muscle and liver. Adult male (3-4 months old) CD1 mice were used for all the experiments. The tissues of interest were rapidly collected from mice sacrificed by cervical dislocation and conserves in ice-cold PBS. Tissues were washed twice with ice-cold PBS in order to remove the blood. The tissues were minced into small pieces using scissors in a small volume of homogenization buffer (HB, 250 mM Sucrose,

20 mM HEPES, 10 mM KCl and 1 mM EGTA). The pieces were homogenized using a glass potter and the homogenates were collected in a 50 mL tube. The samples were centrifuged for 10 minutes at 1000xg in a 4°C refrigerated centrifuge. The supernatants containing mitochondria were collected and centrifuged at 10000xg for 20 minutes to precipitate the mitochondria enriched fraction. The pellets were washed with ice-cold HB and pelleted at 10000xg for 3 times. Mitochondrial protein extraction was performed with lysis buffer provided in the NativePAGE Sample Prep Kit (Thermo Fisher Scientific) with 1% DDM.

BlueNative-Polyacrylamide gel electrophoresis (BN-PAGE)

BlueNative-gels were provided by Thermo Scientific and BN-PAGE was performed following the manufacturing protocol. In BN-PAGE, the Coomassie G-250 was used to confer a net negative charge to the proteins, while maintaining the proteins in their native state without any protein denaturation. The G-250 is present in the cathode buffer to provide a continuous flow of G-250 into the gel, and is added to samples containing non-ionic detergent prior to loading the samples onto the gel. The binding of G-250 to proteins offers several advantages resulting in high-resolution native electrophoresis [103]. First, the proteins with basic isoelectric points (pI) normally have a net positive charge that are converted to proteins with a net negative charge, allowing the proteins to migrate in one direction towards the anode. Second, membrane proteins and proteins with significant surface-exposed hydrophobic area are less prone to aggregation as G-250 binds non-specifically to hydrophobic sites converting them to negatively charged sites. The mitochondria were lysed using the NativePAGE sample buffer (Thermo Fisher Scientific) supplemented with 0.5% DDM (Sigma Aldrich). Crude extracts were centrifuged at 15000xg for 10 minutes to remove debris, and proteins in the supernatant were quantified using the BCA Protein Assay Kit (Thermo Fisher Scientific). 20 µg of proteins were dissolved in 1x NativePAGE sample buffer (Thermo Fisher Scientific) and the samples were loaded in a NativePAGE Novex 4–16% Bis-Tris Gels, that is able to resolve proteins in the molecular weight range

of 15-1,000 kDa. We used the NativeMark Unstained Protein Standard designed for molecular weight estimation of proteins, that was stained with Colloidal Blue Staining Kit (Thermo Fisher Scientific).

Baculovirus/insect cells system and protein affinity purification

Mus musculus MICU1, MICU1.1 and MICU2 coding sequences were cloned in the pFH vector suitable for expression in insect cell. MICU1 and MICU1.1. were cloned in frame with a 6xhistidine-tag sequence at the N-terminus. The baculovirus production and insect cells infection were performed as previously described [104].

The insect cells were collected by centrifugation at 6,000xg for 10 minutes at 4 °C. The cell pellet was resuspended in lysis buffer (50mM Tris HCl pH 8, 200mM NaCl, 10% glycerol, 10mM imidazole, 1 mM DTT and 1 mM PMSF) and lysed in a French press (at 1.35 kbar; One Shot Constant System Cell Disrupter, from Constant Systems Ltd). A clarified crude extract was then obtained by centrifugation (20.000xg, 40 minutes, 4°C) and incubated 2 hours at 4 °C under mild shaking with 1 ml of nickel affinity gel (HIS-Select nickel affinity gel, Sigma-Aldrich). At the end of this incubation, the mix was transferred into a chromatography column. The column was then washed with 5 volumes of lysis buffer, and after that the tagged proteins were eluted with 5 volumes of lysis buffer containing 300 mM imidazole. The elution fractions were pooled together, analysed by 12% Bis-Tris gel (NuPage, Thermo Fisher Scientific). For immunoblotting analysis, the gel was blotted on a nitrocellulose membrane that was probed with a monoclonal α-6xHis tag (Cell Signaling) or α-MICU2 (AbCam) antibody. To isolate the oligomeric state corresponding to the heterodimer MICU1-MICU2 and MICU1.1-MICU2, the affinity purified fractions were subjected to gel filtration chromatography. Gel filtration was performed with a Superdex 200GL 10/30 (GE Healthcare), equilibrated in 25 mM Tris-HCl pH 7,4, 150mM NaCl. The run was performed by injecting 500 µl of the sample at a flow rate of 0.5 ml/min.

For bilayer experiments 2 mM EGTA is added to the samples to remove the residual Ca^{2+}. The buffer is then replaced with 25 mM Tris-HCl pH 7,4, 150mM NaCl using PD10 column (GE Healthcare).

Heterologous proteins expression

Mus musculus MCU cDNA sequence was cloned in pIVEX1.4WG, suitable for *in vitro* expression. *In vitro* expression of pIVEX1.4WG:MCU was performed by using Wheat Germ CECF Kit (Roche), as previously reported [50]. After expression, the MCU was incorporated into proteoliposomes for bilayer experiments as previously described [47,50,52].

Mus musculus MICU1 and MICU1.1 cDNAs were cloned into a pACYC Duet vector (Novagen), suitable for heterologous expression in *Escherichia coli*, in frame with a StrepII tag coding sequence at the N-terminus. The sequences were optimized for prokaryotic expression and the first 96 amino acids were deleted to avoid aggregation, as previously observed [82]. *E. coli* BL21(DE3) cells were transformed with the recombinant plasmids and positive clones selected by antibiotic resistance. Transformed cells were grown overnight in selective LB medium and then subcultured the following day in fresh medium. The expression of the proteins was induced by adding 0.5 mM isopropyl-thiogalactopyranoside and incubating the cells at 22°C overnight. For protein purification, cells were harvested by centrifugation, resuspended in lysis buffer (25 mM Tris-HCl, pH 7.4, 200 mM NaCl, and 1 mM PMSF) and lysed by French press (at 1.35 kbar; One Shot Constant System Cell Disrupter, from Constant Systems Ltd). The supernatant fractions were isolated from the cells debris by centrifugation (20.000xg, 30 minutes, 4°C). Both proteins were purified to homogeneity by combining an affinity chromatography (StrepTactin-Sepharose suspension, IBA) and a gel filtration chromatography. Gel filtration was performed with a Superdex 200HR 10/30 (GE healthcare). For bilayer experiments 2 mM EGTA was added to the samples to remove the residual Ca^{2+}. The buffer is then replaced with 25 mM Tris-HCl pH 7,4, 150mM NaCl using PD10 column (GE Healthcare).

Electrophysiological experiments

A Warner Instruments electrophysiological planar bilayer apparatus was used. Bilayers were prepared using purified soybean asolectin dissolved in decane (Sigma-Aldrich) containing 1% chloroform (Sigma-Aldrich) across a 250 μM hole in a polystyrene cuvette (Warner Instruments). Asolectin was purified by precipitation with cold acetone from a chloroform solution. The lipid membrane divided the *trans* and the *cis* compartments.

When a bilayer membrane was formed, currents across the membrane elicited by different voltage pulses were measured and the membrane resistance could be determined. A bilayer membrane was considered to be satisfactory for further experiments if it exhibited an approximately 150–200 pF capacity. The volumes of the *cis* and *trans* compartments were 3 ml, that were stirred with a small magnetic bar upon need (e.g. after addition of proteins). Both sides were connected to the electrodes via salt bridges (1 M KCl) in series with Ag/AgCl electrodes. All voltages reported are those of the *cis* chamber, zero being assigned by convention to the *trans* (grounded) side. Currents are considered as positive when carried by cations flowing from the *cis* to the *trans* compartment.

The standard experimental medium was 100 mM Na-gluconate, 10 mM HEPES and 5 mM EDTA (pH 7.4). The Ca^{2+}-containing solution was the same but we added $CaCl_2$ resulting in 1 μM free Ca^{2+} as calculated on WebMaxC version 2.2 (http://www.stanford.edu/~cpatton/maxc.html).

20 control experiments with empty membrane or with regulators alone (no MCU in the experiments) showed no activity in any of the above solutions. All measurements were carried out at room temperature.

Data were acquired using a Bilayer Clamp amplifier (Warner Instruments, USA) at 100 μs/point, filtered at 300 Hz and analysed offline using the pClamp program set (Axon Instruments, Union City, CA, USA). Histograms were fitted using Origin6.0 program set. Leak was not subtracted.

Aequorin Ca^{2+} measurements

Aequorin is a 22 KDa photoprotein isolated from jellyfish *Aequorea victoria* that emits blue light in the presence of Ca^{2+}. In its active form, the photoprotein includes an apo-protein and a covalently bound prosthetic group, coelenterazine. The apo-protein contains four helix-loop-helix EF-hand domains, three of which are Ca^{2+}-binding domains [105]. When Ca^{2+} ions bind to the high affinity EF-hand sites, coelenterazine is oxidized to coelenteramide, with a concomitant release of CO_2 and emission of light. Reconstitution of an active aequorin, expressed after cells transfection, can be obtained also in living cells by simple addition of coelenterazine into the medium. The advantage of genetically encoded probes is the possibility to target the probe to specific subcellular regions by fusing specific targeting sequences [106–108]. The possibility of using aequorin as Ca^{2+} indicator is based on the existence of a well characterized relationship between the rate of photon emission and the [Ca^{2+}] [109].

The aequorin detection system is derived from Cobbold and Lee description [110] and is based on the use of a low noise photomultiplier placed in close proximity (2-3 mm) of aequorin expressing cells. The cell chamber is adapted to fit 13 mm diameter coverslips. Cells are continuously perfused via peristaltic pump with medium thermosted at 37°C. The photomultiplier (Hamamatsu H7301) is kept in a dark box. The output of the amplifier-discriminator is captured by C8855-01 photon counting board in an IBM compatible microcomputer and stored for further analysis.

Experimental procedure

Cells transfection. HeLa cells were seeded on 13 millimetres (mm) coverslip at 60% confluency in a 24 wells plate. The day after cells were transfected with calcium phosphate procedure with the appropriate mix of DNA (in an aequorin/total DNA ratio of 1:4). The plasmids encoding aequorin based Ca^{2+} probes are cytosolic aequorin (cytAEQ) [111] and mutant aequorin targeted to mitochondria (mitAEQmut) [112,113]. The cytAEQ displays a range of [Ca^{2+}] sensibility between 10^{-4} and 10^{-7} M under physiological conditions of pH,

temperature and ionic strength. The mtAEQmut construct includes the targeting pre-sequence of subunit VIII of human cytochrome c oxidase fused to the aequorin cDNA. To expand the range of Ca^{2+} sensitivity that can be monitored the photoprotein was also mutated (Asp119>Ala). This point mutation affects specifically the second EF-hand motive of wild type aequorin. The affinity for Ca^{2+} of this mutated aequorin (mtAEQmut) is about 20 fold lower than that of the wild type [35].

Reconstitution. After 24 hours of transfection, 2 hours before the experiment, aequorin apoprotein was reconstituted by adding the prosthetic group, native coelenterazine (Molecular Probe). Cells were washed with Krebs–Ringer modified buffer (KRB: 135 mM NaCl, 5 mM glucose, 5 mM KCl, 1 mM $CaCl_2$, 1 mM $MgSO_4$, 0.4 mM K_2HPO_4, 20 mM HEPES, pH=7.4) and then incubated with 5 μM coelenterazine for 2 hours in KRB saline.

Ca^{2+} measurements. After the reconstitution phase, cells were transferred to the perfusion chamber. All aequorin measurements were carried out in modified KRB saline solution. Agonists and other drugs were added to the same solution. The agonist stimuli used for maximal stimulation was 100 μM histamine, which is an agonist of G proteins-coupled receptor H1, that is able to induce the generation of GAG and IP_3, and thus the release of Ca^{2+} from the ER through IP_3R. The experiments were terminated by lysing cells with 100 μM digitonin (Sigma-Aldrich) in a hypotonic Ca^{2+}-rich solution (10 mM $CaCl_2$ in H_2O), thus discharging the unbound aequorin pool.

Alternatively, aequorin measurements were carried out on a PerkinElmer EnVision plate reader equipped with a two-injector unit. Cells were transfected as described above in 24-well plates and then re-plated on 96-well plates (1:5 dilution) the day before the experiment. After reconstitution with 5 μM coelenterazine, cells were placed in 70 μl of KRB and luminescence from each well was measured for 1 min. During the experiment, histamine was first injected at the desired concentration to activate Ca^{2+} transients, and then a hypotonic, Ca^{2+}-rich, digitonin-containing solution was added to discharge the remaining aequorin pool. Output data were analysed and calibrated with a custom-made macro-enabled Excel workbook.

Mitochondrial Ca^{2+} uptake in permeabilized cells. HeLa cells were transfected with the mtAEQmut construct, using calcium phosphate procedure (see above). 24 hours after transfection, 2 hours before the experiment, the protein was reconstituted by adding the prosthetic group, native coelenterazine. After aequorin reconstitution, cells were perfused for 60 seconds with a buffer mimicking the cytosolic ionic composition (IB: 130 mM KCl, 10 mM NaCl, 2 mM K_2HPO_4, 5 mM succinic acid, 5 mM malic acid, 1 mM MgCl, 20 mM HEPES, 1 mM pyruvate, at pH 7) supplemented with 100 μM EGTA (IB/EGTA). Cells were then perfused with IB/EGTA buffer with 50 μM digitonin for 60 second to permeabilize the plasma membrane. After that, cells were washed with IB/EGTA buffer for other 60 second. Then cells were perfused with a known EGTA-buffered [Ca^{2+}] solution, at the indicated concentration of free-Ca^{2+}. Calculated $[Ca^{2+}]_{free}$ was predicted with CHELATOR software [114] and confirmed fluorimetrically with the Fura2 free acid form. After mitochondrial Ca^{2+} uptake, the experiments were terminated by lysing cells with 100 μM digitonin (Sigma-Aldrich) in a hypotonic Ca^{2+}-rich solution (10 mM $CaCl_2$ in H_2O), thus discharging the unbound aequorin pool. Mitochondrial Ca^{2+} uptake speed was calculated as the first derivative, by using the SLOPE Excel function smoothed for three time points. The higher value reached during Ca^{2+} addition represents the maximal Ca^{2+} uptake speed.

Measurement of Mitochondrial Membrane Potential

The measurement of mitochondrial membrane potential is based on the distribution of the mitochondrion-selective lipofilic cation tetramethyl-rhodamine methyl ester dye (TMRM, Thermo Fisher Scientific). This indicator is fluorescent and membrane permeable and its distribution into intracellular compartments is triggered by electrochemical gradients thanks to its positive charge. Hence, at low concentrations, its accumulation into mitochondria was shown to be driven by mitochondrial membrane potential (almost -180mV). In order to promote the correct distribution of the probe, cells were loaded with the dye-solution at very low concentration (20 nM). Changes in mitochondrial membrane potential cause a redistribution of the dye between mitochondria and cytoplasm. Cells were loaded

with TMRM stock solution (in modified KRB saline solution) for 20 min at 37°C. The probe was excited at 560 nm and the emission light was recorded in the 590-650 nm range.

Images were taken every 5 seconds with a fixed 200 ms exposure time. FCCP (carbonyl cyanide p-trifluoromethoxyphenylhydrazone, 10 μM), an uncoupler of oxidative phosphorylation, was added after 12 acquisitions to completely collapse the electrical gradient established by the respiratory chain ($\Delta\Psi$). Data are expressed as difference between the TMRM fluorescence before and after FCCP depolarization. TMRM imaging were performed on an inverted Zeiss Axiovert 200 equipped with a 40x 1.3N.A. objective. Images were collected with a back-illuminated EMCCD camera (Photometrics Cascade 512B) at 200-300 ms exposure time. Probe was excited by a 300W Xenon arc lamp (Sutter Lambda LS) with a 543/22 nm filter and collected through a 593/40 nm emission filter.

Immunofluorescence

HeLa cells were grown on 13 mm coverslips and transfected with MICU1-HA or MICU1.1-HA constructs and/or mtRFP encoding plasmid. After 24/36 hours, cells were washed with PBS, fixed in 4% formaldehyde for 10 minutes and quenched with 50 mM NH_4Cl in PBS. Cells were permeabilized for 10 minutes with 0.1% Triton X-100 in PBS and blocked in PBS containing 2% BSA for 1 hour. Cells were then incubated with primary antibodies (α-HA, Cell Signaling Technologies) for 3 hours at room temperature and washed 3 times with PBS. 488 AlexaFluor conjugated secondary antibodies (Thermo Fisher Scientific) were used and coverslips were mounted with ProLong Gold Antifade reagent (Thermo Fisher Scientific). Images were acquired on a Leica TCS-II SP5 STED CW system equipped with a 100×/1.4 N.A. Plan Apochromat objective. For all images, pinhole was set to 1 airy unit, pixel size was about 100 nm. 488 nm Ar-laser line was used to excite Alexa-488 and its signal collected in the 492-537 nm range, while RFP fluorescence was excited by the 543 nm HeNe laser and its emission was collected in the 555-700 nm range. For each image, PMT gain was slightly adjusted in order to maximize signal and avoid saturation.

Mitochondrial targeted GCaMP6f measurements

HeLa cells were grown on 24 mm coverslips and transfected with 4mtGCaMP6f-encoding plasmids together with the indicated constructs (ratio probe/other constructs 1:8). After 24 hours, coverslips were placed in 1ml of modified KRB (5.5 mM glucose, 1 mM $CaCl_2$) and imaging was performed on a Zeiss Axiovert 200 microscope equipped with a 63×/1.4 N.A. Plan Apochromat objective. Excitation was performed with a DeltaRAM V high-speed monochromator (Photon Technology International) equipped with a 75 W xenon arc lamp. Images were captured with a high-sensitivity Evolve 512 Delta EMCCD (Photometrics). The system is controlled by MetaMorph 7.5 (Molecular Devices) and was assembled by Crisel Instruments. In order to test resting $[Ca^{2+}]_{mt}$ with high sensitivity, a Ca^{2+} probe based on the last-generation GCaMP probe was generated [115] targeted to the mitochondrial matrix. The GCaMP6 family of is a collection of ultrasensitive, green fluorescent indicator proteins that enable reliable detection of fast Ca^{2+} transient (excitation $[Ca^{2+}]$-dependent at 474 nm). HeLa cells were alternatively illuminated at 474 and 410 nm and fluorescence was collected through a 515/30 nm band-pass filter (Semrock). Exposure time was set to 200 ms at 474 nm and to 400 ms at 410 nm, in order to account for the low quantum yield at the latter wavelength. At least ten fields were collected per coverslip, and each field was acquired for 10 s (1 frame/s). Analysis was performed with the Fiji distribution of ImageJ. Both images were corrected for the background frame by frame by subtracting the mean pixel values of a cell-free region of interest. Data are presented as the mean of the averaged ratio of all time points.

Cut of the sciatic nerve of CD1 mice

Four right hindlimbs for each time points of 3 months old CD1 mice were denervated cutting unilaterally the sciatic nerve. The animals were anesthetized by an intraperitoneal injection of ketamine (75 mg/Kg) and xylazine (20 mg/Kg). The sciatic nerve was unilaterally cut at the level of trochanter. About 0.5-1 cm of the

peripheral nerve stump was removed and the proximal stump was sutured into a superficial muscle to avoid reinnervation and obtain a permanent denervation of the lower hindlimb. 3 and 7 days after the injury, the animals were sacrificed by cervical dislocation. At the indicated time point the tibialis anterior (TA) and extensor digitorum longus (EDL) muscles were dissected out from the denervated hindlimbs and frozen in liquid nitrogen. The muscles were utilized for gene expression studies (see above for RNA extraction and Real-Time PCR procedures). The contralateral, innervated muscles were used as control. The experiments were approved by institutional review boards.

References

[1] R. Rizzuto, D. De Stefani, A. Raffaello, C. Mammucari, Mitochondria as sensors and regulators of calcium signalling., Nat. Rev. Mol. Cell Biol. 13 (2012) 566–78. doi:10.1038/nrm3412.

[2] K.J. Kamer, V.K. Mootha, The molecular era of the mitochondrial calcium uniporter., Nat. Rev. Mol. Cell Biol. 16 (2015) 545–553. doi:10.1038/nrm4039.

[3] F. Fieni, S.B. Lee, Y.N. Jan, Y. Kirichok, Activity of the mitochondrial calcium uniporter varies greatly between tissues., Nat. Commun. 3 (2012) 1317. doi:10.1038/ncomms2325.

[4] I.M. Kramer, Signal Transduction, Academic Press, 2015. https://books.google.com/books?id=QZq6AQAAQBAJ&pgis=1 (accessed January 23, 2016).

[5] D.E. Clapham, Calcium signaling., Cell. 131 (2007) 1047–58. doi:10.1016/j.cell.2007.11.028.

[6] S. Nakayama, R.H. Kretsinger, Evolution of the EF-hand family of proteins., Annu. Rev. Biophys. Biomol. Struct. 23 (1994) 473–507. doi:10.1146/annurev.bb.23.060194.002353.

[7] R. Rizzuto, Microdomains of Intracellular Ca2+: Molecular Determinants and Functional Consequences, Physiol. Rev. 86 (2006) 369–408. http://physrev.physiology.org/content/86/1/369.long (accessed October 12, 2015).

[8] R. Rizzuto, Calcium mobilization from mitochondria in synaptic transmitter release., J. Cell Biol. 163 (2003) 441–3. doi:10.1083/jcb.200309111.

[9] G. Hajnóczky, L.D. Robb-Gaspers, M.B. Seitz, A.P. Thomas, Decoding of cytosolic calcium oscillations in the mitochondria, Cell. 82 (1995) 415–424. doi:10.1016/0092-8674(95)90430-1.

[10] P. Pinton, T. Pozzan, R. Rizzuto, The Golgi apparatus is an inositol 1,4,5-trisphosphate-sensitive Ca2+ store, with functional properties distinct from those of the endoplasmic reticulum., EMBO J. 17 (1998) 5298–308. doi:10.1093/emboj/17.18.5298.

[11] M.J. Berridge, Inositol trisphosphate and calcium signalling mechanisms., Biochim. Biophys. Acta. 1793 (2009) 933–40. http://www.sciencedirect.com/science/article/pii/S0167488908003522 (accessed December 3, 2015).

[12] A. Rasola, P. Bernardi, Mitochondrial permeability transition in Ca(2+)-dependent apoptosis and necrosis., Cell Calcium. 50 (2011) 222–33. doi:10.1016/j.ceca.2011.04.007.

[13] F. Di Lisa, P. Bernardi, Mitochondria and ischemia-reperfusion injury of the heart: fixing a hole., Cardiovasc. Res. 70 (2006) 191–9. doi:10.1016/j.cardiores.2006.01.016.

[14] J.M.N. Duarte, P.F. Schuck, G.L. Wenk, G.C. Ferreira, Metabolic disturbances in diseases with neurological involvement., Aging Dis. 5 (2014) 238–55. http://www.pubmedcentral.nih.gov/articlerender.fcgi?artid=4113514&tool=pmcentrez&rendertype=abstract (accessed January 14, 2016).

[15] E. Gaude, C. Frezza, Defects in mitochondrial metabolism and cancer., Cancer Metab. 2 (2014) 10. http://www.pubmedcentral.nih.gov/articlerender.fcgi?artid=4108232&tool=pmcentrez&rendertype=abstract (accessed October 30, 2015).

[16] F. Celsi, P. Pizzo, M. Brini, S. Leo, C. Fotino, P. Pinton, et al., Mitochondria, calcium and cell death: a deadly triad in neurodegeneration, Biochim Biophys Acta. 1787 (2009) 335–344. doi:S0005-2728(09)00082-6 [pii]10.1016/j.bbabio.2009.02.021.

[17] F. Di Lisa, M. Canton, R. Menabò, N. Kaludercic, P. Bernardi, Mitochondria and cardioprotection., Heart Fail. Rev. 12 (2007) 249–60. doi:10.1007/s10741-007-9028-z.

[18] C. a Mannella, Structure and dynamics of the mitochondrial inner membrane cristae., Biochim. Biophys. Acta. 1763 (2006) 542–548. doi:10.1016/j.bbamcr.2006.04.006.

[19] P. Mitchell, J. Moyle, Chemiosmotic hypothesis of oxidative phosphorylation., Nature. 213 (1967) 137–9. http://www.ncbi.nlm.nih.gov/pubmed/4291593 (accessed January 16, 2016).

[20] P. Mitchell, Chemiosmotic Coupling in Oxidative and Photosynthetic Phosphorylation, (1966). http://fqb.fcien.edu.uy/docs/PDFS teorico 3/Chemiosmotic coupling in oxidative and photosynthetic phosphorylation - Mitchell - 1966 facs%C3%ADmil.pdf (accessed January 16, 2016).

[21] P. MITCHELL, CHEMIOSMOTIC COUPLING IN OXIDATIVE AND PHOTOSYNTHETIC PHOSPHORYLATION, Biol. Rev. 41 (1966) 445–501. http://doi.wiley.com/10.1111/j.1469-185X.1966.tb01501.x (accessed January 22, 2016).

[22] P. Mitchell, J. Moyle, Chemiosmotic hypothesis of oxidative phosphorylation., Nature. 213 (1967) 137–9.

[23] F.D. VASINGTON, J. V MURPHY, Ca ion uptake by rat kidney mitochondria and its dependence on respiration and phosphorylation., J. Biol. Chem. 237 (1962) 2670–7. http://www.ncbi.nlm.nih.gov/pubmed/13925019 (accessed January 16, 2016).

[24] H.F. DELUCA, G.W. ENGSTROM, Calcium uptake by rat kidney

mitochondria., Proc. Natl. Acad. Sci. U. S. A. 47 (1961) 1744–50. http://www.pubmedcentral.nih.gov/articlerender.fcgi?artid=223205&tool=pmcentrez&rendertype=abstract (accessed January 16, 2016).

[25] A.L. LEHNINGER, C.S. ROSSI, J.W. GREENAWALT, Respiration-dependent accumulation of inorganic phosphate and Ca ions by rat liver mitochondria., Biochem. Biophys. Res. Commun. 10 (1963) 444–8. http://www.ncbi.nlm.nih.gov/pubmed/13929376 (accessed January 16, 2016).

[26] P. Bernardi, Mitochondrial Transport of Cations: Channels, Exchangers, and Permeability Transition, Physiol Rev. 79 (1999) 1127–1155. http://physrev.physiology.org/content/79/4/1127.short (accessed January 22, 2016).

[27] R. Rizzuto, A.W. Simpson, M. Brini, T. Pozzan, Rapid changes of mitochondrial Ca2+ revealed by specifically targeted recombinant aequorin., Nature. 358 (1992) 325–7. doi:10.1038/358325a0.

[28] R. Rizzuto, M. Brini, M. Murgia, T. Pozzan, Microdomains with high Ca2+ close to IP3-sensitive channels that are sensed by neighboring mitochondria., Science. 262 (1993) 744–7. http://www.ncbi.nlm.nih.gov/pubmed/8235595 (accessed January 16, 2016).

[29] G. Csordás, P. Várnai, T. Golenár, S. Roy, G. Purkins, T.G. Schneider, et al., Imaging interorganelle contacts and local calcium dynamics at the ER-mitochondrial interface., Mol. Cell. 39 (2010) 121–32. doi:10.1016/j.molcel.2010.06.029.

[30] C.A. Mannella, K. Buttle, B.K. Rath, M. Marko, Electron microscopic tomography of rat-liver mitochondria and their interaction with the endoplasmic reticulum., Biofactors. 8 (1998) 225–8. http://www.ncbi.nlm.nih.gov/pubmed/9914823 (accessed December 28, 2015).

[31] G. Szalai, G. Csordás, B.M. Hantash, A.P. Thomas, G. Hajnóczky, Calcium signal transmission between ryanodine receptors and mitochondria., J. Biol. Chem. 275 (2000) 15305–13. http://www.ncbi.nlm.nih.gov/pubmed/10809765 (accessed December 28, 2015).

[32] G. Csordás, A.P. Thomas, G. Hajnóczky, Quasi-synaptic calcium signal transmission between endoplasmic reticulum and mitochondria., EMBO J. 18 (1999) 96–108. doi:10.1093/emboj/18.1.96.

[33] M. Giacomello, I. Drago, M. Bortolozzi, M. Scorzeto, A. Gianelle, P. Pizzo, et al., Ca2+ hot spots on the mitochondrial surface are generated by Ca2+ mobilization from stores, but not by activation of store-operated Ca2+ channels., Mol. Cell. 38 (2010) 280–90. doi:10.1016/j.molcel.2010.04.003.

[34] T. Hayashi, R. Rizzuto, G. Hajnoczky, T.-P. Su, MAM: more than just a housekeeper., Trends Cell Biol. 19 (2009) 81–8.

doi:10.1016/j.tcb.2008.12.002.

[35] R. Rizzuto, M. Brini, M. Murgia, T. Pozzan, Microdomains with high Ca2+ close to IP3-sensitive channels that are sensed by neighboring mitochondria., Science. 262 (1993) 744–7.

[36] R. Rizzuto, P. Pinton, W. Carrington, F.S. Fay, K.E. Fogarty, L.M. Lifshitz, et al., Close contacts with the endoplasmic reticulum as determinants of mitochondrial Ca2+ responses., Science. 280 (1998) 1763–1766. doi:10.1126/science.280.5370.1763.

[37] L.S. Jouaville, F. Ichas, E.L. Holmuhamedov, P. Camacho, J.D. Lechleiter, Synchronization of calcium waves by mitochondrial substrates in Xenopus laevis oocytes., Nature. 377 (1995) 438–41. doi:10.1038/377438a0.

[38] G. Hajnóczky, R. Hager, A.P. Thomas, Mitochondria suppress local feedback activation of inositol 1,4, 5-trisphosphate receptors by Ca2+., J. Biol. Chem. 274 (1999) 14157–62. http://www.ncbi.nlm.nih.gov/pubmed/10318833 (accessed January 17, 2016).

[39] H. Tinel, J.M. Cancela, H. Mogami, J. V Gerasimenko, O. V Gerasimenko, A. V Tepikin, et al., Active mitochondria surrounding the pancreatic acinar granule region prevent spreading of inositol trisphosphate-evoked local cytosolic Ca(2+) signals., EMBO J. 18 (1999) 4999–5008. doi:10.1093/emboj/18.18.4999.

[40] N.B. Pivovarova, J. Hongpaisan, S.B. Andrews, D.D. Friel, Depolarization-induced mitochondrial Ca accumulation in sympathetic neurons: spatial and temporal characteristics., J. Neurosci. 19 (1999) 6372–84. http://www.ncbi.nlm.nih.gov/pubmed/10414966 (accessed January 17, 2016).

[41] M. Murgia, C. Giorgi, P. Pinton, R. Rizzuto, Controlling metabolism and cell death: At the heart of mitochondrial calcium signalling, J. Mol. Cell. Cardiol. 46 (2009) 781–788. doi:10.1016/j.yjmcc.2009.03.003.

[42] D. Gramaglia, A. Gentile, M. Battaglia, L. Ranzato, V. Petronilli, M. Fassetta, et al., Apoptosis to necrosis switching downstream of apoptosome formation requires inhibition of both glycolysis and oxidative phosphorylation in a BCL-X(L)- and PKB/AKT-independent fashion., Cell Death Differ. 11 (2004) 342–53. doi:10.1038/sj.cdd.4401326.

[43] L. Scorrano, M. Ashiya, K. Buttle, S. Weiler, S.A. Oakes, C.A. Mannella, et al., A Distinct Pathway Remodels Mitochondrial Cristae and Mobilizes Cytochrome c during Apoptosis, Dev. Cell. 2 (2002) 55–67. doi:10.1016/S1534-5807(01)00116-2.

[44] P. Pinton, D. Ferrari, E. Rapizzi, F. Di Virgilio, T. Pozzan, R. Rizzuto, The Ca2+ concentration of the endoplasmic reticulum is a key determinant of ceramide-induced apoptosis: significance for the molecular mechanism of Bcl-2 action., EMBO J. 20 (2001) 2690–701.

doi:10.1093/emboj/20.11.2690.

[45] J.G. McCormack, A.P. Halestrap, R.M. Denton, Role of calcium ions in regulation of mammalian intramitochondrial metabolism., Physiol. Rev. 70 (1990) 391–425.

[46] L. Contreras, P. Gomez-Puertas, M. Iijima, K. Kobayashi, T. Saheki, J. Satrústegui, Ca2+ Activation kinetics of the two aspartate-glutamate mitochondrial carriers, aralar and citrin: role in the heart malate-aspartate NADH shuttle., J. Biol. Chem. 282 (2007) 7098–106. doi:10.1074/jbc.M610491200.

[47] D. De Stefani, A. Raffaello, E. Teardo, I. Szabò, R. Rizzuto, A forty-kilodalton protein of the inner membrane is the mitochondrial calcium uniporter., Nature. 476 (2011) 336–40. doi:10.1038/nature10230.

[48] J.M. Baughman, F. Perocchi, H.S. Girgis, M. Plovanich, C.A. Belcher-Timme, Y. Sancak, et al., Integrative genomics identifies MCU as an essential component of the mitochondrial calcium uniporter, Nature. 476 (2011) 341–345. doi:10.1038/nature10234.

[49] D.J. Pagliarini, S.E. Calvo, B. Chang, S.A. Sheth, S.B. Vafai, S.-E. Ong, et al., A mitochondrial protein compendium elucidates complex I disease biology., Cell. 134 (2008) 112–23. doi:10.1016/j.cell.2008.06.016.

[50] A. Raffaello, D. De Stefani, D. Sabbadin, E. Teardo, G. Merli, A. Picard, et al., The mitochondrial calcium uniporter is a multimer that can include a dominant-negative pore-forming subunit., EMBO J. 32 (2013) 2362–76. doi:10.1038/emboj.2013.157.

[51] Y. Sancak, A.L. Markhard, T. Kitami, E. Kovács-Bogdán, K.J. Kamer, N.D. Udeshi, et al., EMRE is an essential component of the mitochondrial calcium uniporter complex., Science. 342 (2013) 1379–82. doi:10.1126/science.1242993.

[52] M. Patron, V. Checchetto, A. Raffaello, E. Teardo, D. Vecellio Reane, M. Mantoan, et al., MICU1 and MICU2 Finely Tune the Mitochondrial Ca2+ Uniporter by Exerting Opposite Effects on MCU Activity, Mol. Cell. 53 (2014) 726–737. doi:10.1016/j.molcel.2014.01.013.

[53] E. Kovács-Bogdán, Y. Sancak, K.J. Kamer, M. Plovanich, A. Jambhekar, R.J. Huber, et al., Reconstitution of the mitochondrial calcium uniporter in yeast., Proc. Natl. Acad. Sci. U. S. A. 111 (2014) 8985–90. doi:10.1073/pnas.1400514111.

[54] H. Vais, K. Mallilankaraman, D.-O.D. Mak, H. Hoff, R. Payne, J.E. Tanis, et al., EMRE Is a Matrix Ca(2+) Sensor that Governs Gatekeeping of the Mitochondrial Ca(2+) Uniporter., Cell Rep. (2016). doi:10.1016/j.celrep.2015.12.054.

[55] G. Csordás, A.P. Thomas, G. Hajnóczky, Quasi-synaptic calcium signal transmission between endoplasmic reticulum and mitochondria., EMBO J. 18 (1999) 96–108. doi:10.1093/emboj/18.1.96.

[56] M. Giacomello, I. Drago, M. Bortolozzi, M. Scorzeto, A. Gianelle, P. Pizzo, et al., Ca2+ hot spots on the mitochondrial surface are generated by Ca2+ mobilization from stores, but not by activation of store-operated Ca2+ channels., Mol. Cell. 38 (2010) 280–90. doi:10.1016/j.molcel.2010.04.003.

[57] J.D. Martell, T.J. Deerinck, Y. Sancak, T.L. Poulos, V.K. Mootha, G.E. Sosinsky, et al., Engineered ascorbate peroxidase as a genetically encoded reporter for electron microscopy., Nat. Biotechnol. 30 (2012) 1143–8. doi:10.1038/nbt.2375.

[58] N.E. Hoffman, H.C. Chandramoorthy, S. Shamugapriya, X. Zhang, S. Rajan, K. Mallilankaraman, et al., MICU1 Motifs Define Mitochondrial Calcium Uniporter Binding and Activity, Cell Rep. 5 (2013) 1576–1588. doi:10.1016/j.celrep.2013.11.026.

[59] G. Csordás, T. Golenár, E.L. Seifert, K.J. Kamer, Y. Sancak, F. Perocchi, et al., MICU1 controls both the threshold and cooperative activation of the mitochondrial Ca^{2+} uniporter., Cell Metab. 17 (2013) 976–87. doi:10.1016/j.cmet.2013.04.020.

[60] S.S. Lam, J.D. Martell, K.J. Kamer, T.J. Deerinck, M.H. Ellisman, V.K. Mootha, et al., Directed evolution of APEX2 for electron microscopy and proximity labeling, Nat. Methods. 12 (2014) 51–54. doi:10.1038/nmeth.3179.

[61] F. Perocchi, V.M. Gohil, H.S. Girgis, X.R. Bao, J.E. McCombs, A.E. Palmer, et al., MICU1 encodes a mitochondrial EF hand protein required for Ca(2+) uptake., Nature. 467 (2010) 291–6. doi:10.1038/nature09358.

[62] M.R. Alam, L.N. Groschner, W. Parichatikanond, L. Kuo, A.I. Bondarenko, R. Rost, et al., Mitochondrial Ca2+ uptake 1 (MICU1) and mitochondrial ca2+ uniporter (MCU) contribute to metabolism-secretion coupling in clonal pancreatic β-cells., J. Biol. Chem. 287 (2012) 34445–54. doi:10.1074/jbc.M112.392084.

[63] K. Mallilankaraman, P. Doonan, C. Cárdenas, H.C. Chandramoorthy, M. Müller, R. Miller, et al., MICU1 is an essential gatekeeper for MCU-mediated mitochondrial Ca(2+) uptake that regulates cell survival., Cell. 151 (2012) 630–44. doi:10.1016/j.cell.2012.10.011.

[64] C. V Logan, G. Szabadkai, J.A. Sharpe, D.A. Parry, S. Torelli, A.-M. Childs, et al., Loss-of-function mutations in MICU1 cause a brain and muscle disorder linked to primary alterations in mitochondrial calcium signaling., Nat. Genet. 46 (2014) 188–93. doi:10.1038/ng.2851.

[65] M. Plovanich, R.L. Bogorad, Y. Sancak, K.J. Kamer, L. Strittmatter, A.A. Li, et al., MICU2, a paralog of MICU1, resides within the mitochondrial uniporter complex to regulate calcium handling., PLoS One. 8 (2013) e55785. doi:10.1371/journal.pone.0055785.

[66] K.J. Kamer, V.K. Mootha, MICU1 and MICU2 play nonredundant roles in the regulation of the mitochondrial calcium uniporter., EMBO Rep. 15

(2014) 299–307. doi:10.1002/embr.201337946.

[67] K. Mallilankaraman, C. Cárdenas, P.J. Doonan, H.C. Chandramoorthy, K.M. Irrinki, T. Golenár, et al., MCUR1 is an essential component of mitochondrial Ca2+ uptake that regulates cellular metabolism., Nat. Cell Biol. 14 (2012) 1336–43. doi:10.1038/ncb2622.

[68] V. Paupe, J. Prudent, E.P. Dassa, O.Z. Rendon, E.A. Shoubridge, CCDC90A (MCUR1) is a cytochrome c oxidase assembly factor and not a regulator of the mitochondrial calcium uniporter., Cell Metab. 21 (2015) 109–16. doi:10.1016/j.cmet.2014.12.004.

[69] H. Vais, J.E. Tanis, M. Müller, R. Payne, K. Mallilankaraman, J.K. Foskett, MCUR1, CCDC90A, Is a Regulator of the Mitochondrial Calcium Uniporter, Cell Metab. 22 (2015) 533–535. doi:10.1016/j.cmet.2015.09.015.

[70] E. Carafoli, A.L. Lehninger, A survey of the interaction of calcium ions with mitochondria from different tissues and species., Biochem. J. 122 (1971) 681–90. http://www.pubmedcentral.nih.gov/articlerender.fcgi?artid=1176837&tool=pmcentrez&rendertype=abstract (accessed January 21, 2016).

[71] T. Pozzan, R. Rudolf, Measurements of mitochondrial calcium in vivo., Biochim. Biophys. Acta. 1787 (2009) 1317–23. doi:10.1016/j.bbabio.2008.11.012.

[72] Y. Kirichok, G. Krapivinsky, D.E. Clapham, The mitochondrial calcium uniporter is a highly selective ion channel., Nature. 427 (2004) 360–4. doi:10.1038/nature02246.

[73] M.-L.A. Joiner, O.M. Koval, J. Li, B.J. He, C. Allamargot, Z. Gao, et al., CaMKII determines mitochondrial stress responses in heart., Nature. 491 (2012) 269–73. doi:10.1038/nature11444.

[74] Y. Lee, C.K. Min, T.G. Kim, H.K. Song, Y. Lim, D. Kim, et al., Structure and function of the N-terminal domain of the human mitochondrial calcium uniporter., EMBO Rep. 16 (2015) 1318–1333. doi:10.15252/embr.201540436.

[75] F. Fieni, D.E. Johnson, A. Hudmon, Y. Kirichok, Mitochondrial Ca2+ uniporter and CaMKII in heart, Nature. 513 (2014) E1–E2. doi:10.1038/nature13626.

[76] S. Marchi, L. Lupini, S. Patergnani, A. Rimessi, S. Missiroli, M. Bonora, et al., Downregulation of the mitochondrial calcium uniporter by cancer-related miR-25., Curr. Biol. 23 (2013) 58–63. doi:10.1016/j.cub.2012.11.026.

[77] L. Pan, B.-J. Huang, X.-E. Ma, S.-Y. Wang, J. Feng, F. Lv, et al., MiR-25 protects cardiomyocytes against oxidative damage by targeting the mitochondrial calcium uniporter., Int. J. Mol. Sci. 16 (2015) 5420–33. doi:10.3390/ijms16035420.

[78] X. Pan, J. Liu, T. Nguyen, C. Liu, J. Sun, Y. Teng, et al., The physiological

role of mitochondrial calcium revealed by mice lacking the mitochondrial calcium uniporter., Nat. Cell Biol. 15 (2013) 1464–72. doi:10.1038/ncb2868.

[79] C. Mammucari, G. Gherardi, I. Zamparo, A. Raffaello, S. Boncompagni, F. Chemello, et al., The mitochondrial calcium uniporter controls skeletal muscle trophism in vivo., Cell Rep. 10 (2015) 1269–79. doi:10.1016/j.celrep.2015.01.056.

[80] F. Chemello, C. Mammucari, G. Gherardi, R. Rizzuto, G. Lanfranchi, S. Cagnin, Gene expression changes of single skeletal muscle fibers in response to modulation of the mitochondrial calcium uniporter (MCU)., Genomics Data. 5 (2015) 64–7. doi:10.1016/j.gdata.2015.05.023.

[81] Y. Lee, C.K. Min, T.G. Kim, H.K. Song, Y. Lim, D. Kim, et al., Structure and function of the N-terminal domain of the human mitochondrial calcium uniporter., EMBO Rep. 16 (2015) 1318–1333. doi:10.15252/embr.201540436.

[82] L. Wang, X. Yang, S. Li, Z. Wang, Y. Liu, J. Feng, et al., Structural and mechanistic insights into MICU1 regulation of mitochondrial calcium uptake, EMBO J. 33 (2014) 594–604. doi:10.1002/embj.201386523.

[83] G. Hajnóczky, G. Csordás, S. Das, C. Garcia-Perez, M. Saotome, S. Sinha Roy, et al., Mitochondrial calcium signalling and cell death: approaches for assessing the role of mitochondrial Ca2+ uptake in apoptosis., Cell Calcium. 40 553–60. doi:10.1016/j.ceca.2006.08.016.

[84] T.-W. Chen, T.J. Wardill, Y. Sun, S.R. Pulver, S.L. Renninger, A. Baohan, et al., Ultrasensitive fluorescent proteins for imaging neuronal activity., Nature. 499 (2013) 295–300. doi:10.1038/nature12354.

[85] C. Petrungaro, K.M. Zimmermann, V. Küttner, M. Fischer, J. Dengjel, I. Bogeski, et al., The Ca(2+)-Dependent Release of the Mia40-Induced MICU1-MICU2 Dimer from MCU Regulates Mitochondrial Ca(2+) Uptake., Cell Metab. 22 (2015) 721–733. doi:10.1016/j.cmet.2015.08.019.

[86] M. Sandri, J. Lin, C. Handschin, W. Yang, Z.P. Arany, S.H. Lecker, et al., PGC-1alpha protects skeletal muscle from atrophy by suppressing FoxO3 action and atrophy-specific gene transcription., Proc. Natl. Acad. Sci. U. S. A. 103 (2006) 16260–5. doi:10.1073/pnas.0607795103.

[87] A. Raffaello, G. Milan, E. Masiero, S. Carnio, D. Lee, G. Lanfranchi, et al., JunB transcription factor maintains skeletal muscle mass and promotes hypertrophy., J. Cell Biol. 191 (2010) 101–13. doi:10.1083/jcb.201001136.

[88] J.M. Sacheck, J.-P.K. Hyatt, A. Raffaello, R.T. Jagoe, R.R. Roy, V.R. Edgerton, et al., Rapid disuse and denervation atrophy involve transcriptional changes similar to those of muscle wasting during systemic diseases., FASEB J. 21 (2007) 140–55. doi:10.1096/fj.06-6604com.

[89] S.H. Lecker, R.T. Jagoe, A. Gilbert, M. Gomes, V. Baracos, J. Bailey, et al., Multiple types of skeletal muscle atrophy involve a common program of changes in gene expression., FASEB J. 18 (2004) 39–51. doi:10.1096/fj.03-

0610com.

[90] S. Schiaffino, K.A. Dyar, S. Ciciliot, B. Blaauw, M. Sandri, Mechanisms regulating skeletal muscle growth and atrophy., FEBS J. 280 (2013) 4294–314. doi:10.1111/febs.12253.

[91] C. Cárdenas, R.A. Miller, I. Smith, T. Bui, J. Molgó, M. Müller, et al., Essential regulation of cell bioenergetics by constitutive InsP3 receptor Ca2+ transfer to mitochondria., Cell. 142 (2010) 270–83. doi:10.1016/j.cell.2010.06.007.

[92] J. O-Uchi, B.S. Jhun, S. Xu, S. Hurst, A. Raffaello, X. Liu, et al., Adrenergic Signaling Regulates Mitochondrial Ca 2+ Uptake Through Pyk2-Dependent Tyrosine Phosphorylation of the Mitochondrial Ca 2+ Uniporter, Antioxid. Redox Signal. 21 (2014) 863–879. doi:10.1089/ars.2013.5394.

[93] A. Rana, M. Yen, A.M. Sadaghiani, S. Malmersjö, C.Y. Park, R.E. Dolmetsch, et al., Alternative splicing converts STIM2 from an activator to an inhibitor of store-operated calcium channels., J. Cell Biol. 209 (2015) 653–69. doi:10.1083/jcb.201412060.

[94] A.-M. Miederer, D. Alansary, G. Schwär, P.-H. Lee, M. Jung, V. Helms, et al., A STIM2 splice variant negatively regulates store-operated calcium entry, Nat. Commun. 6 (2015) 6899. doi:10.1038/ncomms7899.

[95] L. Wang, X. Yang, S. Li, Z. Wang, Y. Liu, J. Feng, et al., Structural and mechanistic insights into MICU1 regulation of mitochondrial calcium uptake, EMBO J. 33 (2014) 594–604. doi:10.1002/embj.201386523.

[96] S.J. Smith, J. Buchanan, L.R. Osses, M.P. Charlton, G.J. Augustine, The spatial distribution of calcium signals in squid presynaptic terminals., J. Physiol. 472 (1993) 573–593. doi:10.1113/jphysiol.1993.sp019963.

[97] O. Delbono, E. Stefani, Calcium transients in single mammalian skeletal muscle fibres., J. Physiol. 463 (1993) 689–707. http://www.pubmedcentral.nih.gov/articlerender.fcgi?artid=1175366&tool=pmcentrez&rendertype=abstract (accessed January 22, 2016).

[98] B.L. Sabatini, T.G. Oertner, K. Svoboda, The Life Cycle of Ca2+ Ions in Dendritic Spines, Neuron. 33 (2002) 439–452. doi:10.1016/S0896-6273(02)00573-1.

[99] C. Long, L. Amoasii, A.A. Mireault, J.R. McAnally, H. Li, E. Sanchez-Ortiz, et al., Postnatal genome editing partially restores dystrophin expression in a mouse model of muscular dystrophy., Science. (2015) science.aad5725–. doi:10.1126/science.aad5725.

[100] S. Rozen, H. Skaletsky, Primer3 on the WWW for general users and for biologist programmers., Methods Mol. Biol. 132 (2000) 365–86. http://www.ncbi.nlm.nih.gov/pubmed/10547847 (accessed October 17, 2014).

[101] G.J. Chen, N. Qiu, C. Karrer, P. Caspers, M.G. Page, Restriction site-free

insertion of PCR products directionally into vectors., Biotechniques. 28 (2000) 498–500, 504–5. http://www.ncbi.nlm.nih.gov/pubmed/10723563 (accessed January 20, 2016).

[102] O. Makarova, E. Kamberov, B. Margolis, Generation of deletion and point mutations with one primer in a single cloning step., Biotechniques. 29 (2000) 970–2. http://www.ncbi.nlm.nih.gov/pubmed/11084856 (accessed January 27, 2016).

[103] H. Schägger, Blue-native gels to isolate protein complexes from mitochondria., Methods Cell Biol. 65 (2001) 231–44. http://www.ncbi.nlm.nih.gov/pubmed/11381596 (accessed December 16, 2015).

[104] D.J. Fitzgerald, P. Berger, C. Schaffitzel, K. Yamada, T.J. Richmond, I. Berger, Protein complex expression by using multigene baculoviral vectors., Nat. Methods. 3 (2006) 1021–32. doi:10.1038/nmeth983.

[105] S. Inouye, F.I. Tsuji, Cloning and sequence analysis of cDNA for the Ca 2+ -activated photoprotein, clytin, FEBS Lett. 315 (1993) 343–346. doi:10.1016/0014-5793(93)81191-2.

[106] J. Garcia-Bustos, J. Heitman, M.N. Hall, Nuclear protein localization, Biochim. Biophys. Acta - Rev. Biomembr. 1071 (1991) 83–101. doi:10.1016/0304-4157(91)90013-M.

[107] F.-U. Hartl, N. Pfanner, D.W. Nicholson, W. Neupert, Mitochondrial protein import, Biochim. Biophys. Acta - Rev. Biomembr. 988 (1989) 1–45. doi:10.1016/0304-4157(89)90002-6.

[108] S.F. Nothwehr, J.I. Gordon, Targeting of proteins into the eukaryotic secretory pathway: signal peptide structure/function relationships., Bioessays. 12 (1990) 479–84. doi:10.1002/bies.950121005.

[109] D.G. Allen, J.R. Blinks, Calcium transients in aequorin-injected frog cardiac muscle, Nature. 273 (1978) 509–513. doi:10.1038/273509a0.

[110] P.H. Cobbold, P.K. Bourne, Aequorin measurements of free calcium in single heart cells, Nature. 312 (1984) 444–446. doi:10.1038/312444a0.

[111] R. Marsault, Transfected Aequorin in the Measurement of Cytosolic Ca[IMAGE] Concentration ([Ca[IMAGE]][IMAGE]), J. Biol. Chem. 270 (1995) 9896–9903. doi:10.1074/jbc.270.17.9896.

[112] J.M. Kendall, G. Sala-Newby, V. Ghalaut, R.L. Dormer, A.K. Cambell, Engineering the Ca2+-activated photoprotein aequorin with reduced affinity for calcium, Biochem. Biophys. Res. Commun. 187 (1992) 1091–1097. doi:10.1016/0006-291X(92)91309-E.

[113] M. Montero, M. Barrero, J. Alvarez, [Ca2+] microdomains control agonist-induced Ca2+ release in intact HeLa cells, FASEB J. 11 (1997) 881–885. http://www.fasebj.org/content/11/11/881?ijkey=6e8a1bf880ac828511a59c07a0332638126cf905&keytype2=tf_ipsecsha (accessed January 14, 2016).

[114] T.J. Schoenmakers, G.J. Visser, G. Flik, A.P. Theuvenet, CHELATOR: an improved method for computing metal ion concentrations in physiological solutions., Biotechniques. 12 (1992) 870–4, 876–9. http://europepmc.org/abstract/med/1642895 (accessed January 14, 2016).

[115] T.-W. Chen, T.J. Wardill, Y. Sun, S.R. Pulver, S.L. Renninger, A. Baohan, et al., Ultrasensitive fluorescent proteins for imaging neuronal activity., Nature. 499 (2013) 295–300. doi:10.1038/nature12354.